DEVELOPMENT OF A CARDIOVASCULAR SIMULATOR INCORPORATING A PHANTOM SIMULATION OF THE ARTERIAL SYSTEM

Liam Foley

Supervisor: Dr Andrew Lowe

A thesis submitted to Auckland University of Technology in fulfilment of the requirement of the degree of Master of Engineering

March 2021

School of Engineering

Faculty of Design and Creative Technologies

Auckland University of Technology

Abstract

A mock circulatory loop was constructed to test a new blood pressure device under development. The loop was intended to replicate a range of cardiac conditions with the implementation of an artificial arterial tree.

An in-depth literature review was conducted on the previous construction on mock circulatory loops and arterial phantoms. The methods employed previously were analysed and implemented in this project. Lost core casting methods were used to create complex artery phantoms, using 3D printed moulds and silicone elastomers, yielding an arterial tree that was dimensionally and functionally accurate in reproducing pulse wave amplification and arterial wall compliance.

A synthetic ventricle pump was developed in conjunction with a variable compliance chamber and peripheral resistance. The pump consists of a synthetic ventricle inside a water-filled chamber with a motor actuating a piston to change the volume, successfully reproducing the flow desired. The compliance chamber emulated a bladder accumulator to reproduce capacitances as desired, and a motor actuated gate valve simulates peripheral resistance. The overall system successfully reproduced human pressures and flows, with sufficient damping being observed due to the compliance chamber and the elastic vessels.

Contents

List of Figures

List of Tables

Statement of Authorship

"I hereby declare that this submission is my own work and that, to the best of my knowledge and belief, it contains no material previously published or written by another person nor material which to a substantial extent has been accepted for the qualification of any other degree or diploma of a university or other institution of higher learning, except where due acknowledgement is made in the acknowledgements."

Liam Foley

Signature:

Date: 19/03/2021

Acknowledgements

I want to thank my supervisors, Dr Andrew Lowe and Dr Martin Stommel, there expert advice and guidance through the design and development of this thesis have ensured the successful completion of this work, and I am very grateful.

I would also like to thank my fellow students Aadil Paghdiwala, Ragavan Subburaj and Mayuresh Kulkarni. Aadil for the assistance in deriving the power transfer linkage equations found in this thesis and Ragavan and Mayuresh for assistance in the ultrasound testing conducted.

Liam Foley

Auckland, New Zealand

2021

1 Introduction

A mock circulatory loop is a mechanical representation of the human circulatory system; they are important for the development and testing of medical devices such as ventricular assistance devices, stents, artificial heart valves and blood pressure measurement. Mock circulatory systems are also a good tool for education, as blood pressures and cardiac output can be studied. A phantom artery is a synthetic reproduction of an artery often moulded with silicones. Phantom arteries are used for simulations of the mechanics of the arterial wall, and the contribution of the shape and volume changes to the amplification of pulse pressure waves forms downstream from the heart.

1.1 Aims

This thesis aims to analyse the process undertaken to develop a cardiovascular simulator and the production of a phantom arterial tree to be used to test a new blood pressure device.

The aims of this research are to:

- Develop and implement methods of fabricating arterial phantoms accurately.
- Select appropriate phantom material to emulate the physiological properties through material testing of various silicone elastomers.
- Test the behaviour of the phantom arteries against the expected behaviour from literature.
- Assemble a working mock circulatory loop by designing and constructing mechanically simulated arterial compliance, resistance, and pulsating flow.
- Validate the mock circulatory loop against previous studies and measured human levels of arterial compliance, blood pressure and blood flow.

1.2 Scope

This project's scope included the design, construction, and validation of a cardiovascular simulator, which implements elements of compliance, resistance, and pulsatile flow. A phantom artery tree of major arteries was to be developed from compliant silicone elastomers to be accurate in shape and size.

2 Background and Literature Review

This literature review aims to provide a comprehensive grasp of the mock circulatory loop's design requirements and an in-depth investigation into the human circulation system and its elements to produce an accurate mechanical representation of biological systems.

2.1 The Circulatory System

The circulatory system is illustrated in Figure 1. Blood flows to the right atrium from the vena cava depleted of oxygen. From there, it proceeds to flow into the right vertical through the tricuspid valve, then into the pulmonary artery via the pulmonary valve. Blood is supplied to the right and left lung from the pulmonary artery oxygenation of the blood occurs as the blood passes through the capillaries. Blood leaves the lungs out of the pulmonary vein and proceeds to the heart into the left atrium. The left ventricle is filled as blood passes through the mitral valve from the left atrium, then ejected into the aorta through the aortic valve. The arterial system is divided up throughout the body supplying oxygenated blood to all the extremities and organs before returning to the right atrium through the venous system repeating the cycle.

Figure 1: Blood circulation diagram (Mafi, Rajan et al. 2011)

2.1.1 The Cardiac Cycle

Cardiac function is cyclic; it goes through two stages systole and diastole. The ventricle fills with blood as the heart relaxes during diastole; as the cardiac muscle contracts, blood is ejected from the ventricle; this is the systole stage. The stages can be divided further into more stages, as seen in Figure 2.

The first stage is atrial contraction. A pressure differential between the atrium and ventricle is created due to the contracting atrium enough to force the blood to flow into the ventricle quickly; at the end of this stage, the blood in the ventricle has reached its largest amount of end-diastolic volume or (EDV). Stage 2 is where isovolumetric contraction occurs. Ventricle contraction occurs during this process, resulting in a quick pressure increase while the volume remains the same. The third stage is rapid ejection. This happens when the ventricular pressure is greater than the aortic and pulmonary

Figure 2 : Cardiac Cycle (Richard E. Klabunde 2004)

arterial pressure forcing the blood from the ventricle through the valve.

Stage 4 is where the ejection rate decreases. The ventricular pressure now falls below the aortic, and pulmonary pressures flow continues some due to the inertia of the blood. Stage 5 is isovolumetric relaxation. Pressure in the ventricles falls below the aorta and pulmonary arteries' pressure, causing the valves to close abruptly. A small amount of backflow occurs, represented by the dicrotic notch observed in the wave. During this phase, ventricular volume remains constant as there is no flow in or out; this is the end-systolic volume (ESV), usually around 50 ml.

Phase 6 is the rapid filling stage due to the drop in ventricular pressure below atrial pressures causing blood to flow rapidly from the atria to the ventricles. Atrial pressure drops rapidly at this stage, where aortic pressure drops gradually due to the systemic vascular resistance and compliance of the arteries themselves. Phase 7 sees a reduction in the filling of the ventricles. It is caused by a reduction in ventricular wall compliance as volume increases. Atrial pressure continues to rise as blood pressure falls due to circulation. (Richard E. Klabunde 2004)

2.1.2 Frank-Starling Law

The Frank-Starling law dictates that the heart has an inherent ability to increase its contractile force, an increase in venous return also cause stroke volume to increase (Richard E. Klabunde 2004). Dissecting this law, we can understand that the law says that the heart is a loop with no leaks and that what goes out of the ventricle must cycle back in at some stage. This also means that the more blood that is pumped into the ventricle, the heart discharges more blood, meaning it is working harder to resist backflow. Figure 3 illustrates that the preload of the ventricle increases as more blood enters the ventricle. This leads to increased contraction force, therefore, larger stroke volume to maintain ventricular preload.

Figure 3: Ventricle volume vs pressure (Richard E. Klabunde 2004)

2.2 Windkessel Model

"Haemostatics" by Hales (1733) described the concept of capacitance in a circulatory model as the Windkessel effect. The circulatory system's constant flow was credited to the artery's elasticity, allowing them to expand and contract to accumulate flow between pulses. The damping of flow during the cardiac cycle can be compared to air-

filled accumulators or Windkessel chambers used to dampen fire hoses illustrated in Figure 4.

Figure 4:Firehose compared to Windkessel

The blood pressure wave can be described in terms of the systemic vascular resistance (R), capacitance/compliance (C) and stroke volume (SV) using the Windkessel model. The model can be described as an electrical equivalent circuit, as seen in Figure 5, equating systemic vascular resistance to a resistor and the arteries' elastic properties, the compliance as a capacitor.

Figure 5: Two element Windkessel model

The Windkessel relation can be derived from the circuit observed in Figure 5, where Q is flow and P is pressure.

$$Q(t) = \frac{P(t)}{R} + C\frac{dP(t)}{dt} \quad (1)$$

This model can describe the slow release of pressure observed in Figure 6's aortic pressure wave in red as the pressure is slowly released as a capacitor might discharge voltage. In the aorta, the pressure is slowly released, maintain a minimum pressure at the end of the cycle, the diastolic pressure and peaking when the heart pumps the systolic pressure. The stiff ventricle can be seen remaining at peaking then immediately returning to 0 as the pressure cannot be stored or accumulated.

Figure 6: Aortic and Ventricular pressure (Mitchell and Wang 2014)

From equation 1, a transfer function can be derived relating to the equivalent circuit and incoming pressure to the outgoing pressure. The outgoing pressure $\mathrm{P_{out}}$ is given by the Windkessel transfer function given as:

$$P_{out} = \frac{R}{1 + RCs} P_{in} \quad (2)$$

Where RC is equivalent to the time constant (τ) which is the time it takes to get to 63% of a new steady-state after a step change in flow or pressure.

.

Figure 7: Time constant for pressure wave (Ross, Toshner et al. 2013)

Marcus, Korcarz et al. (1994) tested the non-invasive procedures to determine arterial compliance using pulse tracking. Table 1 indicates the parameters used in this experiment, along with the compliance determined using the two and three-element Windkessel model.

Table 1: Haemodynamic profile of a normal population (Marcus, Korcarz et al. 1994)

2.3 Mock Circulatory Loops

Mock circulation loops (MCLs) are developed to represent the human circulatory system mechanically to examine various cardiac assisting and testing devices such as blood pressure measurement, artificial replacement valve and ventricular assisting devices. The most basic of mock circulation systems generally consist of a preloading chamber and a pressure drop developed through the use of assorted valves; more modern systems have been designed to represent accurate pulse flow, resistance, compliance atrial contraction, septal defects, and insertion of cardiovascular assistant devices. A thorough background and literature review of previous systems is presented.

The original purpose of mock circulatory loops was to test stepper actuated pulse duplicators in developing an artificial valve to create a heartbeat, as seen in work by Pantalos, Koenig et al. (2004). A lot of the systems used artificial ventricles that were transparent for visualisation of flow through the valve as in (Verdonck, Dumont et al. 2002), (Naemura, Umezu et al. 1999), (Naemura, Umezu et al. 1999), (Grigioni, Daniele et al. 2000), (Morsi and Sakhaeimanesh 2000) and (Walther, Lehmann et al. 2002).

The MCL designed by Cornhill (1977), designed to test prosthetic artery valves, using a pressurised box containing a flexible silicon bag for the mock left ventricle compressed air controlled by a solenoid valve was supplied to the box. With total arterial capacitance and characteristic peripheral resistance included, natural haemodynamic conditions were simulated.

An older MCL design by Kolff (1959) incorporated pulmonary and systemic systems where the pulmonary system circulates blood between the heart and lungs. The systemic system circulates between the heart and the rest of the body. Compressed air was used to actuate ventricles, and aortic pressure was achieved through water columns; changing the column height changed the diastole pressure. For water to move

up the tube, more inertia was needed due to the columns' height, which is undesirable. To minimise this, the flow up the tube was assisted by a pressurised air chamber at the bottom. No simulation of compliance was attempted, and no resistance was added to the system as the increased flow was observed to increase resistance.

Reul, Tesch et al. (1974) assembled a mock circulatory loop consisting of an aorta and its branches simulated by transparent tubing. The system was placed in a perspex box filled with water and fixed to a variable compliant Windkessel pressure vessel. Each branch used pinch valves as resistance. The heart was simulated by a cam driven system supplying pulsating pressure to the ventricle. This MCL emulated the circulatory system satisfactorily.

Donovan (1975) designed and constructed one of the most widely replicated MCLs since its conception. An acrylic sheet was used to build a box with four chambers to replicate pulmonary arterial, systemic, pulmonary venous and ventricular components. A compact design only 605x403x202 mm for the whole system. This system produced quite promising data and has been replicated many times since.

Rosenberg (1981) described the design of another commonly repeated MCL, the Pennsylvania State University Mock Circulatory system or the Penn state MCL. Designed in 1971 for the testing of Ventricular assistance devices (VADs) and has been refined many times since. It included VADs connections, pulmonary circulation, resistance, compliance, and adjustable cardiac conditions. The values used in the reproduction of the MCL with a right atrial pressure of 2.2 mmHg, mean left atrial pressure of 7.5 mmHg, mean pulmonary arterial pressure of 15 mmHg, mean arterial pressure of 100 mmHg, and cardiac output of 5 L/min, are shown in Table 2. This MCL represented the human circulatory system adequately for the purposes required.

Table 2: MCL parameter chosen by (Rosenberg 1981)

Scotten, Walker et al. (1979) developed a mock circulatory loop for testing a mitral valve prosthesis. The heart was simulated by a cam driving fluid into a sealed box containing a transparent synthetic ventricle. The fluid was pumped into the synthetic aorta from the ventricle flowing into compliant and resistant components. Cellulose fibre water filters were used to simulate resistance 50 and 5 µm pore sizes for peripheral and characteristic resistances. The tube lengths could be changed by inserting a tube while

the system was operating intern altering the resistance; the limitation to this is that it was only discreetly variable instead of continuously variable. Variable air volume above a chamber of water was used to simulate compliance. The ventricle, working fluids and hydraulic accumulator were clear to visualise the system flow.

Verdonck, Dumont et al. (2002) developed an MCL for testing mitral valves. The system was designed to enable easy replacement of aortic and mitral valves. Water flowed into the MCL from a tank emulating the lungs, carrying fluid through the replacement mitral valve from the pulmonary veins. From the left ventricle, water travelled through a replacement aortic valve into a Windkessel chamber, simulating arterial compliance and a resistance valve. The system included a tank to simulate venous pressure of 5 mmHg. A latex atrium and left silicon ventricle were developed to replicate human anatomy and inserted in a Perspex box filled with water where an external circuit controlled the pressure. A feedback system controlled the amount of pressure delivered to the ventricle, which used a model of a pressure wave to vary the amount of air in the system to replicate the haemodynamic pressure wave. Systole and diastole pressures were simulated using positive and negative pressure, respectively. Later Vandenberghe, Van Loon et al. (2003) used the same loop to evaluate an intra-arterial LVAD.

Trittenwein, Zamberger et al. (1998) designed a neonatal MCL to investigate the effect of extracorporeal membrane oxygenation. The loops purpose was to emulate neonatal circulation and produced a slower heart rate and overall lower cardiac output to mimic those seen in the real situation. They simulated increased arterial resistance, a low cardiac output and volume reduction of the mock loop (hypovolemia) to test this loop. The conclusions the authors drew were that the loop was successful in simulating cardiac conditions in a neonate. Still, the inability to replicate the effects of medication could not replace the use of real patients in clinical studies. Though good results were obtained from this system, the absence of pulmonary circulation yielded imprecise preload of the ventricle, making the MCL unable to simulate right ventricle heart failure.

There have been various arrangements of MCLs created. They differ from a basic two Windkessel model to more complex five-element models. Sharp and Dharmalingham (1999) studied the advantage of different arrangements and used the study to compare the Penn state loop, the Donovan loop and the human body. A computer analysis of RCLRC, RCRC, RLR and RC models was undertaken, where L is inertiance, C is capacitance,

and R is resistance. The results from this study showed improvement when compared to human physiological levels when adding an extra element; the difference between RCR and RLRC was only a small increase in accuracy, whereas the jump between the accuracy of RLRC and RCLRC was significant. Due to the complexity of the RCLRC system, it was ignored in favour of the RCR system to take to a physiological stage. When compared to the human circulatory system, both the Penn State and Donovan models were favourable. The small elements (25 mm) in the Penn state model contributed to the undesirable inertial properties of the MCL.

Baloa, Boston et al. (2001) conducted a study to investigate the elastance based control of an MCL. The idea used elastance, described as instantaneous ventricle pressure versus ventricle volume, to create a new control method for mock circulatory loops. They measured the maximum elastance at the end of the systole and is used as a measure of the contractility of the ventricle. Compliance and resistance were manually controlled. The values can be seen in Table 3.

Table 3: Resistance and compliance of the Baloa, Boston et al. (2001) loop

It was concluded that the design succeeded in changing the contraction of the ventricle using an elastic control method to develop a unique mock circulatory loop to simulate cardiac conditions accurately.

Fiore, Redaelli et al. (2003) developed a model left ventricle with physiologic-like diastolic behaviour for studying mitral valve surgical correction. The study involved developing a flexible ventricle and studying the change in shape during the cardiac cycle. The information was gathered for the use of creating an acceptable mock ventricle for studying ventricle filling fluid dynamics. The ventricle shape at its end-systole point was chosen for reproduction. This shape was chosen for the ventricle to keep its shape as it fills, as opposed to if the end-diastolic shape was used the true shape as systole may not be achieved due to potential buckling of the ventricle due to forced contraction. An FEA model was used to develop a ventricle shape with a volume of 71 mL at its systolic point. Negative pressure was applied around the mock ventricle to induce filling of the ventricle until the injection point is reached. Wall curvature values were examined at seven sections around the mock ventricle and compared to those in literature. The system was accurate within 3.5%, and the publishers determined that the design

behaved similarly to those found in human anatomy. However, the system could not replicate conditions such as cardiomyopathy, resulting in the system only being used to replicate normal cardiac conditions.

A systemic mock circulation to test pulsatile and continuous ventricular assisting devices was developed by Koenig, Pantalos et al. (2004). A hemi-ellipsoid shape with a semi-rigid dome was used to create a mock ventricle with mitral and aortic valve mounts. A pressurised chamber controlled the heart rate. A pressure-volume catheter measured ventricular volume and pressure. A compliant latex tube within a sealed chamber was used to mimic resistance pressure supplied to the chamber changed the area of the tube throttling the flow. This study was limited because of the lack of a pulmonary circulation component to the systemic side.

Pantalos, Koenig et al. (2004) constructed a loop intending to mimic the frank starling response in normal conditions and partial recovery and heart failure situations. Table 4 illustrates the reproduced values of human conditions in the mock circulatory loops by Pantalos. a flexible polyurethane ventricle and atrium were used in this system. The ventricle was pressurised in a chamber capable of mounting in and outflow valves using a semi-rigid dome. However, it was not anatomically shaped. Coronary and systemic vasculature was connected to a synthetic ventricle. Good representations of natural pressure-volume loops were produced, mimicking the desired Frank-Starling response. For all conditions tested, and accurate waveform, morphology and magnitudes were produced by this MCL and could incorporate cardiac devices for testing. The system's main limitations were the lack of pulmonary vasculature and noise in the pressure waveform from valve closure.

Table 4: Values chosen for reproduction in mock circulation in (Pantalos, Koenig et al. 2004)

Litwak, Koenig et al. (2005) constructed an MCL incorporating coronary vasculature for studying ascending aorta graft location continuous and pulsatile flow ventricular assisting devices. Table 5 **Error! Reference source not found.**illustrates the MCL values used to emulate normal and heart failure conditions. This loop incorporated a ventricle and atrium fabricated from flexible polymer sacs where the ventricle is in a pressurised chamber. A systemic and coronary vasculature included an aorta and carotid artery

connected downstream from the ventricle into a mock vasculature. Increased precision was achieved by including carotid artery and coronary circulation and ignoring venous return. Resistance was simulated with a pressure vessel to contracting a latex tube and restrict flow using the same pulse as the ventricle, resulting in coronary resistance being elevated during systole and reduced resistance during diastole producing a biphasic waveform developing most of the flow during diastole.

Table 5: Values for MCL study (Litwak, Koenig et al. 2005)

An MCL was constructed for testing continuous-flow left ventricular devices and can be seen in Figure 8, constructed by Liu, Allaire et al. (2005). Ellipsoid silicon diaphragm was used to simulate the ventricles in pressurised chambers receiving pulses of air for systolic pressure and light negative pressure for diastolic pressure. One-way valves were used to ensure one-directional flow. Each component in the loop was connected by clear tubing, the ventricular assisting device to the loop through the top of the ventricle tank. Several conditions were tested, which include healthy sleeping, partially recovered congestive heart failure, congestive heart failure, resting, healthy exercise and healthy resting. Table 6 illustrates the flow and pressure values used for the conditions. The loop was suitable for testing the left ventricular devices under multiple conditions. The inability to mimic the Frank-Starling response makes the system unable to predict the left ventricle device's performance during the transition between cardiac conditions and ventricular failure.

Figure 8 : MCL by (Liu, Allaire et al. 2005)

Table 6:Simulation values chosen by(Liu, Allaire et al. 2005)

Timms, Hayne et al. (2005) developed a complete MCL for test ventricular assisting devices. The studies aim was to design and construct a new MCL to reproduce normal and heart failure conditions. The Frank-Starling law seemed to be followed by this rig; however, no ventricular volume measurement was mentioned; therefore, it cannot be confirmed with a quantitative measurement. The loop produced accurate flow and pressure wave in heart failure and normal conditions with various parameters. The study was limited by replacing the heart valve with check valves, the inability to measure ventricular volume change and the small orifice in the flow meter used restricting flow.

Kozarski, Ferrari et al. (2003) designed an MCL using current electrical and hydraulic simulation methods and merged them to develop a cheap, precise system. Electrical signals were converted into a flow on the loop's hydraulic side produced by a flow generator. The studies components were accurate to human resistance and capacitance.

Many of the previously developed MCLS previously developed; however, factors like pulmonary circulation, variable compliance and frank starling law are not included. An MCL that can test a varied range of cardiovascular conditions requires a complex system containing many components, including attachments for various measurement devices for flow volume and pressure, arterial compliance and vascular resistance.

2.4 Blood Flow

Predominantly laminar flow is observed when measuring the human circulatory system at the arterial branches; there is often some more turbulent flow. A healthy adult at rest exhibit a typical blood flow of around 5 L/min; heart failure situations see this drop to 2-3 L/min. Blood flow in an artery is proportional to the pressure differential in the artery and the artery's resistance (R). Blood always flows from the high pressure to the low pressure ($P_1 \; to \; P_2$) flow thought the artery (Q) could be represented by the following:

$$Q = \frac{P_1 - P_2}{R} \tag{3}$$

2.5 Blood Pressures

Blood pressure is highly significant in the development and evaluation of mock circulatory systems and the evaluation of human health. Pulse pressure is the difference between the systole and diastole pressure, usually 120 mmHg and 80 mmHg. Compliance and stroke volume are the primary influencers of pulse pressure. Increasing vascular compliance or decreasing stroke volume will decrease pulse pressure and vice versa. Pulse is slowly dampened in between pulses due to compliance.

The average pressure over one cycle is known as the mean arterial pressure; typically, it is less than the average systole and diastole pressures; this is the result of the pressure wave spending more time in diastole (approx. 60%) than in systole (approx. 40%). Mean

arterial pressure can be determined by multiplying the peripheral resistance and the cardiac output, identifying a direct relationship between these values. Mean pressures can be seen in Figure 9.

Figure 9: Blood pressure volumes and pressures in major vessels

Timms, Hayne et al. (2005) used the following values for the basis of resting conditions when developing a mock circulatory system seen in Table 7.

Table 7: Pressure values used by Timms, Hayne et al. (2005)

"High Blood Pressure or hypertension is an ongoing anomalous increase of the pressure in the arteries which transport blood to the entire body. An adult's blood pressure is calculated by using two numbers. The heart's pulsing pumping action creates the upper systolic pressure (normal is 120 mm. Hg. or lower), and its resting pressure between heartbeats is the lower diastolic pressure (normal is 80 mm. Hg. or lower)". Figure 10 the stages of hypertension determined by the American heart association (AHA 2019).

Figure 10: Hypertensive ranges (AHA 2019)

2.5.1 Pulse wave amplification and reflections

Avolio, Van Bortel et al. (2009). The heart ejects blood into the aorta, circulating it through the whole arterial tree; this ejecting creates flow and pressure within the vessels; this can be identified as the propagation of pulse through the arterial bed. The arterial pulse, measured at a given point of the arterial tree, for instance, the brachial artery, is broken down to systolic and diastolic pressures. The theory of a periodically oscillating wave (pulse wave) is most often ignored when analysing is often ignored when measuring blood pressures.

The pulse wave can be compared to an acoustic wave. From this relation, it can be said that the wave can be amplified and reflected, has a frequency and an amplitude and that these features can be measured in the time domain seen in Figure 11 and as harmonic sinusoidal waves seen in Figure 12.

Figure 11: Time-domain analysis Avolio, Van Bertel et al. (2009)

Figure 12:Frequency domain analysis Avolio, Van Bortel et al. (2009)

The forward flowing pressure wave is reflected at many sites of the arterial tree due to changes in geometry such as calcifications, branches or tapering, or changes in stiffness/elasticity of the artery wall. The recording of forward pressure and the reflected wave combine to create a single pulse wave creating waves shapes; as seen in Figure 13, the brachial pressure wave is a lot more notched and amplified due to the reflections.

Figure 13: Pulse wave amplification Avolio, Van Bortel et al. (2009)

In a study into the importance of wave reflection comparing wave intensity analysis and separation of pressure into forward and backward components by Hughes, Davies et al. (2013), the following equation set was derived. They outline the separation of forward and backward pressure. P_f is the forward pressure, P_b is the backward pressure, Z_c is the characteristic impedance, P is the total pressure, A is the area of the section, U is the velocity, and ρ is the desity of the fluid.

$$P_f = \frac{1}{2}(P + Z_c AU) \tag{4}$$

$$P_b = \frac{1}{2}(P - Z_c AU) \tag{5}$$

$$Z_c = \frac{\rho c}{A} \tag{6}$$

An expansion of these methods can yield equations for arterial branches and area reductions.

2.6 Compliance

Compliance describes a blood vessel's elasticity and its ability to change its volume due to a change in pressure. The following equation expresses this relationship:

$$C = \frac{\text{Change in Volume } (\Delta V)}{\text{Change in Pressure } (\Delta P)} \tag{7}$$

Venous compliance is roughly 24 times more than arterial compliance, which means that veins ability for holding blood is greater than arteries. The distinct shape of the pressure waveform is developed from arterial compliance. As seen in Figure 14, the end-diastolic pressure increases as the vessel's compliance increases.

Figure 14: Effect of ventricular compliance

Donovan (1975) achieved a range of 1 ml/mmHg to 10 ml/mmHg for systemic venous compliance and pulmonary arterial compliance, respectively and varied the compliance by changing the air volume above the above tank fluid. Woodruff, Sharp et al. (1997) developed a mock circulatory system incorporating a more compact compliance chamber. The size was reduced using a set of springs with varying spring constants K relating to different compliances; the equation below illustrates the relationship between compliance and the spring constant for the Woodruff, Sharp et al. (1997) design in Figure 15.

$$K = \frac{A_c^2}{C} \tag{8}$$

K is the spring constant, C is the desired capacitance, and Ac it the piston area. A concave seat was incorporated into this design to allow a range of spring sizes to be fitted. This design was limited because specific spring constants for specific compliance were hard to come by, so exact compliance values were hard to achieve. The process of changing the spring was an arduous, time-consuming task that required a complete shutdown of the whole system.

Figure 15:Spring Compliance Chamber (Woodruff, Sharp et al. 1997)

Garrison, Frangos et al. (1994) designed a mock circulatory loop for haemolysis studies. Because the working fluid was going to be blood, biocompatible material could only be used, and the system would have to be free of air. It was desired that only one unit of blood per study would be used, so the system's volume would have to be kept small. A combination of 200 ml of saline solution and one unit of blood could be used to run two of these loops when the design was finished. One of these loops was the test loop, and one was a control loop. A sealed chamber containing two 70 ml sacs were used as the compliance chamber. The chamber was sized to fit one empty and one full sack inside. The top sack would be pressurised as the bottom sack would fill, keeping the system at a constant pressure. The blood sack would empty as the air sack filled for diastole, and the reverse would occur for systole. The chambers size limited the volume changes; therefore, the compliance was limited. The method was successful in emulating both natural venous and arterial compliance.

Marcus, Korcarz et al. (1994) determined arterial compliance by studying 70 healthy people and comparing the two and three-element Windkessel model. Table 8 is the haemodynamic profile of the studied population.

Table 8: : Haemodynamic profile of population (Marcus, Korcarz et al. 1994)

More recent MCLs like the one developed by Gregory et al. (2009) used diaphragm accumulators to simulate arterial compliance shown in Figure 16. The chambers separate the air and fluid chamber using a thin rubber diaphragm. Changing the initial air pressure (pre-charge) or volume changes the compliance creating a compact pressure vessel capable of high operating pressures allowing for an extensive range of compliances.

Figure 16: Diaphragm accumulator (Gregory et al. 2009)

Arabia and Akutsu (1984) used a spring capacitor seen in Figure 17, much like Woodruff, Sharp et al. (1997), to develop compliance. The author used 10, 4.8, 82.5 and 3.6 ml/mmHg for pulmonary venous, pulmonary arterial, systemic venous and systemic

arterial compliance, respectively. A spring-loaded piston was used in this instance to achieve compliance.

Figure 17: Spring compliance (Arabia and Akutsu 1984)

In a study conducted by Lick, Zwischenberger et al. (2001), compliance was achieved by using a cast polyurethane inflatable segment open to the air so no external pressure would be generated. This system worked much like natural arteries, building pressure and volume in the inflatable segment due to its elasticity. Changing compliance meant changing the inflatable segment. Results of this study were significantly improved using this method.

Dumont, Yperman et al. (2002) developed a new pulsatile bioreactor for tissue engineered aortic heart valve formation. The system used the air variation above a chamber of water to control arterial compliance. Under the assumption that air volume does not change when altering the air pressure, compliance would be generated. The circulatory loop only took into account systemic circulation when developing this method; it is not ideal for the use in a loop that represented the entire circulatory system because of the variable pressure of the entire system when changing compliance. Dumont, Yperman et al. (2002) used values between 0.4 and 1.2 mL/mmHg as their compliance range. The study was limited by the lack of pulmonary circulation and could only produce a small number of conditions.

Papaioannou, Mathioulakis et al. (2002) studied if arterial compliance is a primary variable determining intra-aortic balloon counter pulsation effectiveness. A Windkessel chamber was used as the compliance in this simulation. previously mentioned in determining compliance. The benefit of this is that the compliance could be readily determined by the pressure and volume of air above the water. A range between 1 and 2.6 mL/mmHg for compliance, 80 to 120 bpm for heart rate and aortic pressure between 50 and 110 mmHg during testing. The study determined that intra-aortic balloon counter pulsation is highly influenced by compliance disregarding heart rate and pressure.

Haft, Bull et al. (2003) designed an artificial lung compliance chamber for pulmonary replacement. A mock circulatory loop was constructed to rest this but ignored variable resistance and inertia elements. The right atrium was mimicked using a tank to deliver

a consistent pressure by elevating it above the system cause flow through a compliance chamber to an artificial lung. Figure 18 illustrates the compliance chamber used, a flexible bag encased in an airtight container; compliance is changed by the amount of compressed air entering the box.

Figure 18: Compliance of (Haft, Bull et al. 2003)

able 9 illustrates the values used by Loh and Yu (2004) for compliance. The values used here are reasonably higher than the previous values identified in this literature review. The left ventricle compliance is significantly greater than expected.

able 9: Compliance values from the MCL by Loh and Yu (2004)

As seen previously, many of the studies in the literature use air above water in airtight pressure vessels (Loh and Yu 2004), (Litwak, Koenig et al. 2005), (Haft, Bull et al. 2003), (Avrahami, Rosenfeld et al. 2006), (Athanassiou, Hancock et al. 2005), (Ayre, Lovell et al. 2003), (Andrade, Nicolosi et al. 1999) and (Orime, Takatani et al. 1994) all used these in their mock circulation systems. The loop would have to be shut down to vary the compliance in these cases; nevertheless, they were all effective in producing a wide range of compliance values; this is why they are favoured by so many. Litwak, Koenig et al. (2005) used chambers of 5.6L, 43.6L and 4.9l for the pulmonary, venous, and arterial compliance, respectively. To determine compliance accurately, they modified derived equation 9 to add the water volume to the systems calculation; the equation is a follows:

$$C = \frac{\Delta \mathrm{V_{fluid}}}{\Delta \mathrm{P_{fluid}}} = \frac{\Delta \mathrm{V_{air}}}{\Delta \mathrm{P_{air}}} = \frac{\mathrm{V_{tank}} - A_{tank}.\, h_{fluid}}{\mathrm{P_{fluid}} - \rho.\, \mathrm{g}.\, \mathrm{h_{fluid}}} \quad (9)$$

Where g is the acceleration of gravity, ρ is the density of the working fluid, h_{fluid} is the fluid height, $\mathrm{P_{fluid}}$ is the fluid pressure, A_{tank} is the tank area, $\mathrm{V_{tank}}$ is the tank volume, $\Delta \mathrm{P_{air}}$ is the air pressure and $\mathrm{V_{air}}$ is the volume of air. Fluid pressure would vary between 80 and 120 mmHg for aortic pressure so $\mathrm{P_{fluid}}$ is measured at 100 mmHg. Venous and arterial compliance were chosen to be 2.2 mL/mmHg and 50 mL/mmHg, respectively.

There have been many methods of varying and creating compliance in mock circulatory loops; the most effective method has been the trapped air volumes and Windkessel variations used in the studies mentioned.

2.6.1 Hydraulic Accumulators

As observed in this section on capacitance, most of the systems employ some versions of a hydraulic accumulator. Most hydraulic accumulators are used for one of four applications:

- Dampen shock in pneumatic circuits lines or at the outlet of pulsing pumps.
- Have a backup of pressurised fluid for use in the case of power failure.
- Keep pressure in a cylinder while the system pump is turned off.
- Supplement pulsation of pump flow in pneumatic loops

Accumulators can be described as a hydraulic version of an electrical capacitance accumulating and releasing fluid into the circuit. Estimating the capacitance can be achieved using the capacitance equation and the fundamental gas laws where diastolic and systolic pressures are known.

$$P_{precharge}V_{Precharge} = P_{diastolic}V_{diastolic} = P_{systolic}V_{systolic} \quad (10)$$

There are various types of accumulators used in industry, as seen below:

Figure 19: Accumulator Types

The most common accumulators in industry are Gas-charged, Gas over piston, diaphragm and Bladder accumulators.

2.7 Resistance

The resistance to blood flow has a significant effect on the cardiovascular system. The resistance (R) increases as the arterial and venous radius (r) decreases. The viscosity (η) of the blood and the artery length (L) also influence the resistance. The flowing equation illustrates the relationship between these.

$$R \propto \frac{\eta \mathrm{L}}{\mathrm{r}^4} \quad (11)$$

Most of the resistance is developed in the smaller vessels like the arterioles and the capillaries; significant pressure drops can be observed in these vessels due to their small radius, whereas, in the aorta, little to no pressure drop can be observed. Constriction and dilation of the vessels by the body can change the resistance to flow. Constriction of the vessel allows less blood through increasing resistance, where dilation allows more flow. Systemic vascular resistance (SVR) is the common terminology for the resistance to blood flow in the circulatory system; the blood vessel's diameter greatly determines it. Knowing mean arterial pressure (MAP), and central venous pressure (CVP), the following equation can be used to calculate SVR where CO is cardiac output in L/min:

$$SVR = \frac{MAP - CVP}{CO} \tag{12}$$

CVP can be assumed to be 0 when it is unknown; most of the time, CVP is close to 0. Pinch valve derivations are used in the majority of MCLs developed in the past, either motorised or manually reducing the flow area developing variable resistance; some studies that have used this method are Timms, Hayne et al. (2005), Litwak, Koenig et al. (2005) and Dumont, Yperman et al. (2002).

A unique method of developing variable resistance was developed by Donovan (1975), seen in Figure 20 for there MCL. A plate attached to a pivot occluded the tube blocking flow and building resistance. The plate angle determined the resistance—the lever was attached to bellows sitting inside a pressure vessel containing water. The bellows would contract when the pulmonary pressure was increased, varying the resistance through the described methods.

Trittenwein, Zamberger et al. (1998) developed a mock circulatory loop employing variable and constant resistances. The former uses an inflatable cuff encompassing a flexible section of tubing to control the tube's constriction, the latter employing a pinch valve. A 3/8” proportional control valve was used in a mock circulatory system developed by Gregory (2009), illustrated in Figure 21. The valve was supplied voltage which raised of lowered a gate occluding the flow area, throttling flow. The valve was chosen to simulate heart failure and healthy heart function.

Figure 20:Bellows operated valve

Figure 21: Proportional control valve

The method Scotten, Walker et al. (1979) designed can be seen in Figure 22, consisting of flexible small tubes flattened by a plate. The flatted the tubes, the higher the resistance.

Figure 22: Resistance used by (Scotten, Walker et al. 1979)

The author developed the flowing two-equations for change in pressure and Resistance, respectively, where L_R is the resistor tube length, μ denoted the viscosity of the working fluid, Q is the volume flow rate, and ΔP is the pressure differential.

$$\Delta P = R \,.\, Q \tag{13}$$

$$R = \frac{8 \,.\, \mu . L_R . \pi}{A_r^2} \tag{14}$$

Pantalos, Koenig et al. (2004) used various densities of open-cell foam in a chamber for peripheral resistance. Sealed pistons compressed the foam to achieve desired resistance. The values for resistance in the study can be seen in Table 10.

Table 10: Resistance by (Pantalos, Koenig et al. 2004)

Patel, Allaire et al. (2003) achieve resistance used a 1.5-inch gate valve. Resistances of 1.2 - 1.4 mmHg.s/mL and 0.85 mmHg.s/mL were chosen for heart failure and healthy respectively. The system was accurate in mimicking pressure drops in the MCL to test left ventricular assisting devices.

2.8 Phantom Fabrication

The scope of the project was to develop an MCL using synthetic arteries. The following section delves into the potential methods and materials to accomplish this.

2.8.1 Lost core casting

The most common synthetic artery creation method is lost core casting. This method involves a sacrificial male component to create the arteries' inner diameter, two female

moulds for the outer diameter, and a choice of silicon mimicking the required properties. These moulds are created mainly by 3D printing or milling; the most beneficial use for this method is for complex shapes that cannot be achieved via other methods.

2.8.1.1 Male mould fabrication

The male mould must be dimensionally accurate as well as easily removable the following section discusses previous fabrication methods and materials used to achieve this. Yazdi, Geoghegan et al. (2018) reviewed arterial phantom fabrication using lost core casting methods for use in flow measurement using PIV techniques. For the male mould construction, 3D printing methods were employed using a filament 3D printer using PVA as the working material to print. PVA is a water-soluble 3D printing material that would allow the work to be easily removed from the mould.

Geoghegan, Buchmann et al. (2012) investigated chocolate, gelatine and wax for male casting materials. The three working material were capable of being fabricated with precise detail; however, they were vulnerable to shrinking.

Smith, Rutt et al. (1999) and Hoi, Woodward et al. (2006) investigated Cerro alloy, which is an alloy with a low melting point, and like chocolate wax and gelatine could be easily removed with some heating, it was found that the material left residue when removed and proved difficult to remove the excess in intricate geometries

In the development of silicon phantoms, Doutel, Carneiro et al. (2015) used both sucrose and wax as the male mould. The wax was heated to 80 °C for removal, where the sucrose could be removed with water, and it is water-soluble. Using X-ray spectroscopy and scanning electron microscopy, they determined the surface's chemical composition discrepancies and any contaminants on the surface. They determined that the surface finish was better for sucrose.

It was suggested by Huetter, Geoghegan et al. (2015) that abs plastic was more structurally sound when compared to the types of materials previously mentioned. Surface smoothing of the print can be achieved by applying acetone to the print. Acetone could again be used after casting to breakdown the ABS and remove them from the phantom. This method was used by Aplin, Geoghegan et al. (2016), Huetter, Geoghegan et al. (2015) and Munro, Becker et al. (2015). Aplin, Geoghegan et al. (2016)

noted that yellowing occurred when soaking the phantom submerged in acetone, effecting its optical properties. A solution was found by using after seven days to ensure complete curing.

2.8.1.2 Female mould fabrication

The female mould determines the external geometry of the phantom. The mould can be generated on software such as SOLIDWORKS and manufactures using subtractive or additive fabrication methods. The male mould must be precisely located in the female. Once silicon is poured and cured, the male and female moulds are removed, producing a phantom.

Geoghegan, Buchmann et al. (2012) fabricated a female mould with a CNC machine cutting aluminium plate to and ABS for the male mould as mentioned previously. The material was cast from the bottom to prevent bubbles, and once cured, the phantom was examined for dimensional accuracy. The error in the area was recorded as 3 to 5%, which is minimal. Cao, Duhamel et al. (2013) 3D printed both male and female moulds and was determined to be accurate within 7%

Meyer, Bertrand et al. (2011) and Deplano, Knapp et al. (2007) CNC milled aluminium for the female mould. Blown glass was used for the male, and destruction of the interior was used to remove the male. Brunette, Mongrain et al. (2004) used CNC to cut five aluminium female moulds to generate a multi-layered coronary phantom. The studying employed different materials for the different layer properties of the artery. After casting, the first and second layers were measured using ultrasound for dimensional accuracy. The intima (second layer) was measured to be 0.64 ± 0.16 mm along the length of the phantom and the first layer thickness of 0.41 ± 0.08 mm.

2.8.2 Lathe moulding

Lathe moulding is a female less moulding method for creating arterial phantoms with multiple layers involving the successive application of different materials to represent the layers of the human system (Bisaillon, Dufour et al. 2011).

Figure 23 demonstrates the system involving extruding the material onto a specific diameter rail for the inner diameter at a specified rate for the desired thickness and length of the artery that is trying to be replicated. This method is ideal for straight arteries.

Figure 23: Lathe moulding

2.8.3 Rotational moulding

Rotational moulding involves the pouring of silicon into a mould rotated on a multi-axial machine to evenly distribute the material as it sets. Of the methods mentioned, rotational moulding it the most difficult to successfully accomplish for various complex shapes requiring different axial speeds for different shapes and materials.

2.8.4 Mould dipping

Mould dipping is an easy method of creating synthetic arteries. The process involves dipping the male specimen many times, allowing it to cure each time to ensure complete coverage. This method is harder to control the wall thickness because it does not use a female mould. Yip, Mongrain et al. (2011) determined that wall thickness variations significantly affect how the phantom behaves. Dip spin uses the rotational force similar to lathe moulding, where the specimen is dipped then spun to uniform wall thickness. Arcaute and Wicker (2008) devised a dip spinning technique to produce elastic phantoms of complex arteries, such as a bypass graft, ascending and descending aorta and the aortic arch. The mould was spun with a machine with two-axis much like rotational moulding but using a male instead of the female phantom. The results showed that wall thickness was harder to control on smaller specimens. Dipping required a vast amount of silicon, and the estimated wasted silicon is around 80%; therefore, it is not very cost-efficient.

2.8.5 Materials

Ionita, Mokin et al. (2014) 3D printed a phantom using an elastic material known as Tango +, various complex flexible geometries were grated using this material. The shape accuracy was within $120\mu m$ indicating little shrinkage or expansion of material upon cooling; this study did not report the material's elastic modulus but is reported in a study by Dalaq, Abueidda et al. (2016). They found that through a compression test, the elastic modulus 340 kPa under their test parameters. Biglino, Verschueren et al. (2013) studied the viability of using a poly jet printer and the Tiger + material to simulate arterial function and properties and observed that it was a suitable replacement for testing purposes.

A polyvinyl alcohol cryogel was Qian, Niu et al. (2014) to mould phantom arteries in a study to determine the effect of blood vessel stiffness on flow dynamics. The material's varying stiffness was achieved by repeatedly freezing and thawing the sample. Twelve hours of thawing and 12 hours of freezing were used as one cycle length; the results of this testing can be observed in Figure 24. The study successfully produced a range of arterial stiffness from 60.9 to 310.3 kPa.

Figure 24: The effect of repeatedly freezing cryo-gel on elastic modulus (Qian, Niu et al. 2014)

Fuard, Tzvetkova-Chevolleau et al. (2008), in a study into the "Optimisation of poly-di-methyl-siloxane (PDMS) substrates for studying cellular adhesion", the elastic modulus of PDMS solutions were analysed regarding baking time and percentage of the cross-linking solution in each batch. The results of this study are illustrated in Figure 25. We can observe that the material is well within the ranges required of a phantom, depending on the material's dilution and baking time.

Figure 25: Young's modulus as a function of the baking time at 100 °C for (a) 3%, (b) 5% and (c) 10% of the cross-linker concentration in the PDMS solution. (Fuard, Tzvetkova-Chevolleau et al. 2008)

In a study using silicone materials to simulate tissue biomechanics related to deep tissue injury, Sparks, Vavalle et al. (2015), three materials were tested for their viability. The three-material tested were from smoothon's range of material Dragon skin, Eco flex 0030 and Eco flex 0010. Compression tests on each material can be seen in Figure 26. From the stress and strain curve, we can identify the elastic moduli of the three materials, 230 kPa, 100 kPa and 50 kPa for Eco flex 0030 and Eco flex 0010, respectively.

Figure 26: Stress and Strain of three materials (Sparks, Vavalle et al. 2015)

2.8.6 Artery dimensions

Suppose phantoms of the human arterial system are to represent accurately. In that case, we must study the arteries' dimensions and properties to produce something of similar size and function. The aorta is one of the most commonly simulated arteries. Figure 27 demonstrates the variation of arteries from the body to body; in the case of the aorta, it can vary greatly.

Figure 27: Aortic dimensions (Chee, Yiu et al. 2018)

The arterial system branches into many vessels from the aorta through the human body of varying size and shape. Table 11 illustrates the lengths and diameters of the vessels vary greatly. There are branches and bifurcations in each artery that affect blood flow in the body, such as reflections and pressure variations (Hench and Jones 2005).

Table 11: Artery dimensions (Ghasemalizadeh, Mirzaee et al. 2014)

2.8.7 Mechanical Properties of Arteries

The arteries' mechanical properties are essential to achieve similar damping properties seen in the human body and be strong enough to handle the required pressures for testing. Figure 28 and Table 12 illustrate the range of elastic moduli in the artery from person to person and with age variation. A range between 160 kPa and 390 kPa was established using ultrafast echography ultrasound imaging.

Table 12: Measured PMV and Elastic moduli during systole (Messas, Pernot et al. 2013)

Figure 28: Elastic modulus measure during diastole (Messas, Pernot et al. 2013)

In a Non-invasive Assessment of Elastic Modulus of Arterial Constructs during Cell Culture using Ultrasound Elasticity Imaging by Dutta, Lee et al. (2013). The samples were isolated from common carotid arteries of 3-year-old male baboons for ultrasound imaging. Comparisons between a UEI estimate were taken, the results of which can be seen in *Figure 29*. A range between 130 kPa and 200 kPa was established across 21 days of specimen cultures.

Figure 29:Elastic modulus comparison between UEI estimate and Pressure diameter tests (Dutta, Lee et al. 2013)

(Sokolis, Lampropoulos et al. 2010) established a range between 200 and 300 kPa for aortic stiffness in a study on the effect of aortic stiffness and heart disease. Many other studies follow these lines, but it is hard to pinpoint the specific elasticity for every artery in the human body; our best estimate is to work within a range established in previous studies.

2.9 Conclusions

This literature review aimed to identify potential improvement areas in mock circulatory loops design. Current MCLs may consist of simple continuous flow devices or more intricate representations of atria, ventricles, and arteries.

The five-element mock circulation loops seem to be the most accurate; however, decidedly the most complex for our applications; the two or three-element loops may be less accurate but are a lot simpler with less room for era whilst still being able to achieve relatively accurate results as well as being simple in design.

It is important that vascular resistance in mechanical simulation is represented accurately to build pressure. Arterial compliance is also an essential part of the human arterial system to produce the gradual release of pressure we see in the literature; most of these devices use a pressure vessel to achieve this phenomenon. Some previous loops achieved accurate representation of ventricle shapes; however, these systems required many resources to develop this system accurately. None of the studies identified has developed a full phantom arterial tree. This feature would be useful in developing the pulse wave amplification effect due to the artery's geometry and the mechanical properties of the arterial wall.

This literature review identifies the components required to develop a complete mock circulatory loop. The culmination of information in this report will allow the construction of an accurate representation of the human circulator system to test a new blood pressure measurement device.

3 Design and development of a phantom arterial system

3.1 Aims

This section aims to dictate the process to develop a basic synthetic representation of the arterial system. The system should produce dimensionally accurate arteries and assume similar properties to those seen in the literature. To achieve this, various tests were undertaken on different materials and moulding methods to achieve a process that successfully meets these requirements.

3.2 Refining and employing methods of phantom fabrication

This section describes the processes undertaken to develop and refine moulding methods and select appropriate materials for use as phantom arteries.

3.2.1 Materials

From the culmination of literature on arterial stiffness, it was concluded that a good working range would be a material that exhibits an elastic modulus of between 150 and 250 kPa. After determining these materials were selected to conduct our testing into their mechanical properties to determine suitability in the moulding of phantoms.

The materials were selected from the literature. Three potential materials were identified, Smooth on dragon skin 10, Smooth on Eco flex 50, and Barnes Platsil 00. The study by Sparks, Vavalle et al. (2015) Identified dragon skin having a desirable elastic modulus for our purpose approximately 230 kPa; the same study identified Eco flex 0030 as having an elastic modulus of approximately 100 kPa knowing that the 0040 and 0050 range of Eco flex to stiffer than the 0030 the Eco flex 0050 material was also selected to see if the elastic modulus was within the desired range. Platsil 00 was also tested as it was the most readily available material when this study was undertaken and has also been used in the phantom development of other human body parts such as the arm.

The material was tested using the TA.XT plus texture analyser and Exponent software version 6.1.4.0 from Stable Micro Systems and the ISO 37 standard for tensile testing of rubber. Background information on the material tested was obtained to gauge the potential silicon rubber to test and eventually mould into arteries. The following is a description of the methods used in identifying such a material.

3.2.1.1 Ring Testing

The following values outline the dimensions used in the materials testing in relating to the equations provided in ISO 37 Rubber, vulcanised or thermoplastic - determination of tensile stress-strain properties and about Figure 30.

$$d_1 = 26mm \quad d_2 = 32mm$$

$$L = 40mm \quad A = B = 8mm$$

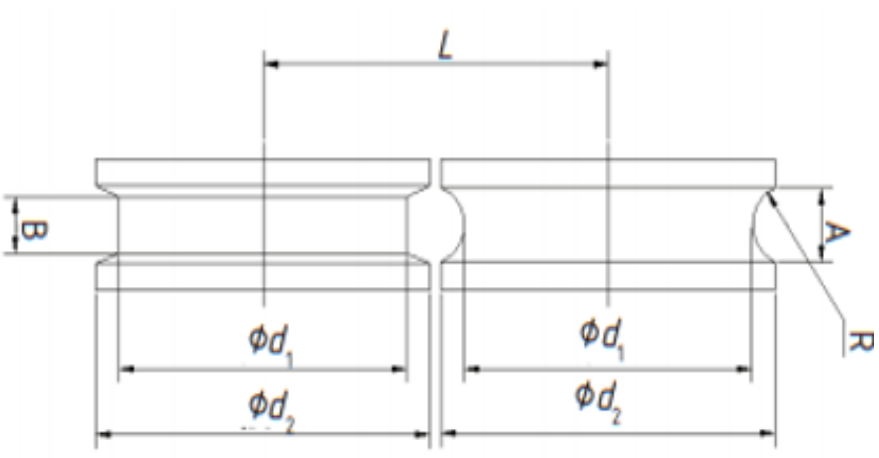

Figure 30:Pully arrangement for tensile testing ISO_37 (2017)

Before conducting the tests, the machine was calibrated as per the user guide. A 730g weight was placed on top of the calibration platform, and the weight measurement was set. Then it was rechecked in the check calibration menu to confirm the settings.

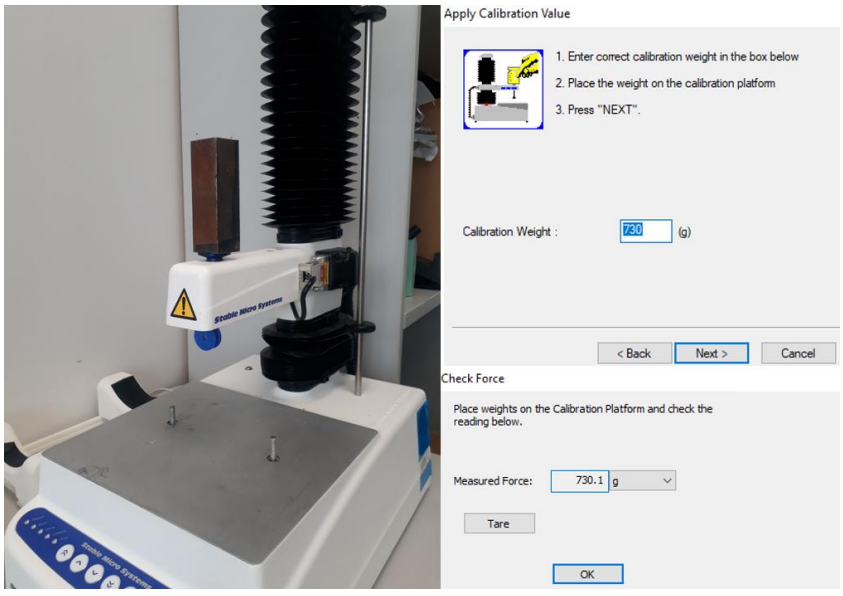

Figure 31: Calibration of a texture analyser

The test was conducted with three samples of each material; as seen in Figure 32, each sample was tested four times and averages were taken to determine the elastic modulus. All samples were cast on the same pour for consistent results.

Figure 32: Dragon skin ring test samples

Figure 33 demonstrates the arrangement of the pullies and the ring within the texture analyser recommended by ISO 37 and used in this instance to test the three mentioned materials.

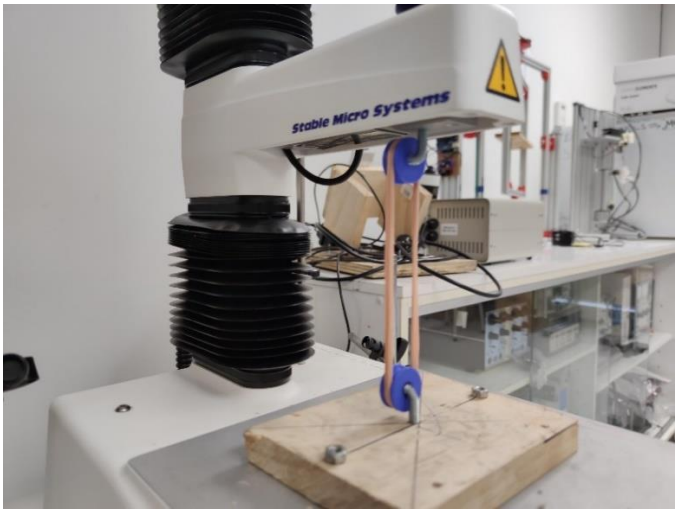

Figure 33: Texture analyser, ring and pully set up.

3.2.1.2 Ring Test Results and Discussion Comparing silicon

The following graphs are the ring test results outlined in the previous section measured on the exponent program. The Ecoflex 50 illustrates the potential differences from sample to sample as each sample peaked at three distinct different points enforcing the decision to test multiple samples multiple times. The graphs illustrate twelve total tests, four tests on each sample.

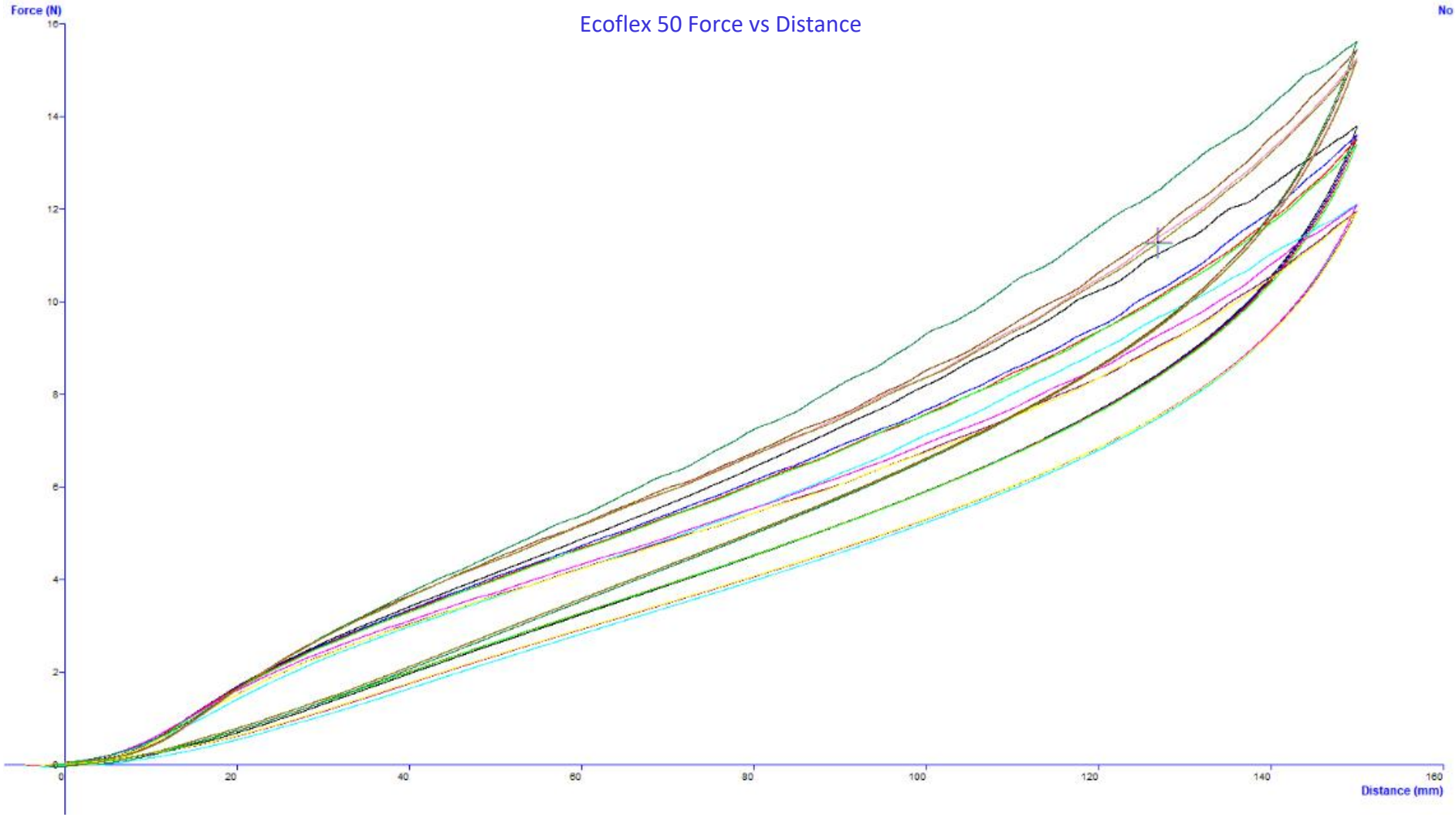

Figure 34: Tensile ring test Ecoflex 50

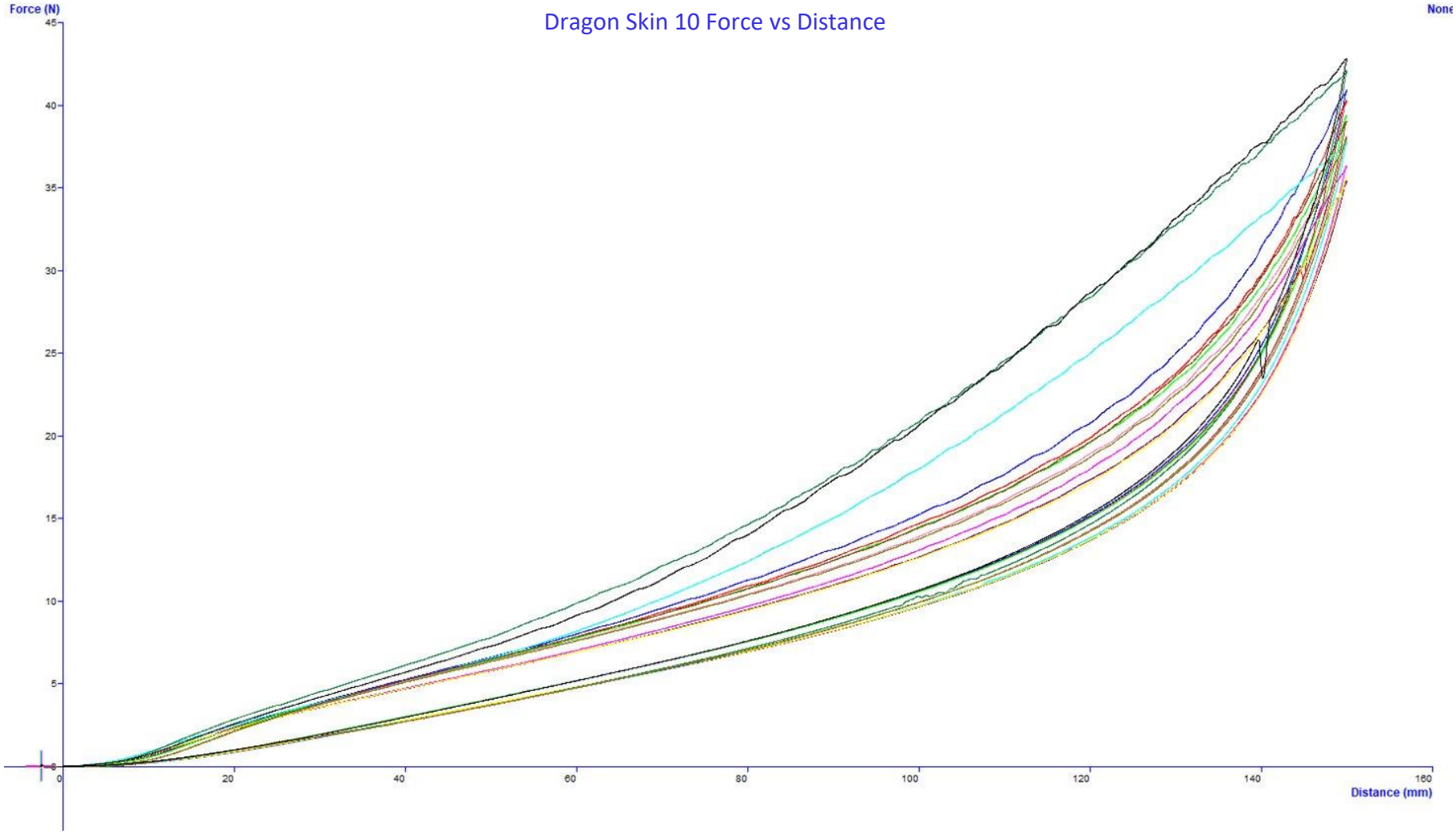

Figure 35: Tensile ring test Dragon Skin 10

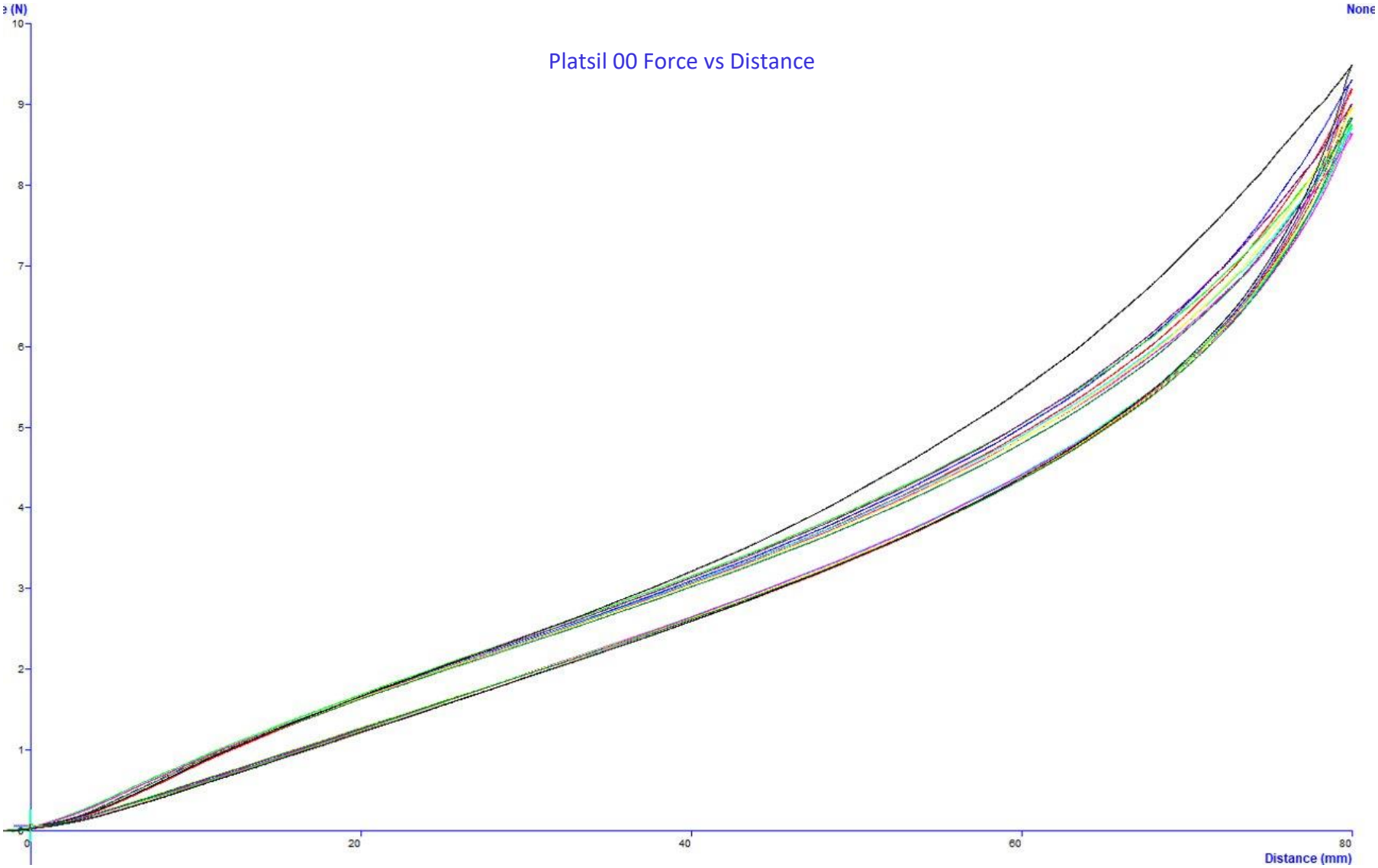

Figure 36: Ring test Platsil 00

Figure 37 illustrates the most considerable test discrepancy observed. The orange line indicates the difference in slope magnitude for the dragon skin samples between test 1, 2 and 3 for each sample. It is believed that this is due to the sample plastically deforming slightly from test to test because of the reasonably large strain range tested. It can also be observed that there is little to no variation between the third and fourth test in each sample. This indicates that the material may have been permanently deformed, decreasing the slope of the then levelling out to accommodate the constantly reproduced strain of the tensile testing.

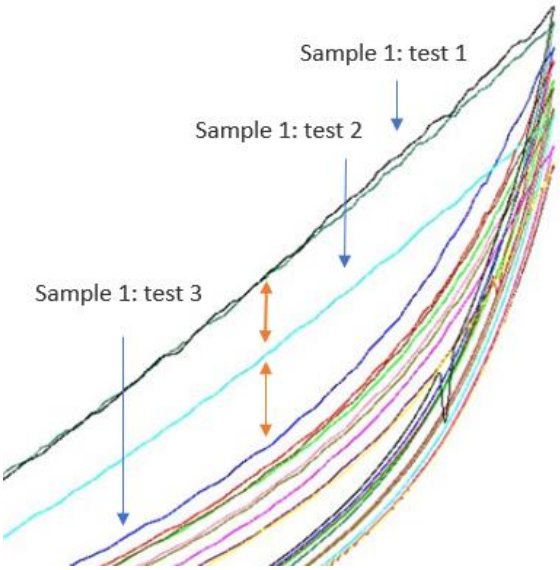

Figure 37: Slope variation in dragon skin

It can also be observed from the graphs, especially in the dragon skin's stiffer material, the plotted line begins to trend upwards from a linear trend to an exponential trend after a given point. We can assume that the material has deformed hyperelastically at these points, and measurement should be taken from the linear portion as they are more realistic to our working range. Materials' average elastic modulus can be determined using the formulas outlined in the ISO 37 handbook from the graphs. Starting by calculating tensile stress at yield, δ_y, expressed in megapascals, using the equation where F_y is the force at yield:

$$\delta_y = \frac{F_y}{2Wt} = \frac{37}{2 * 6 * 6} = 0.51\ MPa$$

Calculate the elongation at yield ε_y, expressed as a percentage where L_y is the distance between the pullies at yield and C_i is the circumference of the ring:

$$\varepsilon_y = \frac{100(\pi d_1 + 2L_y - C_i)}{C_m} = \frac{100(\pi * 27 + 2 * 175 - \pi * 44)}{\pi * 44} = 210\%$$

Calculate the elastic modulus E of the material as a function of δ_y and ε_y:

$$E = \frac{\delta_y}{\varepsilon_y} = \frac{0.51}{2.1} = 0.24 \text{ MPa}$$

Subsequent testing was conducted on Smooth on Eco flex 50 and Barnes platsil 00 yielding an elastic modulus of 0.088 MPa and 0.077 MPa, respectively, using the testing method above. Using the exponent plots seen in Figure 34, Figure 35 and Figure 36, a plot was generated by exporting the data from the exponent into a MATLAB array and repeating the method mentioned above of determining stress and strain at even intervals. The results were taken between 0 and 80mm to work with the plastic range. The results of the and stress/strain curves developed in MATLAB can be seen in Figure 38.

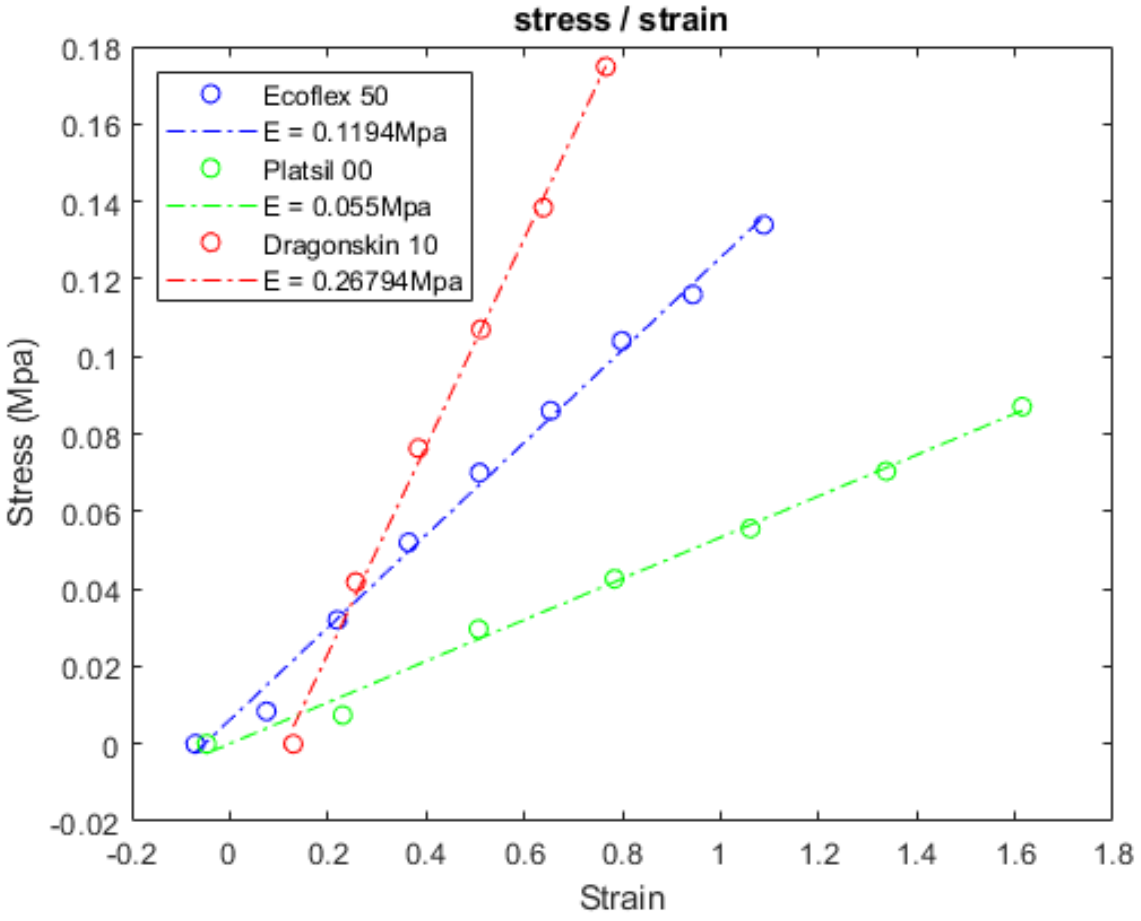

Figure 38: Stress and strain curve

The stress and strain curve provides a more accurate and averaged prediction of the material's elastic modulus by determining the line's slope. In this case, the Elastic moduli were 0.119 MPa, 0.055 MPa and 0.267 MPa for Eco flex 50, Plastic 00 and Dragonskin 10, respectively. From the plot, we can observe that the tests were well within the elastic range as each line follows a linear trend. Given these values, the process of moulding synthetic arteries proceeded using the smooth on dragon skin 10 material as its elastic modulus was closest to what we desired an elastic modulus of 0.25 MPa to properly emulate the damping of the arterial system and sustain the required pressures. Although determined to be higher than needed, the alternative, for example, using platsil 00, would yield worse results when incorporating them into the MCL as a pressure test determined as shown below where the artery has expanded exploded before reaching 80 mmHg. Another potential factor in the tearing of the arteries was determined to be the thickness of the arterial wall. It was decided to conduct further tests on the relation between the thickness of the sample and the material's elastic modulus as the arteries' thickness varies throughout the circulatory system.

Figure 39: Pressure tested platsil 00 artery

3.2.1.3 Ring testing discussion comparing elastic modulus and wall thickness.

This section discusses the results of conducting a ring test on the Dragonskin 10 silicon selected from the previous section, comparing different materials. The test was conducted using a sample with a width and thickness to the ring of 3 mm, 6 mm and 12 mm, where the internal diameter remained the same at 44 mm for each ring. These samples can be seen in Figure 40 to determine whether material thickness affects the material's elastic modulus.

Figure 40: Variable sized rings

These tests were conducted using the methods previously mentioned in the section on Ring Testing above, testing each sample 3 times to ensure the results are consistent. The test was also conducted at a lower strain range than the previous ones. We found that the previous range was much greater than the working strains and minimised hyper-elastic deformations in the material, affecting the measurement. The results of this test can be seen in Figure 41.

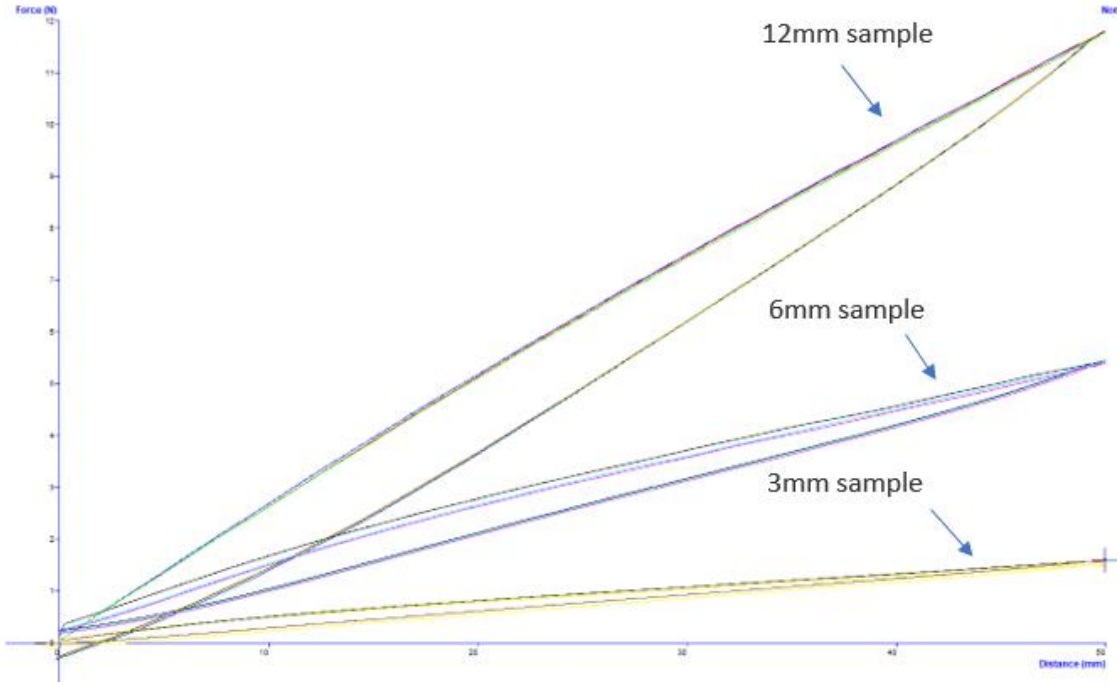

Figure 41: Variable thickness ring test

It was be observed from Figure 41 the effect of reducing the strain range at which the material was tested. There was little to no different from test to test validating our previous assumption that the excessive strain on the material was the cause of the discrepancy. The exponent software plots also output a more linear relationship than those observed in Figure 35 again; this is likely the result of reducing the strain range. Not much more can be observed from this plot, so the data was exported to MATLAB, where Figure 42 was created plotting stress and strain of the 3 sample sizes. The slope of which can be determined to Identify the material's elastic modulus.

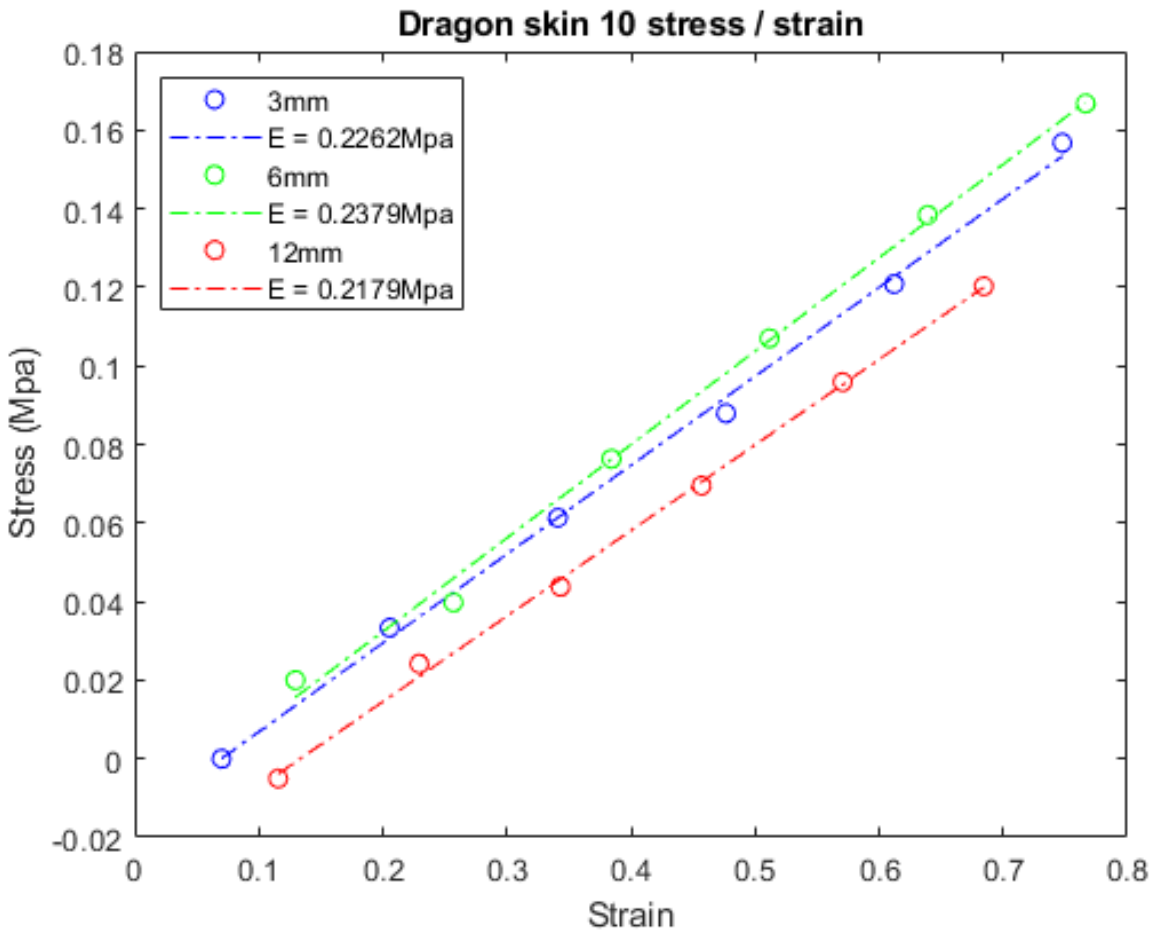

Figure 42: Stress-strain curve comparing sample sizes.

By observing the results in Figure 42, it was observed that the silicon elastic modulus is reasonably consistent across each thickness of the material lying within 10% of each other, which is not significant for our application because arterial stiffness may differ slightly from person to person. These results also confirm that the material is suitable for simulating arteries as it comes within the range of arterial stiffness found in literature, those being a range between 150 kPa and 250 kPa. Unfortunately, the manufacturer does not specify the elastic moduli of the material; however, our results are consistent with compression tests conducted by Sparks, Vavalle et al. (2015), where the elastic modulus was determined to be 230 kPa with a maximum variance of 5% between our test and the literature. We can determine that our test were reasonably sound, and once the material properties were determined suitable, we proceeded to the development of fabrication methods in the following section.

3.2.2 Fabrication

The three methods mentioned in the literature review, lathe moulding, lost core casting and rotational moulding, were tested to identify the best method to proceed with the moulding procedure. A comparison between the lost core casting and rotational mould was conducted for complex arteries. A comparison between all three methods for the straight portions of the arterial system's benefits was recorded in the following selection matrix to determine the best method for each. The matrix uses a scale of +, 0 and – rated in reference to the datum method; in this case, lost core casting is the datum where + is better – is worse and 0 is the same. Shape and thickness accuracy was the most important aspects of the arteries' moulding; as mentioned in the literature, the shape and thickness greatly influence how the phantoms perform more, especially related to thickness as edemas form under loading. The second most important aspect was the simplicity of the moulding method. The more complex the method, the more room for error, potentially creating waste and inaccuracies. Lastly, we must ensure that the bubbles are minimized in the moulding process as they may affect the arterial wall's performance and material properties. This was rated lowest because a vacuum chamber can be used for each method to bridge the gap in how they perform.

Criteria	Weight	Method		
		lost core casting (Datum)	Lathe moulding	Rotational moulding
Shape accuracy	30%	0	0	0
Thickness accuracy	30%	0	0	-
Simplicity	25%	0	-	-
Bubbles	15%	0	+	+
Sum +		0	1	1
Sum -		0	2	2
Sum 0		4	1	1
Net score		0	-1	--1
Weighted score		0	-10	-40
Rank		1	2	2
Continue?		Yes	No	No

Table 13:Selection Matrix for moulding methods

Table 13 above illustrated the superiority of the lost core casting for this project's purposes and was ultimately the method used to mould the circulatory system. The selection was made from what was observed in the literature test were conducted on each method to validate our choice and confirm the best method. The following sections briefly describe the testing done on these methods and the issues that arose with each.

3.2.2.1 Rotational moulding

Figure 43 illustrates the rotational moulding machine and the moulds used to test this method. The rotational moulding machine rotates on two axes being able to control the speed of the axis independently to adjust for the mould's shape and material used. The mould used was a 3D printed from designs developed on SOLIDWORKS 2018 modelling software to accurately represent the artery's anatomical shape; the one below illustrates the aortic arch.

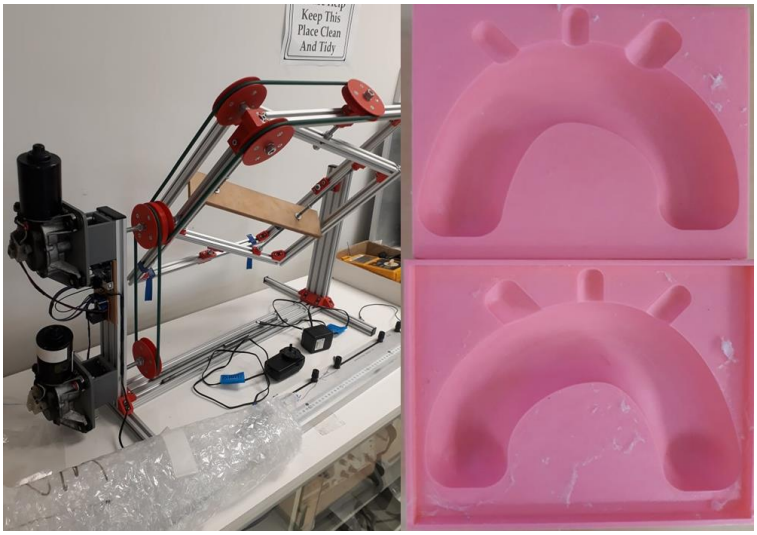

Figure 43: Rotational moulding machine with mould

Testing this method included calculating the required volume of silicon for a given wall thickness before adding the silicon to the mould sealing and inserting it into the rotational moulding device and running till cured. Various axial speeds were tested to get an accurate and consistent spread of material throughout the mould and create the required wall thickness. Despite these efforts, the results were consistently poor when achieving the required wall thickness, as shown in Figure 44.

Figure 44: Rotationally moulded aortic arch

Also, in Figure 49, the absence of large bubbles and smooth surface in this method is the main advantage of the method of moulding. But the large clumps that can be observed were consistent with each test. Many trial and error repetitions adjusting the axial speed would require each shape to achieve a good result.

3.2.2.2 Lathe moulding

Lathe moulding performed very well for medium diameter medium to large diameter arteries 8 mm and above, shown in Figure 45. The process produced smooths even walled arteries at the range mentioned. One of the flaws in this process is the limited amount of material used at one time. The system used only a 10ml syringe that limited the length of the artery that can be produced depending on the artery's required thickness and diameter. Testing the extruder on the aorta of an inner diameter of 23 mm and a thickness of 3 mm, the lathe only produced a specimen of only 40 mm of the required 400 mm. It determined that it is unsuitable for arteries this size either.

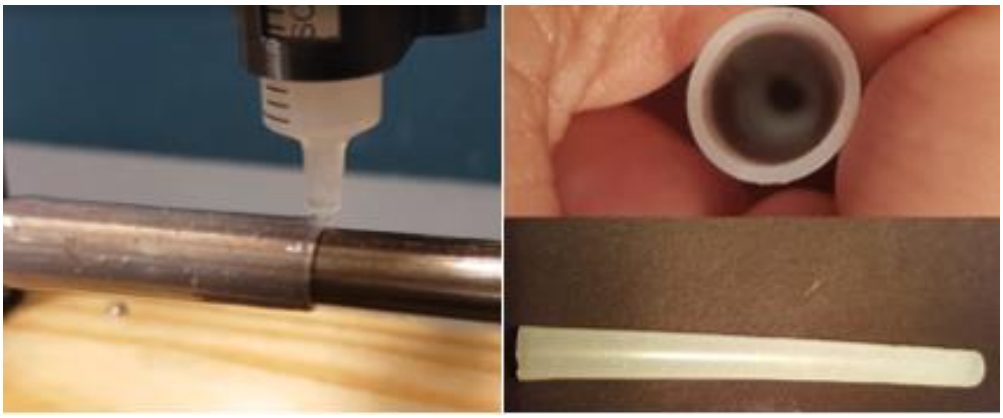

Figure 45: 10 mm artery extrusion

For the small diameters below 8 mm and smaller thicknesses below 0.75 mm, the wall thickness tends to become more and more uneven, which can be seen in Figure 46. The uneven thickness causes edemas to form when pressurised at the thinner sections making them more likely to burst, making it unsuitable for arteries this size either. Overall, the artery size worth producing on this are pretty limited, making it less suitable for arterial production than other methods.

Figure 46: Uneven walled artery

3.2.2.3 Lost core casting

Lost core casting was produced using a 3D printed mould shown in Figure 47; complex moulds such as this aortic arch, such moulds were designed to be reusable; as we see here, the yellow branches can detach and reattach for future use. The inner and outer olds were designed to match a given artery's inner and outer diameter.

Figure 47: 3D printed aortic arch mould.

The material was mixed and added to each half of the mould, and the core was placed inside and clamped together to cure. Figure 48 illustrates the shape and thickness accuracy produced using this method. The arteries' thickness was consistent throughout this initial test for both the aorta and its branches.

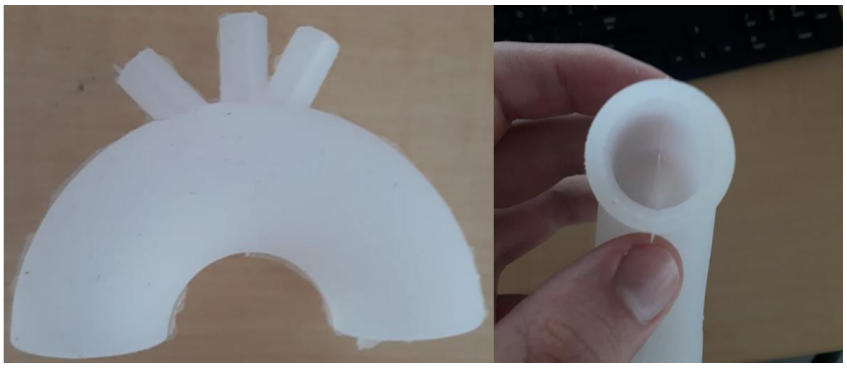

Figure 48: Lost core cast silicon aortic arch

Similarly, smaller arteries were tested and produced arteries of consistent thickness and shape. The main issues with this method were flashing, as shown in Figure 49, and large bubbles are seen in Figure 50. Despite this, this moulding method was the most consistent and straightforward and was chosen to complete the moulding of the arterial system. The flaws mentioned were refined in the following section.

Figure 49: Artery Flashing from casting

Figure 50: Large bubbles from casting

3.2.3 Refining methods

As mentioned in the previous section, the main issues that arose from our lost core casting methods were forming large bubbles, as seen in Figure 50 and flashing seen in Figure 49. This section will outline the tests undertaken to refine the lost core casting methods to minimize these issues.

3.2.3.1 Large and small bubbles

From our initial assessment of the different moulding processes, it was observed that there were tiny bubbles apparent in the silicon phantom after casting. Although the manufacturer states that the material does not need to be vacuumed, the observed tiny bubbles could affect the phantom wall's mechanical properties as studied in the literature, so further processing was needed to remove the remnants. The most obvious choice was using a vacuum chamber to force the bubbles to the surface of the pre-cured material, where they are expelled pre-pour. The result of this proved promising and can be observed in Figure 50. Vacuuming was effective in removing tiny bubbles, but the large bubble was not affected by this method, and refinement of the pouring and curing process was required to eliminate these.

Figure 51: Vacuum chamber

For the large bubbles, three methods were employed. The first method tested was the injection of the material from the bottom of the mould, similar to the method mentioned by (Yazdi, Geoghegan et al. 2018). This process did yield some results decreasing the bubbles formed. Still, it was inconsistent in the absolute elimination of them, as half of the time, large bubbles would occur just smaller than previously.

It was observed that the bubbles would usually form at the top of the phantom whichever way the phantom was orientated during curing; for example, in Figure 52, if the mould were orientated in the way shown, the bubbles would form on the top. This is expected as the bubbles would naturally rise to the surface but could not escape during curing.

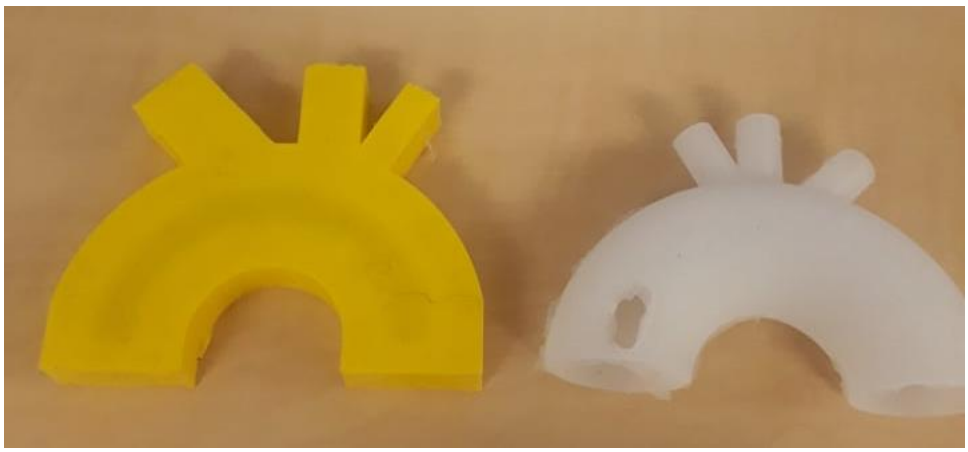

Figure 52: Cured this way up.

This was easily fixed for the straighter sections as they could be orientated, shown in Figure 53, so the bubbles would form on the ends of the phantom and easily be removed by cutting the small, effected section top with a craft knife or scissors. This method was implemented for all the straight arteries moving forward and yields positive results 90% of the time. The minor shortening of the artery would not significantly affect the reflections much as the arterial length is affected by limb length from person to person; there is a significant variation.

Figure 53: Vertical curing of phantom

The last method tested was mainly for the more complex shapes like the aortic arch and branching sections in the arms and legs. Because the bubble primarily formed in the top, as previously mentioned, the complex phantoms were cast by halves, as seen in Figure 54. in doing this, the curing area was always at the bottom, and large bubbles were a lot less likely to form. This method was very successful in the elimination of large bubbles. However, it doubled the moulding time for each complex phantom from 70 mins to 140 mins. The first half must cure before adding the second, eliminating bubbles the extra time as it made up for the potential remoulding time of defective phantoms and wasted material. This method was also carried over to develop the final phantom circulatory system.

Figure 54: Cure one side at a time

3.2.3.2 Flashing

Flashing occurred due to a slight over-pouring of injecting of material into the mould; the material would seep slightly to the female's outer edges. Flashing was quickly and tidily removed using a craft knife without damning the phantom or changing the atrial wall geometry. A before and after of this can be seen in Figure 55.

Figure 55:Before and after flashing removal

3.2.4 Creation of complex shapes

This section will discuss the methods used to design and construct mould and phantoms of complex geometries. It will describe the arteries, shapes and dimensions chosen for the reproduction of a simple arterial tree and the effectiveness of the process.

3.2.4.1 Simplifying the geometry of the arterial tree

The arterial tree is a complex thing; it branches many times throughout the body, becoming smaller and smaller the further downstream it becomes. For our purposes, it was decided that only the larger arteries should be included, excluding those at the ends of the extremities, like those in the hands and feet, also those that branch into the organs. Figure 56 illustrates the arteries chosen for reproduction.

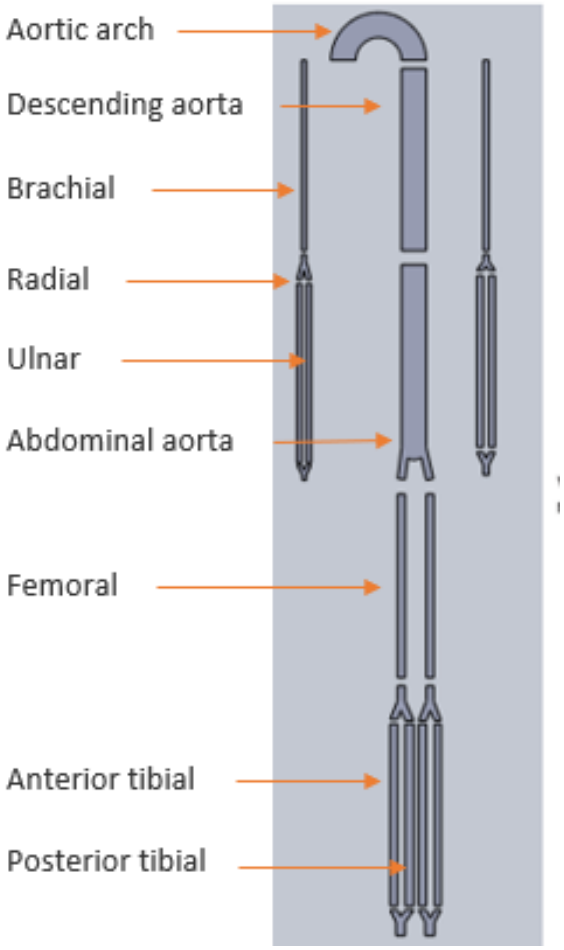

Figure 56: Phantom arterial tree (Left), Actual arterial tree (Right)

The aortic arch, descending aorta, abdominal aorta, brachial, radial, femoral, anterior tibial and posterior tibial arteries were selected for modelling and moulding. The artery shapes were also simplified and can be observed; the arteries are a combination of straight tubes, forked tubes and curbed tubes. This was done for modelling ease and consistency of the vessel for measurement and testing purposes. Simplifying the geometry provides us with a means of control for constant wall thicknesses and diameters through the length of the phantoms when compared to a real vessel like the aorta in Figure 57.

Figure 57: Aorta imaging

3.2.4.2 Arterial modelling

The following table illustrates the process step by developing male and female moulds.

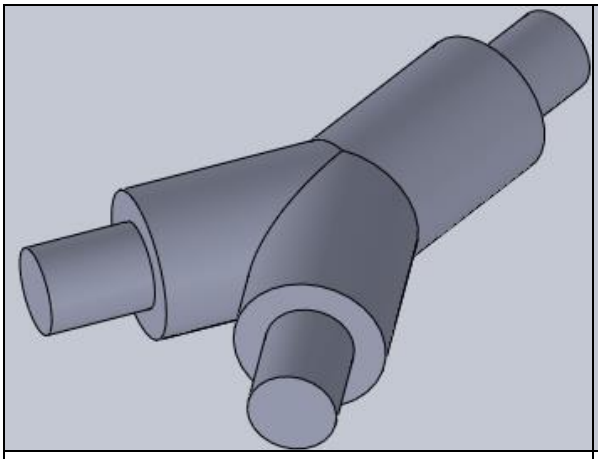	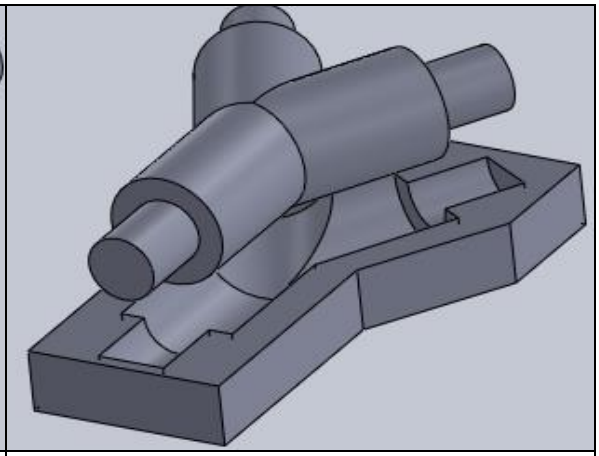
Step 1: 3D modelling of the external surface of the vessel in SOLIDWORKS	Step 2: Using an external surface to create a cavity
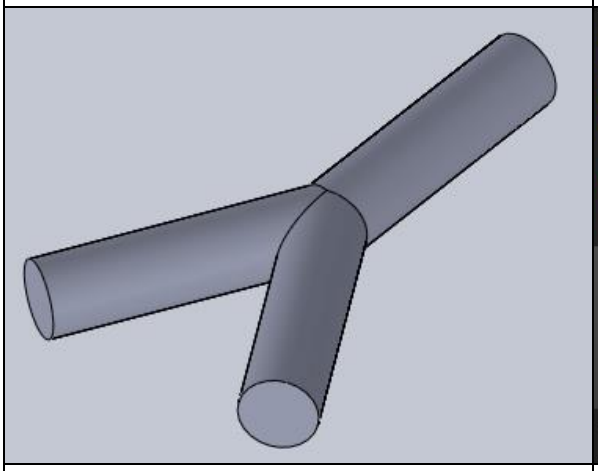	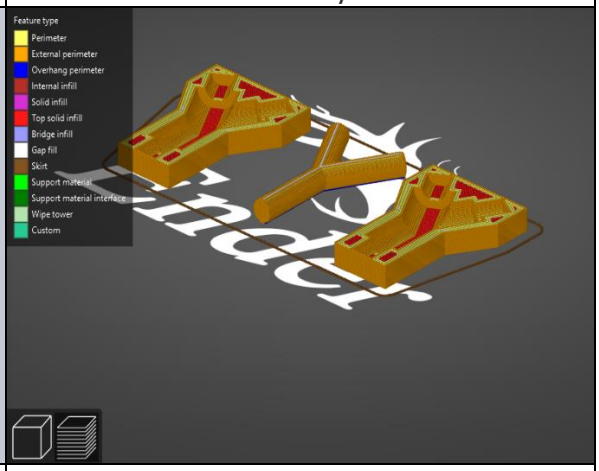
Step 3: 3D modelling of the internal surface of the vessel in SOLIDWORKS	Step 4: Finely slice models in 3D printing slicing software for printing
	
Step 5: 3D printing of male and female mould using PLA+ filament	Step 6: Finish surface of the print with fine sandpaper to refine layer lines

Table 14: Mould creation process

The moulds were printed at a resolution of 0.05 mm layer height to achieve the greatest accuracy. The male moulds for complex shapes were created to be easily broken down into simpler shapes to remove the male from the inside of the phantom. For instance, the fork in the table above is easily broken, meaning one of the forks can be snapped off and removed. This practice is fine for the smaller complex shapes as the printing time and filament used is minimal; however, larger complex shapes, which would be harder to break and take longer to reprint if broken and needed for another mould, were designed to be detachable. For example, in Figure 58, the male aorta moulds branches were made to be removable, transforming it into a much easier shape to remove from the interior of the aortic arch phantom.

Figure 58: Male aorta mould

3.2.4.3 Description of the final moulding process

This section will describe the process used to mould the phantom arterial system.

	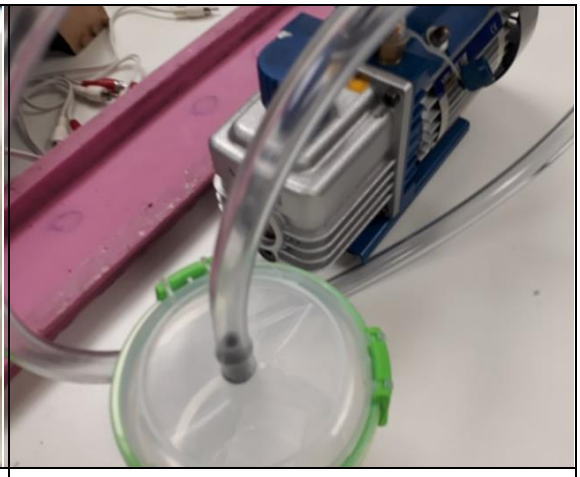
Step 1: Mixing parts A and B of equal volume	Step 2: Vacuuming the mixed solution for 5 minutes to ensure the removal of bubbles
	
Step 3: Pour mixture into a female side and set the male in place, waiting to 70 minutes to cure	Step 4: repeat step 1 and 2 for the second side and add place the first side and the male on top, waiting to cure
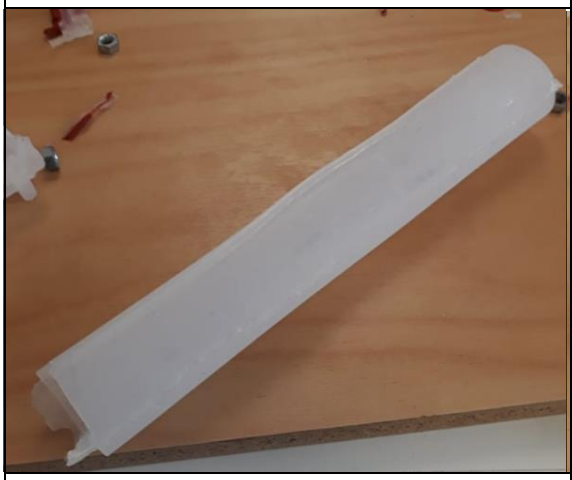	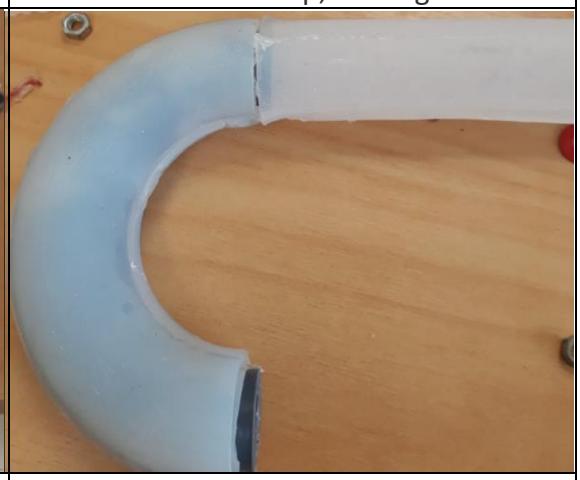
Step 5: remove male and female moulds from the phantom	Step 6: remix silicon and stick to the arterial tree as arranged in Figure 56

Table 15: Phantom moulding process

3.3 Evaluation and testing of the arterial phantoms

This section aims to test the accuracy of the materials and moulding methods developed and employed by evaluating the dimensional accuracy of the phantoms and the mechanical properties of the arterial wall.

3.3.1 Examination of dimensional accuracy using vernier

It was important to examine our moulding method's dimensional accuracy as the dimensions affect the vessel's behaviour, and dimensional accuracy to the designed mould will affect our predictions when testing for compliance in the following section. The aorta was tested of 5 slices down the length of the phantom; in the absence of more advanced testing equipment, the artery's internal and external circumference were measured by cutting it so it could be folded out. By measuring this way, we eliminate error in thickness by compression as the material is not stiff. Five 10 mm wide sections cut equidistant along the length of the moulded phantom and converted to diameter using Diameter = Circumference/π, and the results can be seen in Table 16, and Table 17, data was measured using a vernier calliper as seen in Figure 59

Measurement no.	Sample no.					Average (mm)
	1	2	3	4	5	
1	23.16	23.28	22.91	23.29	22.79	23.08
2	22.81	22.89	22.97	22.86	22.96	22.89
3	22.80	22.75	22.97	23.21	23.16	22.97
Average	22.92	22.97	22.95	23.12	22.97	22.98

Table 16: Internal diameter of aortic samples (mm)

Measurement no.	Sample no.					Average (mm)
	1	2	3	4	5	
1	27.88	28.22	27.97	28.03	28.26	28.07
2	27.83	28.13	27.83	28.09	27.91	27.62
3	28.05	28.12	27.99	28.16	28.15	28.09
Average	27.92	28.16	27.93	28.09	28.11	28.05

Table 17: External diameter of aortic samples (mm)

Figure 59: Measurement of sample circumferences

The Tests identified an internal diameter of $22.98 \pm 0.2\ mm$ and an external diameter of $28.05 \pm 0.2\ mm$, a variance of less than 1% for both internal and external diameters on the moulded phantom across its length. This variance should not be significant in the artery's performance in the following testing section and indicates a successful development of the moulding process to achieve accurate arterial shape and size.

3.3.2 Examination of dimensional accuracy using ultrasound

Ultrasound became available after these tests were conducted, and the arteries were re-measured. The ACUSON Sequola C512 ultrasound machine was used along with the 17L5 HD Pinless ultrasound probe. The specimens were submerged in water and measured, as shown in Figure 60, where the probe and the specimen are parallel. The specimens were measured in the Radiant DICOM viewer software version 4.6.9.

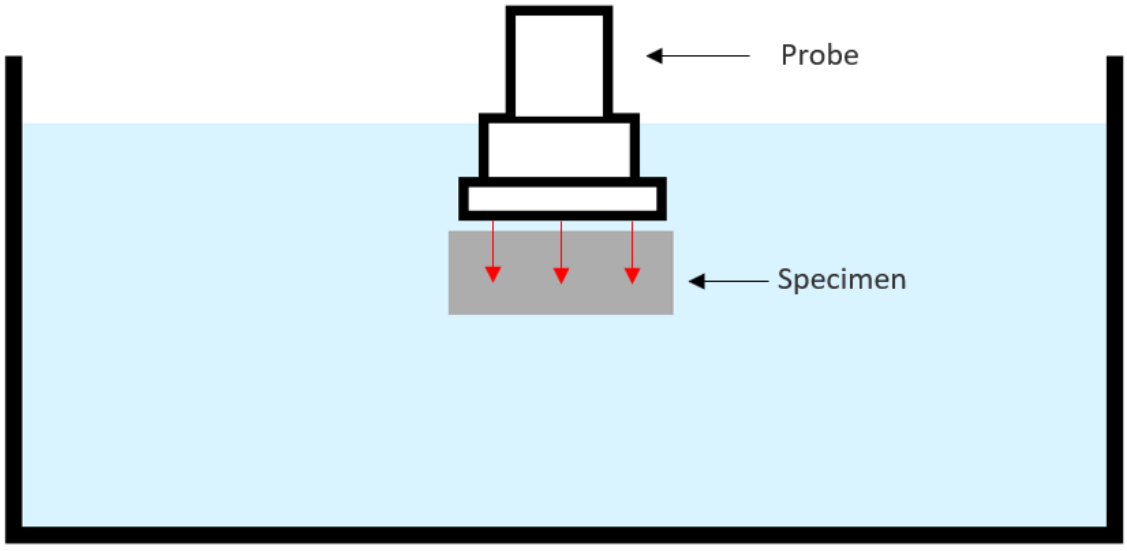

Figure 60:Ultrasound experiment setup

Initial testing would have to determine the speed of sound in the dragon skin material. To do this, a sample seen in Figure 61 was created of a known thickness of 11.5 mm. The sample was then tested with the ultrasound and measured.

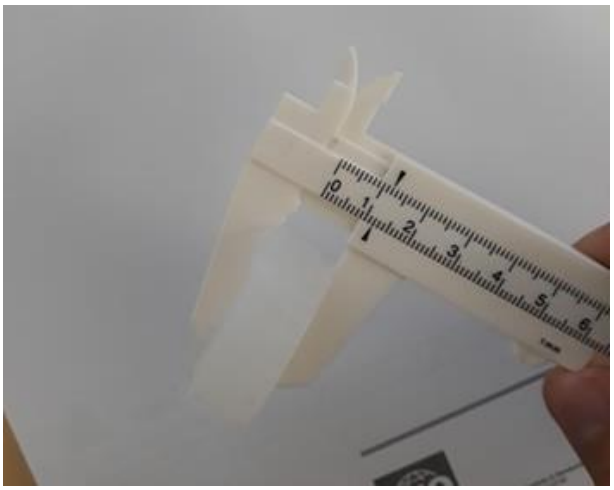

Figure 61: Speed of sound test sample

Figure 62 illustrates the ultrasound measurement taken as observed. The average thickness measured was 17.9 mm; therefore, the ratio for the actual value and the ultrasound measurement is 1.55; this can be used to adjust the arterial thickness measurements gathered in Figure 64.

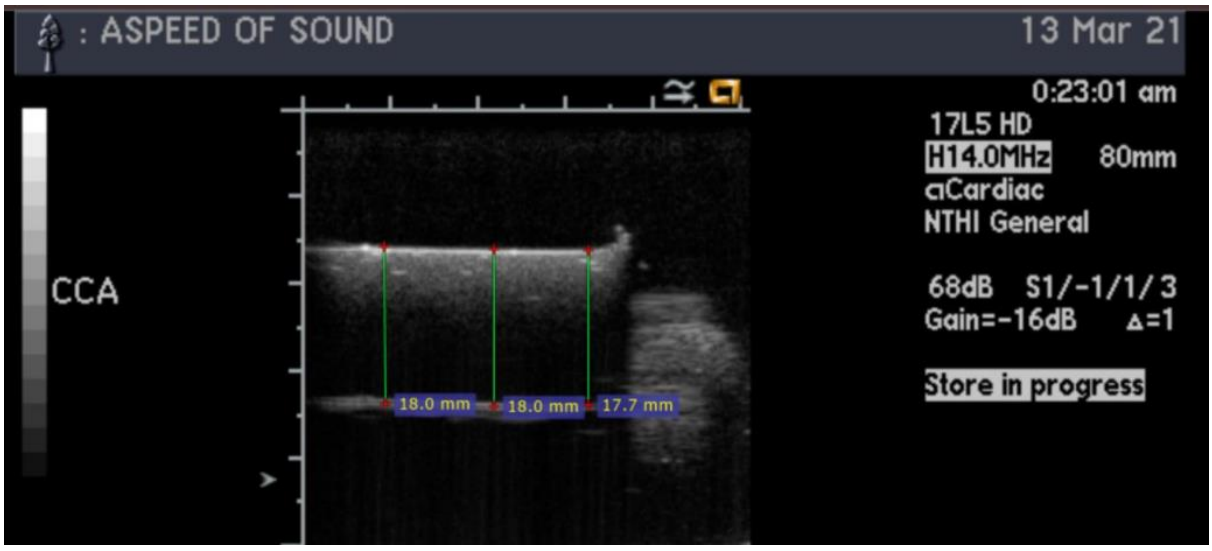

Figure 62: Speed of sound ultrasound experiment

Once the speed of sound ratio in dragonskin was determined, a test was conducted on the brachial artery. This vessel's thickness and diameter were moulded to be 1.5 mm thick and have an internal diameter of 4 mm.

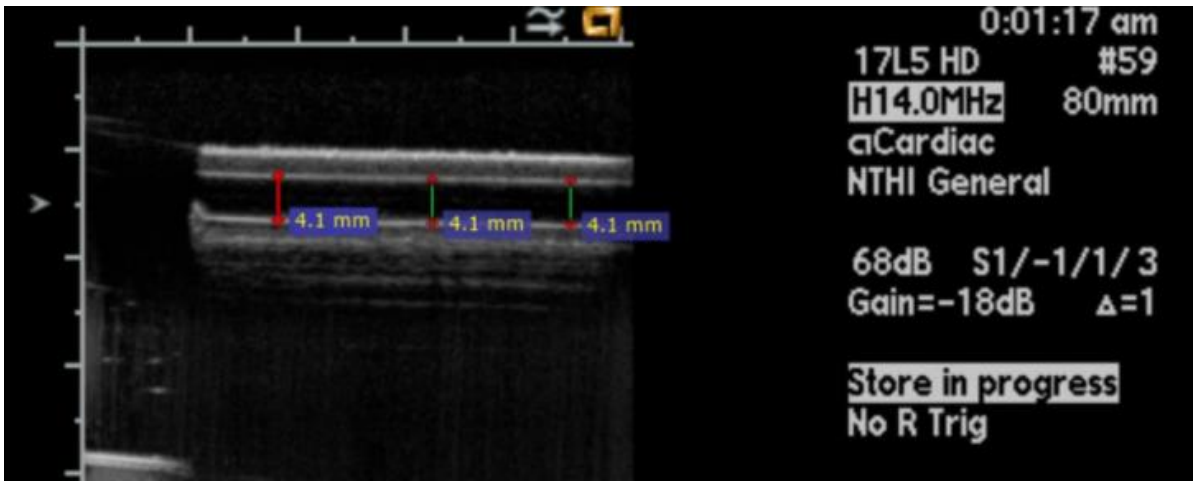

Figure 63: Ultrasound measurement of the brachial artery diameter

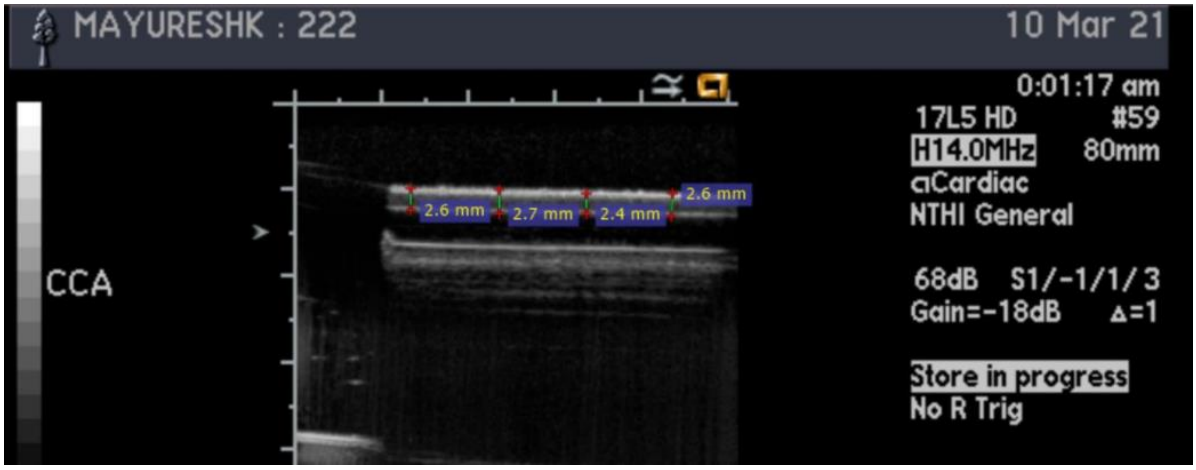

Figure 64: Ultrasound measurement of brachial artery thickness

The internal diameter can be observed to average 4.1 mm, the thickness can be measured to an average of 2.575 mm; considering the speed of sound difference measured earlier, the real measured value for thickness is 1.66 mm. As in the vernier testing, there is a minimal variance between the standard dimensions and those measured. This leads to the conclusion that the moulding process is sound.

3.3.3 Evaluation of arterial emulation in compliance

To evaluate the phantom arteries' compliance, we conducted a test to relate the phantom's expected compliance and the real compliance of the phantom. Bergel (1961) used Laplace's theory of thin-walled tubes to derive the following equation for elastic modulus.

$$E = \frac{\Delta P . D^2}{2 . h . \Delta D} \tag{15}$$

(Gamble, Zorn et al. 1994) derived an equation for an artery's compliance based on its geometry and pressure.

$$C = \frac{\frac{\Delta \mathrm{D}}{\mathrm{D}}}{2\Delta P} \pi D^2 \tag{16}$$

We can use these two equations to determine the compliance and elastic modulus' theoretical values based on the pressure change in the arteries. If we set the following test parameters, we can dictate the following desired capacitance for the test. Elastic modulus E can be taken from the material tests conducted to be an

$$D = 23mm$$

$$\Delta D = 11mm$$

$$h = 3mm$$

$$R = 1.736\ mmHg . s/mL$$

Where D is the Internal diameter of the artery ΔD is the change in internal diameter, h is the wall thickness, and R is the resistance to flow. The following is a brief description of the test conducted.

The Pump, Aorta, Catheter and Resistance valve was set up, as shown in Figure 65. A ring to determine the aorta's expansion limit was placed around the aortic section. The pump was turned on until the aorta reached the meeting ring and then turned off till pressure reached 0. This process was repeated three times. The readings were plotted with the lab chart software for analysis.

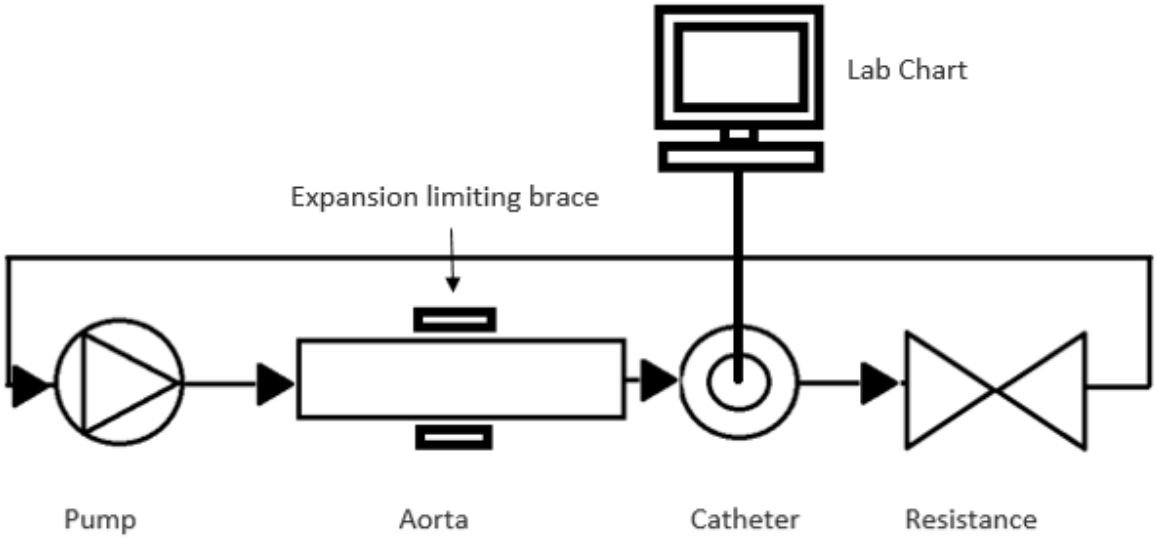

Figure 65: Experimental setup for Aortic compliance

By measuring the pressure as observe at an average of 203 mmHg, we can estimate compliance to be $1.41 \times 10^{-8} \frac{m^3}{Pa}$ Or 1.9 ml/mmHg and an elastic modulus to be 224 kPa, resulting in an elastic modulus as estimated and theoretical compliance. The test results can be seen below in Figure 66 and Table 18.

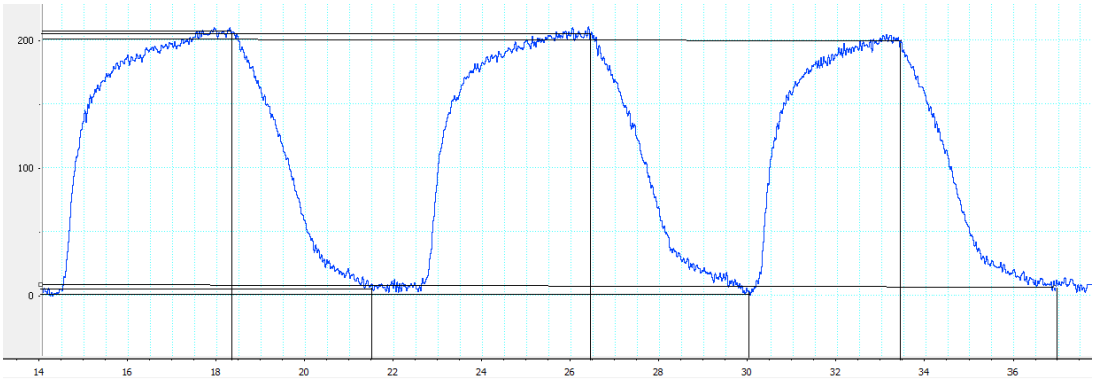

Figure 66: Aorta Pressure/time

	1	2	3	Average
Peak (mmHg)	**205.4**	**203.6**	**200.9**	**203.3**
38.8% of Peak (mmHg)	**5.2**	**4.8**	**4.1**	**4.7**
Time constant (τ)	**3.3s**	**3.5s**	**3.4s**	**3.4s**
C (mL/mmHg)	**1.9**	**2.01**	**1.96**	**1.95**

Table 18: Aorta compliance test

It is known from the literature that the time constant is proportional to RC ($\tau = R.C$). The values for compliance were identified using this relationship and entered in the table above. Through this method, we observed an average compliance of 1.95 ml/mmHg. From the literature, we know that aortic compliance between 1 and 2 ml/mmHg the values determined in the experiment lie within the upper range of the

reference values. The experimental values also lie within 3% of the estimated compliance values previously determined from the material properties and the phantom's dimensions to be 1.9 l/mmHg. From these results, we can determine the precision of the phantom dimensions. The elastic modulus of the material is accurate to the design requirements and those of real arteries, as arterial emulation of compliance is accurate to within 3%.

3.3.4 Evaluation of the wave reflections

The propagation of waves through the arterial tree was studied from the literature. It is known that the pressure and velocity waveforms. A test was conducted to see if the phantom system developed would replicate the expected amplifications as they propagate away from the heart. Figure 67 illustrates the experimental setup pressures were measured at the aorta and the radial artery simultaneously, the results of which can be observed in Figure 68, where the orange waveform is the pressure measured at the radial artery and the pressure measured at the aorta is blue. The test results were measured against a simulation developed in Simulink using the wave propagation equations Identified in the literature. The simulation emulated the cardiac output and the artery compliance and shapes. The simulation output can be observed in Figure 69.

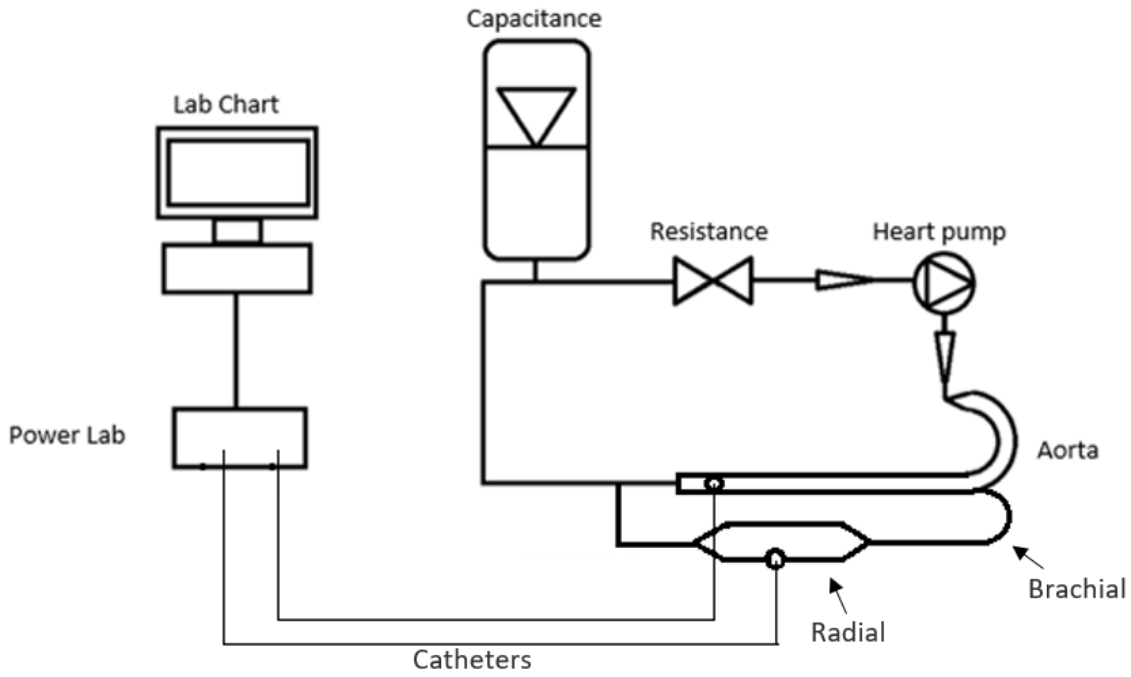

Figure 67: Wave reflection test set up.

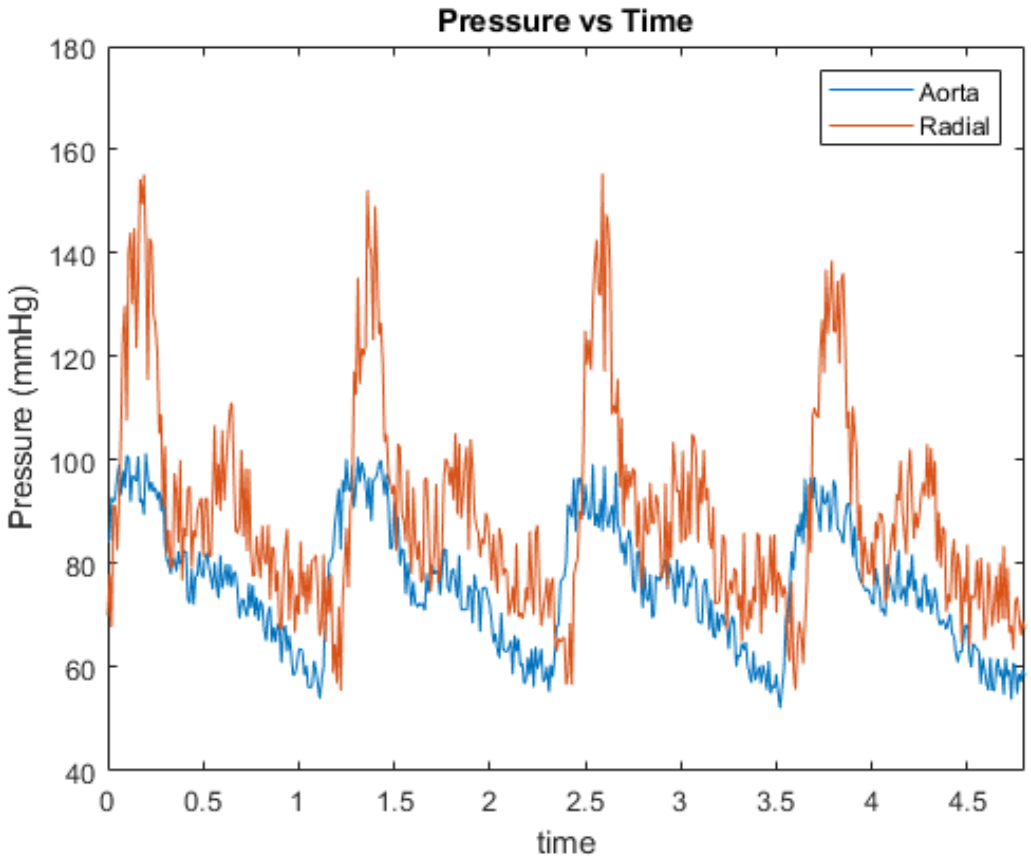

Figure 68: Pressure wave, reflections test

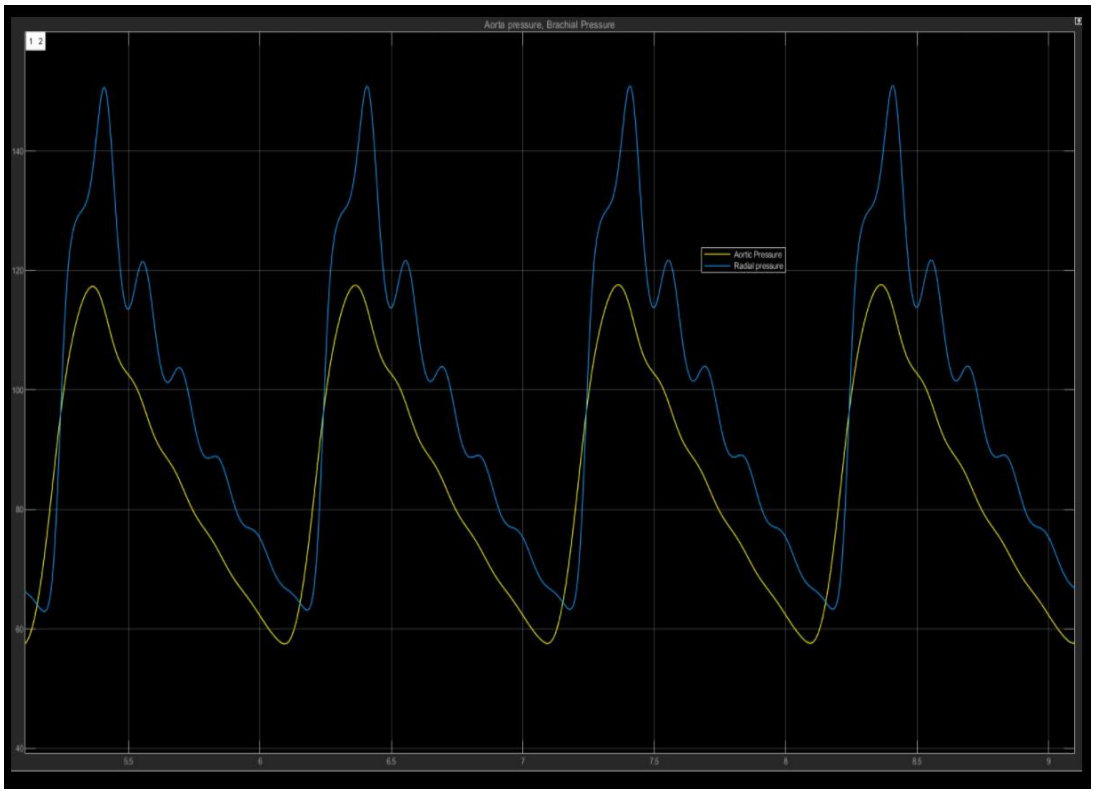

Figure 69:Pressure wave, Simulink simulation

A time delay can be observed in both figures as the two arteries are different distances from the heart; in the Simulink simulation, this was measured as 0.12 s. In the mock circulatory loop 0.13s, these values being within 8% of each other. The average peak systolic pressure in the aorta can be measured as 105 mmHg, and the average radial systolic pressure 153 mmHg, a 45.7% amplification. The radial systolic pressure averaging 152 mmHg and the systolic aortic pressure averaging 113 mmHg a 34.5% amplification. An amplification difference of 10%, however, can be attributed to the ideal circumstances of the simulation. The fact that the mock system amplifies the wave, in general, is a testament to the fabrication of the synthetic arteries as it emulates the pulse wave reflections we desire.

3.4 Summary

The aim of this section was to produce arteries that are dimensionally accurate and assume similar properties to those seen in the literature. To achieve this, various tests were undertaken on different materials and moulding methods to achieve a process that successfully meets these requirements. The materials testing yielded promising results, allowing similar elastic properties to real arteries as discovered in literature as 150 and 250 kPa. The tests on dragon skin 10 indicated an elastic modulus of 230 kPa. Proceeding this discovery, the investigations into different moulding methods yielded geometrically accurate shapes after testing and refining methods to produce phantoms with a high degree of precision in their wall thickness, diameter and shape. Tests conducted on the way phantoms preform about what we expect from our testing, and the human body yielded a damping effect of pulse pressure equivalent to that of the upper desired capacitance.

4 Design and development of the mock circulation loop

4.1 Aims

This section aims to design and develop a method of emulating the circulatory system. The goal is to create a system that can reproduce the pressure and flow waves seen in the literature. This will involve developing a pumping method that can adjust pulsatile flow at the required rates and volume, emulate compliance of the arteries and the damping effect it has on blood pressure and systemic vascular resistance to build and throttle pressure in the system.

4.2 Development of essential mock circulatory components

This section outlines the development of individual components of the mock circulatory loop, the heart, the resistance and the compliance.

4.2.1 The Heart

The heart was designed like some of those used in previous MCLS, but here it was decided that we used water as the compressing factor, not air, so leaks were easier to manage and identify. The system uses a linear motor driving a piston in a cyclic fashion, mimicking the desired cardiac conditions. The piston, in turn, changes the volume of the outer chamber, compressing the mock ventricle inside. The system was designed to be disassembled and reassembled to replace the ventricle if needed. The lid also contains a bleed valve to remove any air from the chamber.

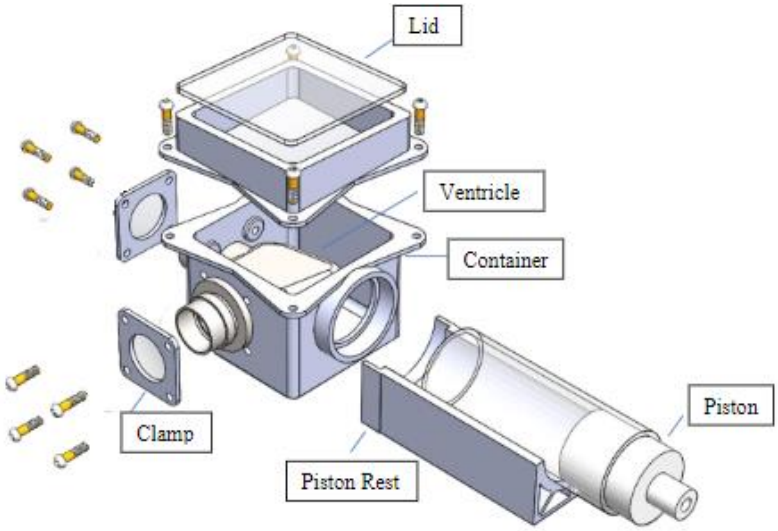

Figure 70: Heart pump chamber design

The system was to be submerged in the water; therefore, the actuator was supported on a frame above the water, driving a linkage to actuate the piston, as shown in Figure 71.

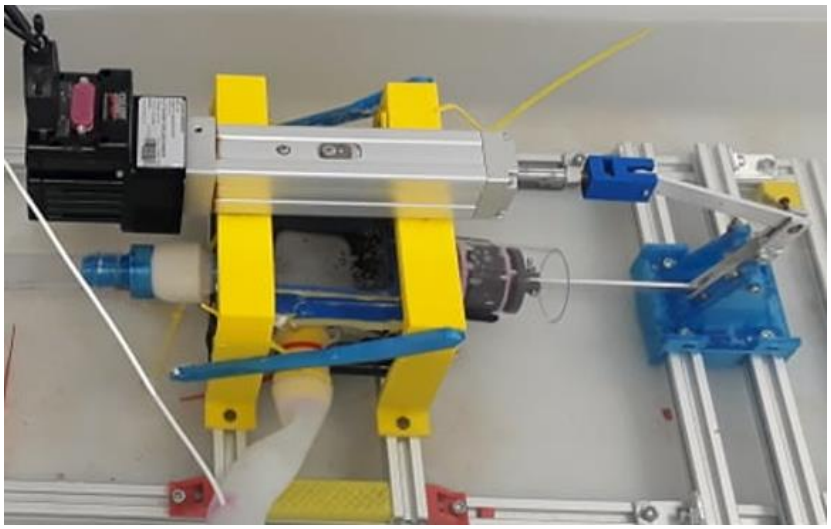

Figure 71: Heart pump

4.2.1.1 Pulse rate, Stroke volume and trajectory planning

The desired pulse rate was modelled from Figure 6 in MATLAB, which can be observed in Figure 72.

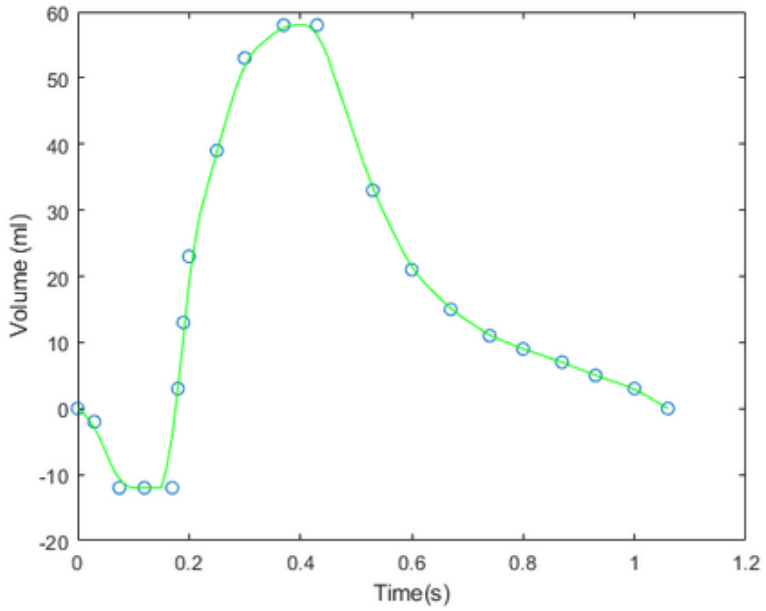

Figure 72: Modelled pulse wave

The system was designed to allow a 40 mm diameter piston to move 60 mm up an acrylic tube, achieving the desired change in volume 70ml per stroke. At a pulse rate of 60 bpm, we can achieve a flow rate of 5L/min. Flow rate can be altered through the pulse rate or the volume change in the ventricle required creating a large possibility for testing flow

ranges. Figure 73 is the dimensioning of the linkage and position of the motor and piston. This image was used to derive the piston's trajectory equations in relation to the motor shaft.

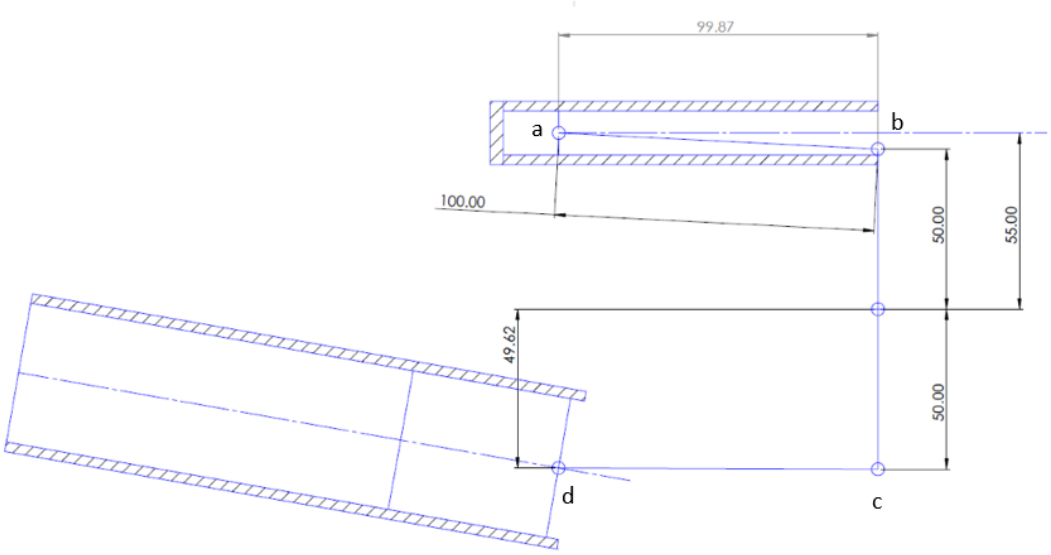

Figure 73: Scaled linage dimensions

The following set of equations were derived by Aadil Paghdiwala from knowing the dimensions above and the distance the piston is required to move along the tube to displace a given amount of fluid in the ventricle, in this case, 70ml. Working backwards from point d using Figure 73 and Figure 74 as a reference, we have the following where r = 50 mm and R = 100 mm (the lengths of the linkages).

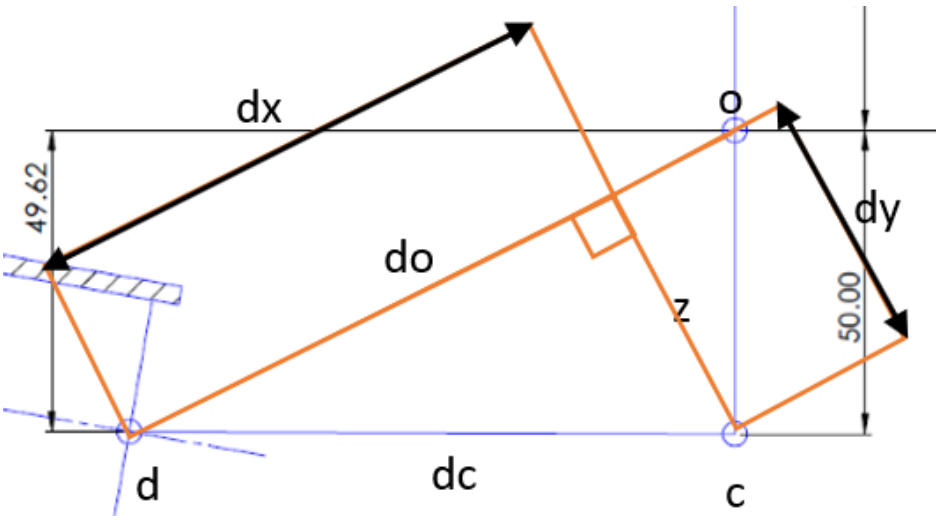

Figure 74: Trajectory derivation reference for motor linkage

The equation of the line the point follows:

$$n = -\frac{\pi}{18m} - 67.05 \tag{17}$$

Coordinates of point d:

$$d = (m, n) \tag{18}$$

Distance between point d and the origin (o):

$$l_{od} = \sqrt{m^2 + n^2} \tag{19}$$

Derived dx and dy:

$$dx = \frac{l_{od}^2 - r^2 + R^2}{2l_{od}} \qquad dy = \sqrt{R^2 - dx^2} \tag{20}$$

Vector do:

$$[-m \quad -n \quad 0]$$

The unit vector of d:

$$d_{unit} = \frac{do}{\det(do)} \tag{21}$$

Finding Z:

$$z = [0 \quad 0 \quad 1] \times d_{unit} \tag{22}$$

Finding dc:

$$dc = dx.d_{unit} - dy.z \tag{23}$$

Fining c:

$$c = dc - do \tag{24}$$

Finding b:

$$b = -c = (bx, by) \tag{25}$$

Finding a:

$$a = \left(-\sqrt{R^2 - (55 - by)^2} + bx, 55\right) \tag{26}$$

After deriving these relations, the equations were entered into MATLAB to develop trajectory plots for the motor shaft in relation to the piston, shown in Figure 75, where the red line it the piston movement and the black is the motor shaft.

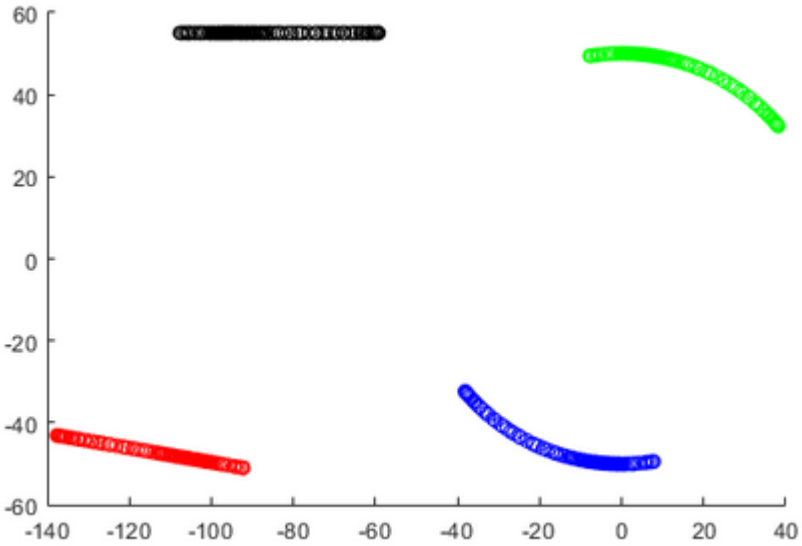

Figure 75: Trajectory plot for motor linkages

Once the Absolute counts found using this program were then exported to a CSV file. The CSV file was then imported to the SMI application using the "Import CAM" tool. The motor's speed can be changed by changing the master increment in the "Import CAM" window. Increasing the Master Increment decreases the motor's speed while decreasing the master increments speeds the motion up. Yielding the steps vs time plot, we see in Figure 76 relation the steps to the ventricular displacement.

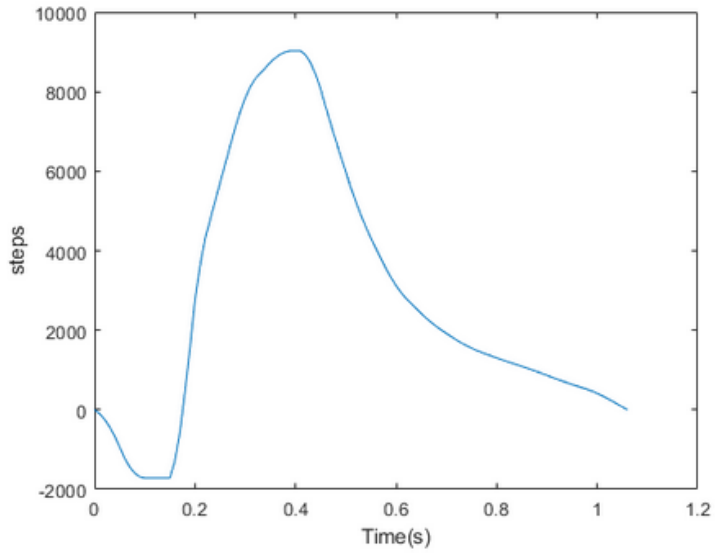

Figure 76: Steps vs time motor table

4.2.1.2 Ventricle

The ventricle was designed relative to the stroke volume required; in this case, little consideration for shape was researched as the volume was the primary driver in the physiological waveforms we desired. Taking into consideration the average ventricle volume change during the heart cycle 125 ml to 50 ml during contraction, the ventricle was modelled to be approximately 75 ml. The ventricle was moulded like the arteries through the same material adding a compliant nature for compression and expansion, adding the potential to hold a greater volume of water if needed. A study was conducted by Fiore, Redaelli et al. (2003), developing a "model left ventricle with physiologic-like diastolic behaviour for studying mitral valve surgical correction". The study involved developing a flexible ventricle and studying the change in shape during the cardiac cycle. The information was gathered for the use of creating an acceptable mock ventricle for studying ventricle filling fluid dynamics. An FEA model was used to develop a ventricle shape with a volume of 71 ml at its systolic point, allowing a decent reference for ventricle size. The ventricle was modelled using the same methods mentioned in section 3 and can be observed in Figure 77.

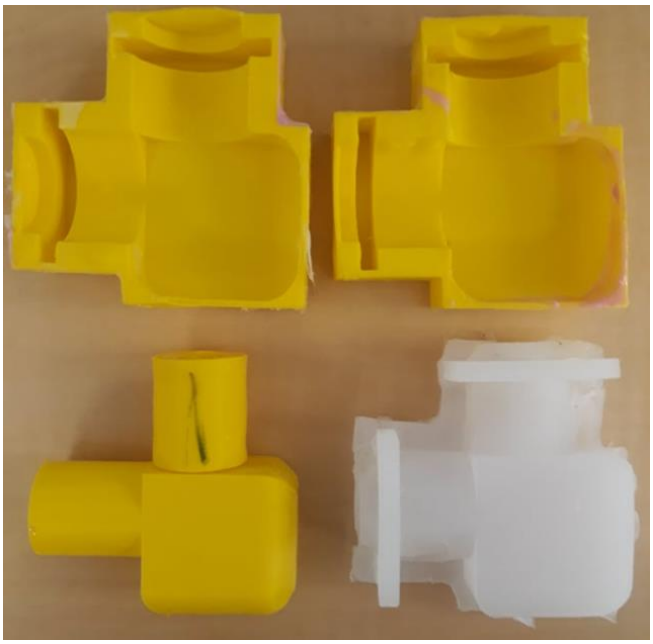

Figure 77: Moulded ventricle

4.2.1.3 Valves

Three different one-way valves were tested for use in the heart system to simulate the atrial and aortic valves. A disk valve, ball valve and synthetic tricuspid valve were tested for their effectiveness. Figure 78 illustrate the three types of valve tested.

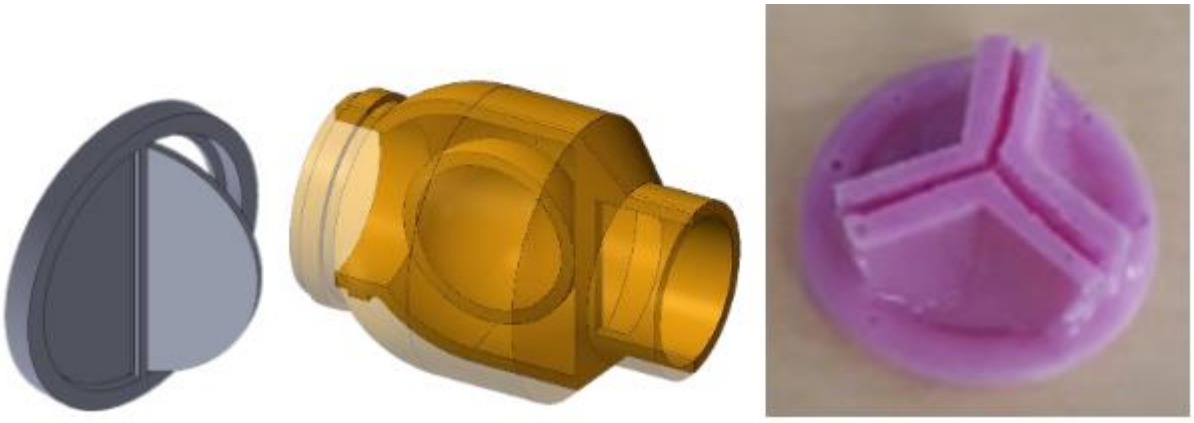

Figure 78: Disk valve, ball valve and tricuspid valve, respectively

The three valves were tested by attaching them to the system intern and running the heart pump with a piece of plastic debris inside the system visible through nylon tubing. The debris indicated the direction of flow and any back flowing in the system. Through observation, the following selection matrix was created.

Criteria	Weight	Method		
		Disk Valve (Datum)	Ball Valve	Tricuspid
Prevent back flow	35%	0	0	0
Allow forward flow	35%	0	0	0
Consistency	30%	0	0	+
Sum +		0	0	1
Sum -		0	0	0
Sum 0		3	3	2
Net score		0	0	1
Weighted score		0	0	30
Rank		2	2	1
Continue?		No	No	Yes

As can be deduced from the table, all three valves effectively prevented backflow and allowed forward flow through the atrium and the ventricle; however, both the disk valve and the ball valve were inconsistent in this. The disks and the ball often would become stuck on a certain cycle, causing backflow or prevent flow at some points, whereas the tricuspid valve was consistent throughout the testing. The assumption is that the disk valve and the ball valve were 3D printed, and the ringed layer lines on inaccuracies in the printing cause the moving components to catch sometimes. Whereas the tricuspid valve was moulded and acted as a true aortic valve would and was chosen for use in this case.

4.2.1.4 Initial Testing and improvements

The initial tests were simply carried out by running the code to the pump and measuring the flow output using a pressure sensor connected to the Arduino software, measuring the flow ten times per second. The Arduino software saved the data to an array and was plotted in MATLAB, yielding the results in Figure 79. The blue line represents the pulsatile flow, and the red is the average flow across the system of which we are looking for approximately 5 L/min.

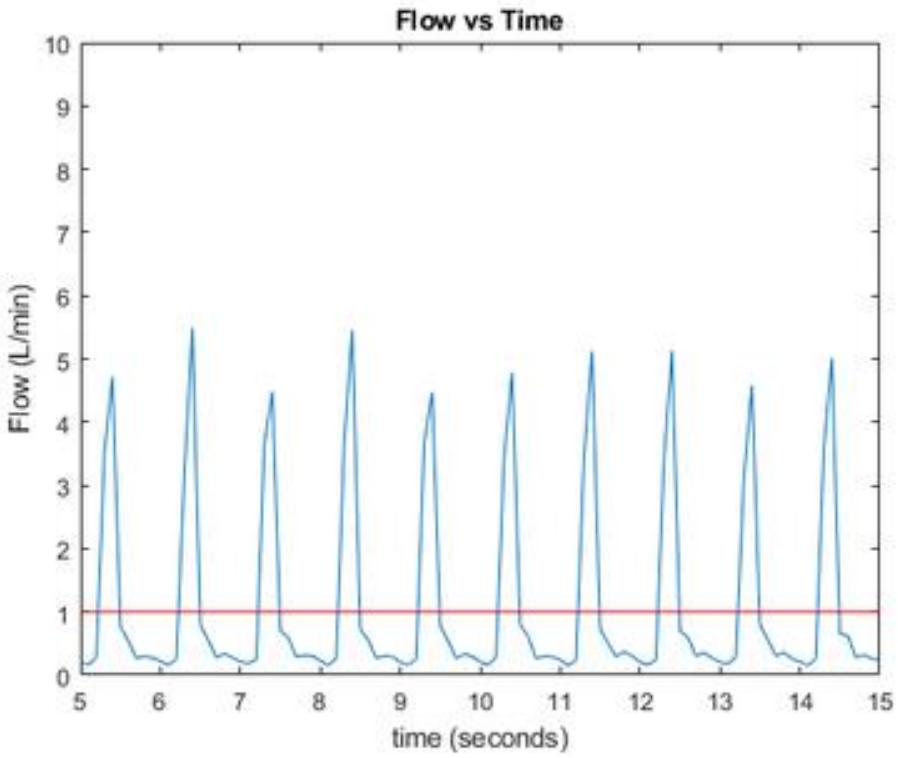

Figure 79: Initial flow test results

It can be observed from Figure 79 that the average flow rate in the system is much lower than we expect. There were four observable problems with the system, which will be illustrated in Figure 80, they were the movement of the motor mount, the movement of the linkage hinge, bubbles being expelled from the chamber indicating that the vessel is not fully sealed and less than half of the motor shaft displacement being translated up the system.

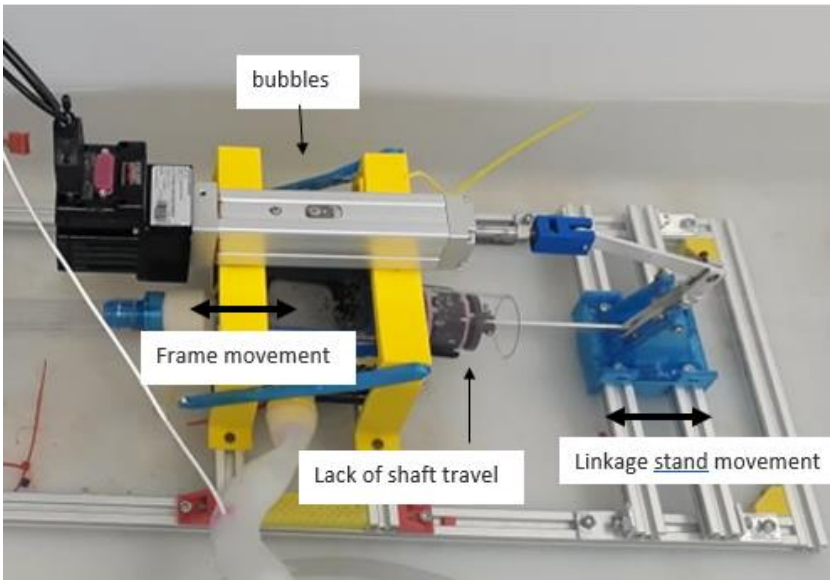

Figure 80: Initial test issues

The bubbles and leaks were prevented by a silicone sealant around the heart chamber's edge, seen in Figure 81. The silicon sealant can seal the system's gaps and be somewhat removable and replaceable if the ventricle should need to be replaced.

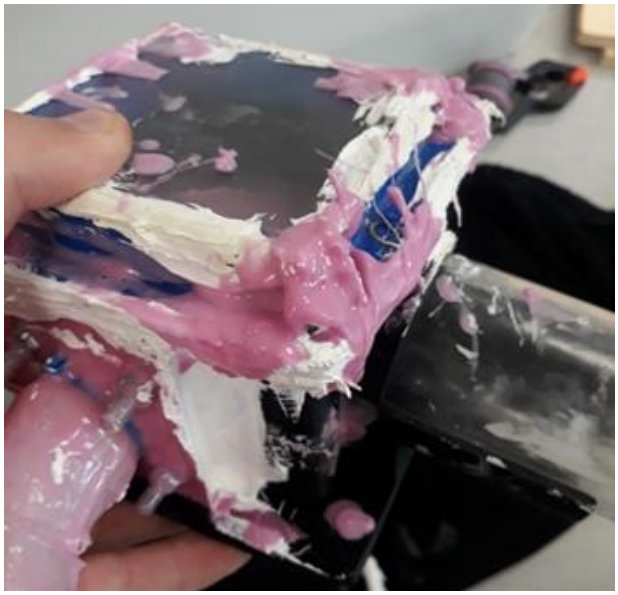

Figure 81: Sealing the heart chamber.

The motor stands and the linage stand were stiffened using aluminium struts to prevent movement, allowing complete translation of the power shaft length to the piston to create a more accurate flow from the ventricle.

Figure 82:Stiffening of the motor stand.

4.2.1.5 Retesting and discussion.

Following the improvements to the system made above, the heart pump was retested; the results from this test are illustrated below.

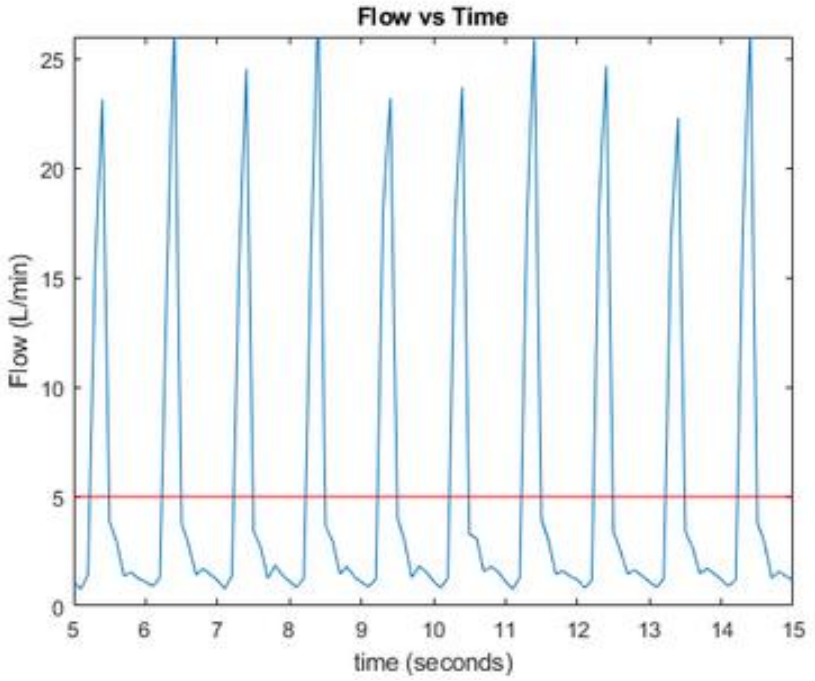

Figure 83: Resetting of flow.

The retesting of the flow yielded an average flow of 4.95 L/min. The desired flow output was 5 L/min the meaning there was a less than 1% difference in the expected flow rate as derived from the trajectory planning section and the design of the pump and the tested values. By stiffening the system and removing the bubbles, an adequate flow was acquired from the system can be tested within the whole circulatory loop to discover how it acts in the face of higher operating pressures. The sensor only measures flow one way, meaning the moulded tricuspid valve's effectiveness cannot be thoroughly evaluated from these results; however, the fact that a flow within the desired range was produced, we can assume that the valve acted as expected.

4.2.2 Resistance

As seen in the literature, vascular resistance can change quite dramatically, requiring a method of variable resistance. Ideally, the resistance would be computer-controlled easily connected to the system. Here we employed the same method Patel, Allaire et al. (2003) used to achieve resistance used a 1.5-inch gate valve as the system was accurate in mimicking pressure drops in the MCL to test left ventricular assisting devices. This was achieved using a motor actuated gate valve, as seen in Figure 84. Our gate valve was produced to make it electronically controlled.

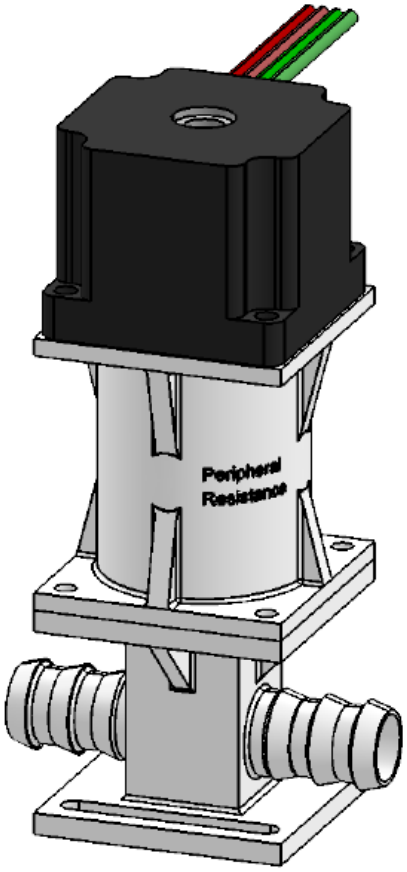

Figure 84: Resistance valve

The Gate valve consisted of a 15 mm orifice section with barbed fittings with a captive stepper motor mounted on top of it. The orifice was occluded by a gate actuated by the stepper motor capable of moving with 0.2 mm increments for throttling accuracy. The following sections will discuss this design's throttling accuracy and the required resistance ranges.

4.2.2.1 Theory

Determining arterial resistance is a fluid mechanics problem; the fundamentals of fluid dynamics can be applied to the resistance design. To determine resistance, we can use the following equation:

$$R = \frac{P_{in} - P_{out}}{\dot{V}} \tag{27}$$

P_{in} is the pressure into the valve from the heart, the arterial side and P_{out} is the pressure out going to the heart, the venous side, $\dot{V}$ The flow rate of volume through the valve and losses are minimal; therefore, we can assume it to be constant across the valve. A flow coefficient K is used in the rating of commercial valves; the relation between pressure and K can be observed below:

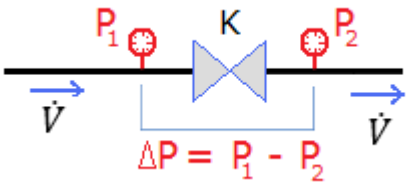

$$\Delta P = \frac{KV^2}{2g} \tag{28}$$

V is the blood velocity, and g is the gravitational acceleration; knowing this, we can derive a relationship between R and K.

$$V = \frac{\dot{V}}{A} \tag{29}$$

$$\Delta P = \frac{KV^2}{2g} = R\,\dot{V} = RVA \tag{30}$$

$$R = \frac{KV}{2gA} \tag{31}$$

A resistance range can also be established from Literature as:

$$70 - 160 \text{ Mpa s/m}^3$$

4.2.2.2 Testing

4.2.2.2.1 Test Rig

The test rig was assembled to represent how the mock circulation loop would be laid out once all parts were developed. A centrifugal pump was used to pump water through the system into the resistance and out the other side back into the tank of water. The pressure was measured on either side of the resistance and plotted on LabChart. Figure 85 and Figure 86 demonstrate the layout of the test rig.

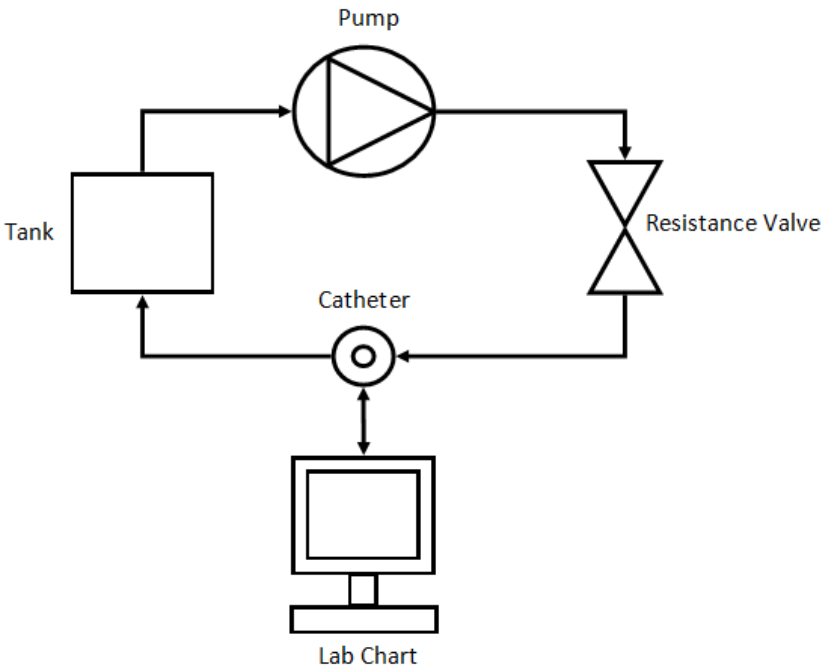

Figure 85: Test Rig Diagram

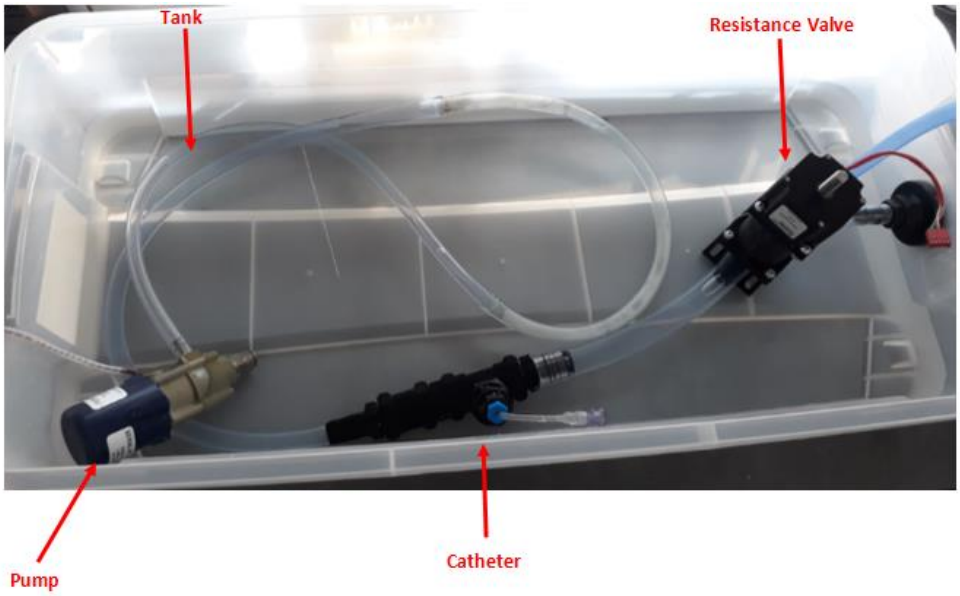

Figure 86: Test Rig Setup

4.2.2.2.2 Experimental Method

1. Calibrating the catheter by measuring two values in a monometer, the first value at 0 mmHg, then at 200 mmHg, inputting the corresponding voltage in the lab chart software.
2. Different flow rates were set and measures by timing the flow of water filling a bucket. These were 1.1,3.7,5.8,7.6,9.4 L/min.
3. For each flow rate, the pressure was measured on either side of the resistance using a catheter. The pressure was measured through a range of gate heights from 100% open to 100% closed.
4. The data was accumulated and turned in to a curve to determine the valve's throttling and the coefficient of flow K for any given pressure.

Table 19 below contains the recorded pressures in and out at each flow rates at different gate heights. The data was used to produce Figure 87 through to Figure 91 the illustrates the pressure drop across the resistance or capillary bed as the gate height of the resistor varies.

Results

Flow Rate (L/min)	Gate % closed	P_{in} (mmHg)	P_{out} (mmHg)	ΔP (mmHg)
1.1	0	37.86049	26.68977	11.17072
	50	20.29782	15.59782	4.7
	80	25.62549	3.138122	22.48737
	90	18.02882	4.91315	13.11567
	95	21.21387	3.102755	18.11112
3.7	0	32.6915	16.73836	15.95313
	50	30.04626	17.46257	12.58369
	80	56.25891	17.46866	38.79025
	90	35.5858	11.24447	24.34134
	95	36.64517	6.455168	30.19
5.8	0	93.95306	76.06183	17.89123
	50	40.20485	30.04853	10.15633
	80	65.39021	20.17638	45.21383
	90	55.20738	13.08297	42.12441
	95	60.24534	7.035888	53.20945
7.6	0	94.39967	86.38645	8.013222
	50	49.70248	38.02481	11.67767
	80	74.90214	21.52875	53.37339
	90	85.19079	15.02344	70.16734
	95	92.53684	7.956819	84.58002
9.4	0	93.75713	87.34017	6.416964
	50	67.82232	56.22319	11.59913
	80	81.8339	22.81461	59.01929
	90	118.6335	16.18288	102.4506
	95	123.2384	8.728364	114.5101

Table 19: Resistance test values

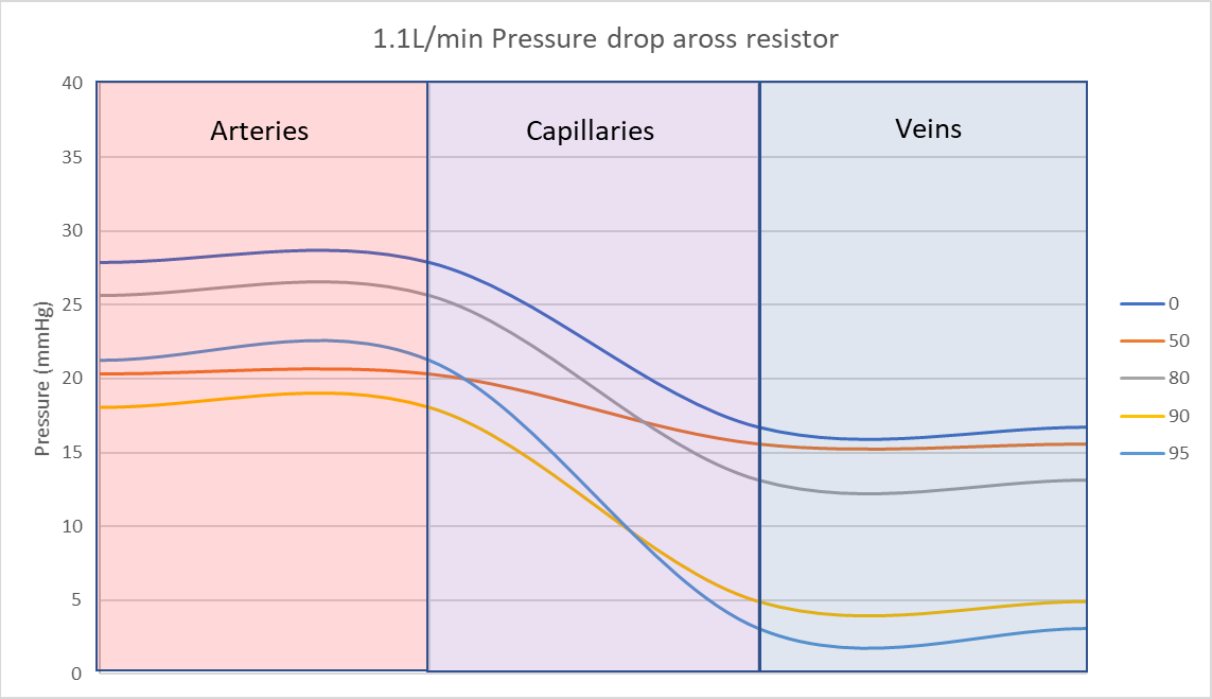

Figure 87: Pressure drop across resistor at 1.1L/min

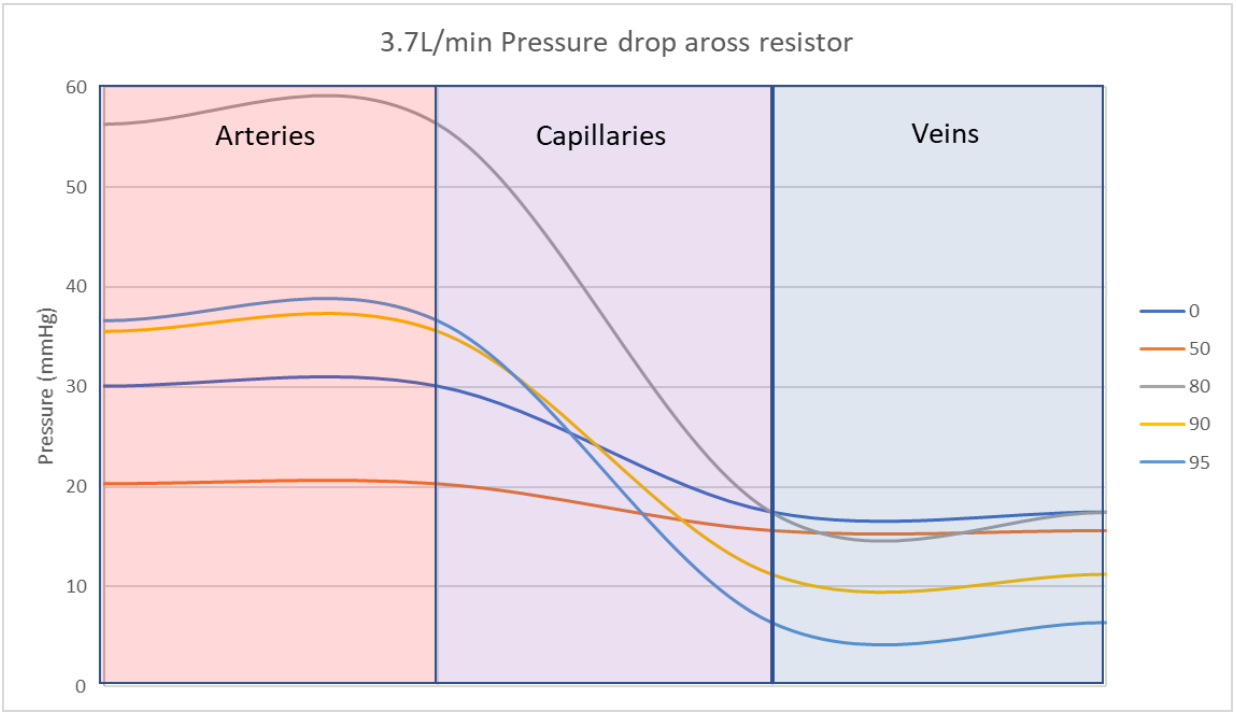

Figure 88: Pressure drop across the resistor at 3.7L/min

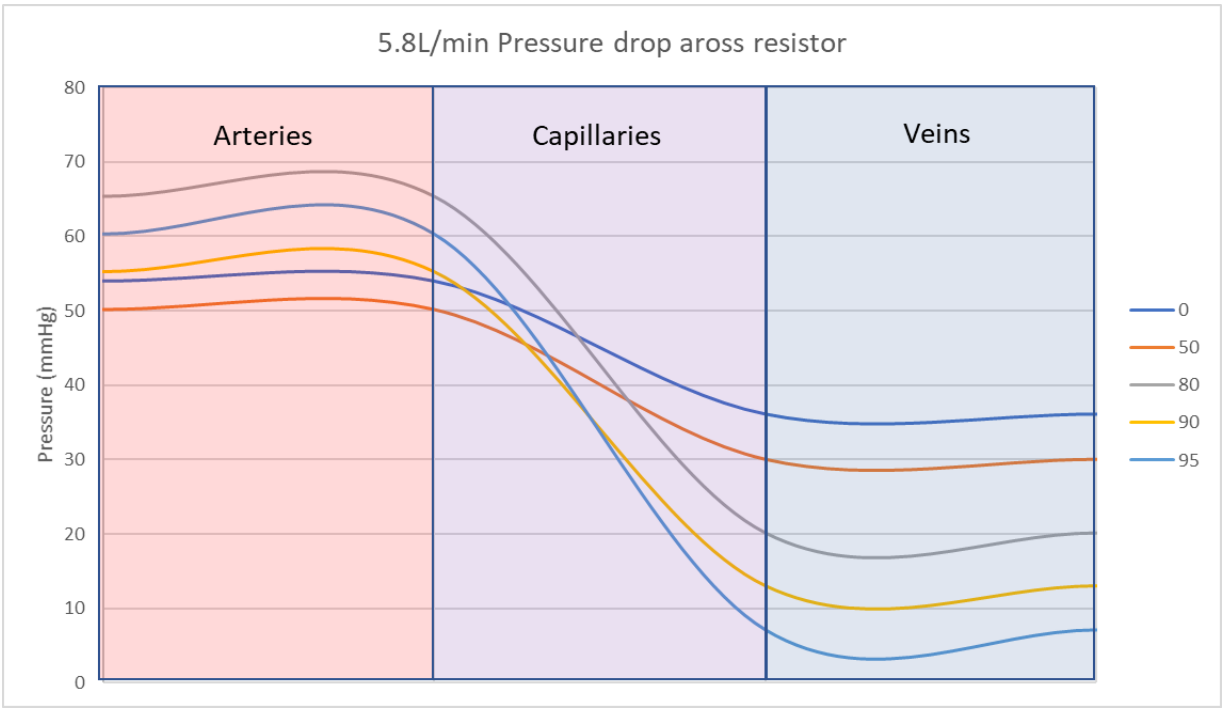

Figure 89: Pressure drop across the resistor at 5.8L/min.

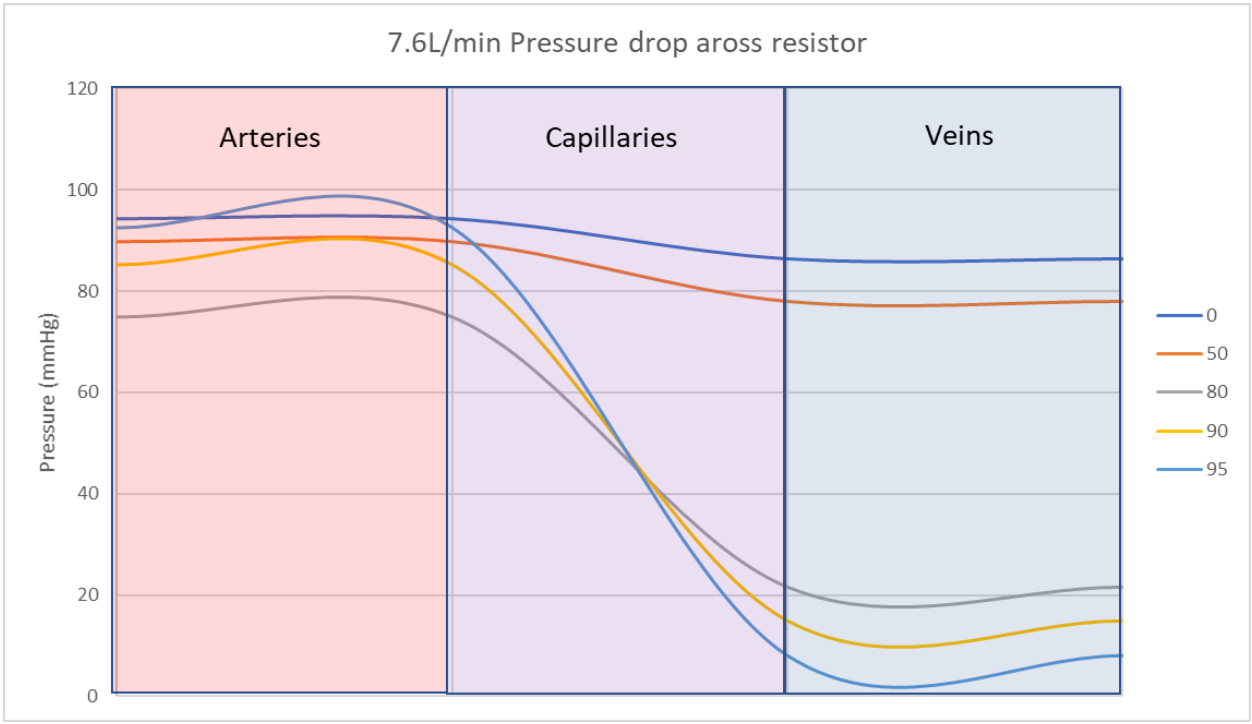

Figure 90: Pressure drop across the resistor at 7.6L/min

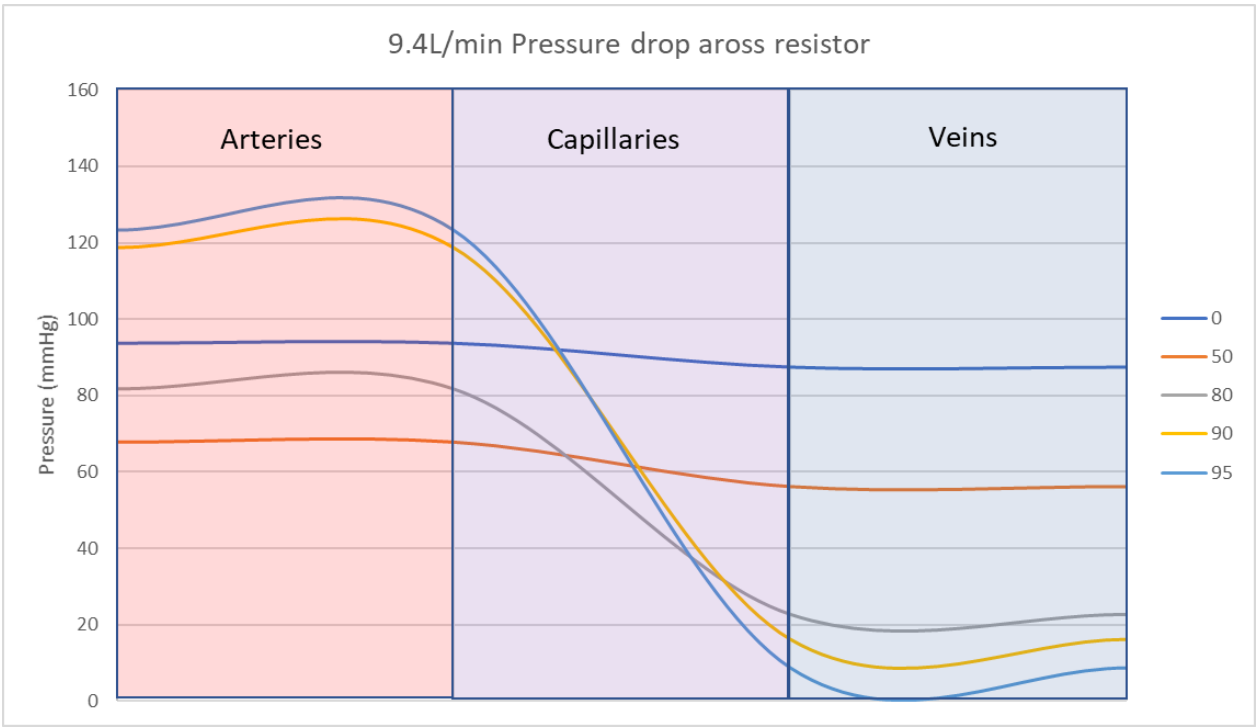

Figure 91: Pressure drop across the resistor at 9.4L/min

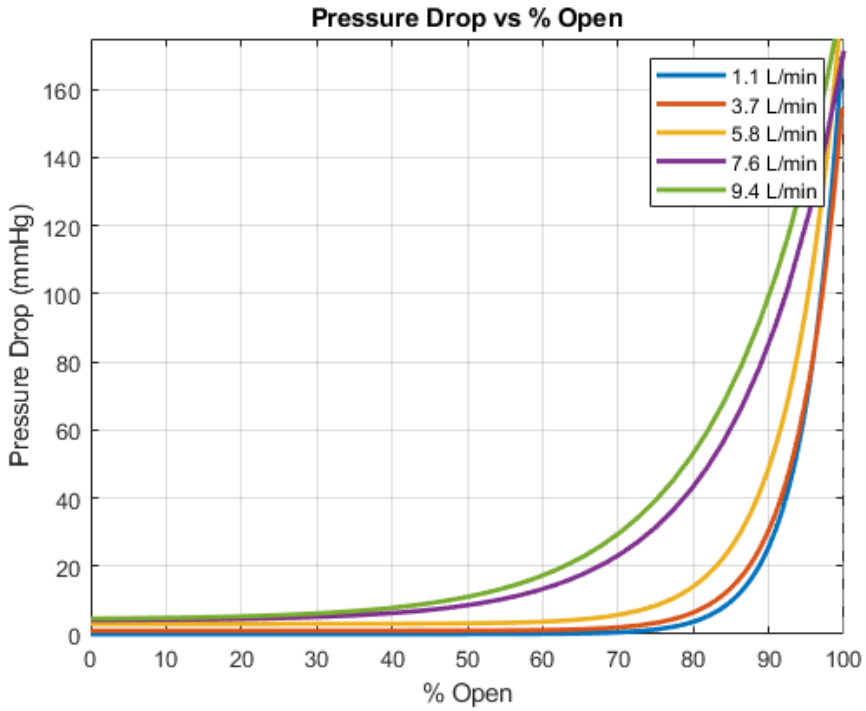

Figure 92:Pressure drop vs % open for each flow rate

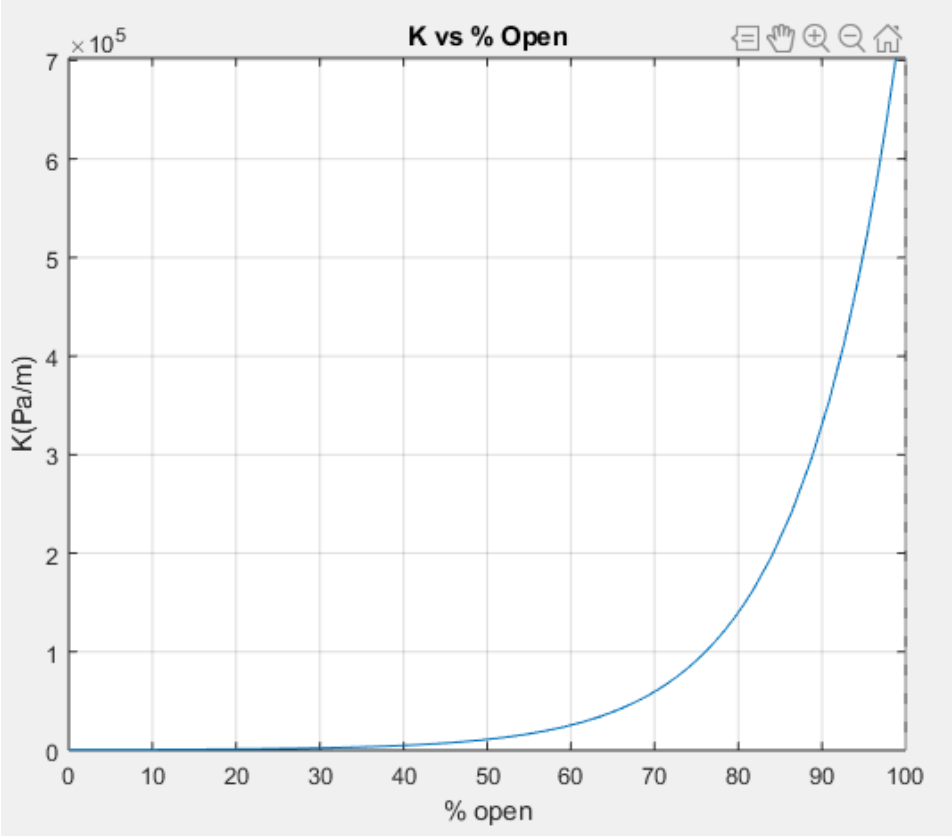

Figure 93: Coefficient of flow K vs % open

The following equation describes the curve in Figure 93:

$$K = 145.14e^{0.085(x)} + 423 \quad (32)$$

4.2.2.2.3 Discussion

As we can see above, a constant flow curve has been established from this curve; we can check the validity of the throttling range knowing the valve diameter of 15 mm flow rate of blood to be 5L/min.

$$A = \frac{0.015^2}{4}\pi = 1.76 \times 10^{-4} m^3$$

$$\dot{V} = \ 5\text{L/ min} = 8.33 \times 10^{-6} \frac{m^3}{s}$$

$$V = \frac{\dot{V}}{A} = \frac{8.33e-6}{1.76e-4} = 0.47 \frac{m}{s}$$

$$R = \frac{KV}{2gA} \ \therefore K = \frac{2gAR}{V}$$

$$R = (70 - 160) \times 10^{-6} \text{ pa s/m}^3$$

$$K = \frac{2 \times 9.81 \times 70000000 \ \times 8.33 \times 10^{-5}}{0.47} = \ 2.43 \times 10^5$$

$$K = \frac{2 \times 9.81 \times 160000000 \ \times 8.33 \times 10^{-5}}{0.47} = \ 5.56 \times 10^5$$

We can see from Figure 93 that these values lie within the range of the valve throttling capabilities. Pressure drops within the second stage of hypertension can be seen in Figure 92. This tests flaw is that we could not control which flow rate we have a which pressure, and vice versa, so we are unable to visually see the ranges we require. This means that the effectiveness of the valve cannot be fully evaluated until we connect the whole loop together. However, the test was sufficient to plot a flow coefficient vs % open graph illustrating the achievable range of resistance. This test was suitable to display the valve capability for achieving vascular resistance within the ranges obtained in the literature. We established the equation of the line for determining flow coefficient $K = 145.14e^{0.085(x)} + 423$ an exponential was used as it suited the K values derived from the testing of the valve and the fact that from our literature on the throttling capabilities of gate valves in general.

4.2.3 Compliance

An artery's compliance can be defined as the pressure change required to produce a given change in volume within the artery. A pulse of fluid travels into the vascular segment; the segment's compliance is how much it can expand. Higher compliance refers to a more stretchable artery wall, indicated that it could absorb a higher volume of blood with each pulse when compared to an artery with lower compliance. This feature is crucial in the development of the MCL as it generates the slowly dissipating wave seen in the literature.

Most systems mentioned in the literature accommodate variation on a Windkessel chamber using trapped air to dampen the system simulating compliance. The larger the volume of air trapped above the system at atmospheric pressure, the larger the compliance, similarly the pressure above the system changes the system's compliance. Developing and using a compliance chamber can easily vary one or both factors to simulate a wider range of potential arterial compliances that coincide with various cardiac conditions.

4.2.3.1 The variable compliance chamber design

A Windkessel chamber, which can be seen in Figure 94, uses a volume of trapped air above a fluid to mimic a spring simulating a system's compliance, essentially a no barrier accumulator. By changing the volume of air, the chamber, we have achieved the ability to vary the system's capacitance.

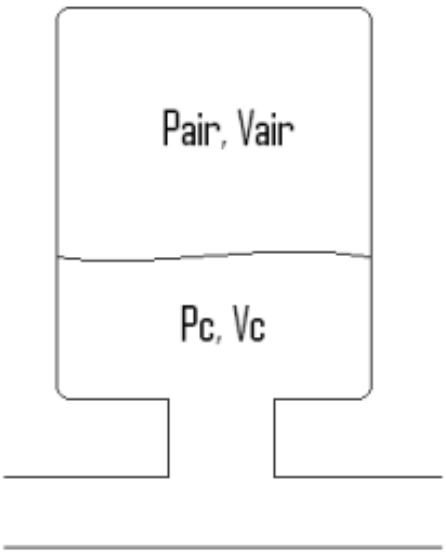

Figure 94: WindKessel Chamber

The design used in this system consists of a 3D printed base, an acrylic tube and 3D printed components. The top component supported a linear non-captive motor used to adjust the piston's position—a solenoid valve connected to the piston to adjust the air in the vessel. The design works like a no barrier accumulator. The piston and solenoid adjust the air volume in the vessel at atmospheric pressure changing the capacitance. This concept is illustrated in Figure 95.

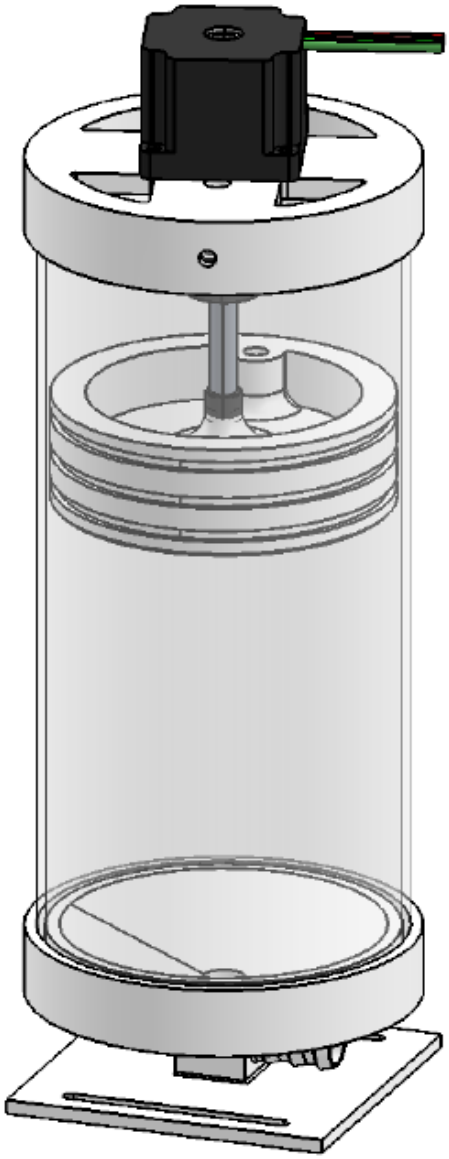

Figure 95: Capacitance Tank

4.2.3.2 Determining Capacitance

Using the theory of hydraulic accumulators, the following method can be used to identify the piston's ideal recharge volume and height. A range between 1 and 2 ml/mmHg can be established from the literature.

Known Variables:

- C_{max} = 2 ml/mmHg = 1.50012e-8 $\frac{m^3}{Pa}$.
- $P_{max\ systolic} = 180mmHg = 23998\ Pa$
- $P_{max\ diastolic} = 140mmHg = 18665\ Pa$
- $P_{atm} = 101e3\ Pa$

Required Change Volume:

$$C = \frac{\Delta V}{\Delta P} \therefore \Delta V = C\Delta P$$

$$\Delta V = 1.50012\text{e} - 8 \times (23998 - 18665) = 9.5e - 5m^3$$

Calculate V1 an V2:

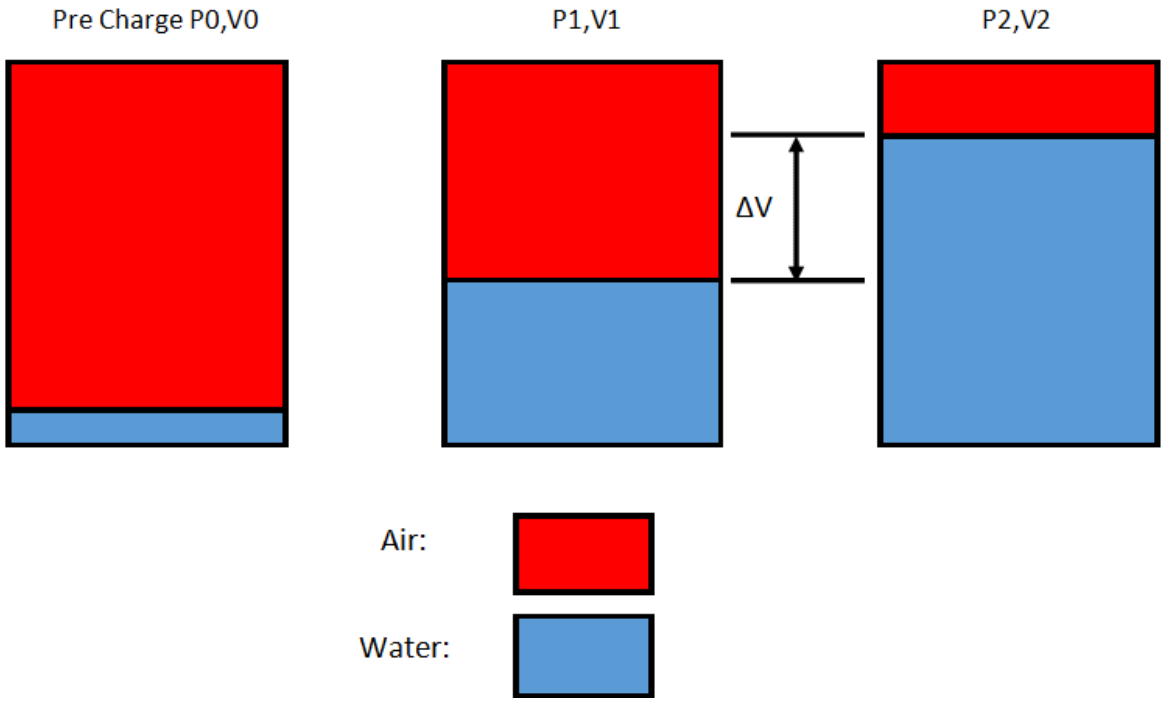

$$P_1V_1 = P_2V_2$$

$$(1)\ P_1V_1 - P_2V_2 = 0 = (101000 + 18665)V_1 - (101000 + 23998)V_2$$

$$(2)\ \Delta V = V_1 - V_2 = 9.5e - 5m^3$$

Solving simultaneous equations 1 and 2 yields:

$$V_1 = 2.2e-3m^3$$

$$V_2 = 2.1e-3m^3$$

Finding V0 (the total container volume):

$$Assume\ P_0 = P_{atm}$$

$$P_0V_0 = P_2V_2$$

$$(101000 + 23998)2.1e-3 = 101000V_0$$

$$V_0 = 2.6e-3m^3 or\ 2.6\ L$$

Find tube height:

$$D_{tube} = 0.124m$$

$$A = \frac{0.124^2}{4}\pi = 0.0121m^3$$

$$H_{minimum} = \frac{V}{A} = \frac{2.6e-3}{0.0121} = 0.215m$$

4.2.3.3 Initial Testing

Once the design was judged to be sound, it was assembled and tested. The following section will explain the testing methods and results obtained from this initial batch of testing.

4.2.3.3.1 Test Rig

The test rig was arranged to replicate the Windkessel model, connecting the capacitance and resistance in series to build up pressure and fluid in the accumulator to dampen the system. The resistor is required so that the pressure and fluid build; if not, the accumulator will not work.

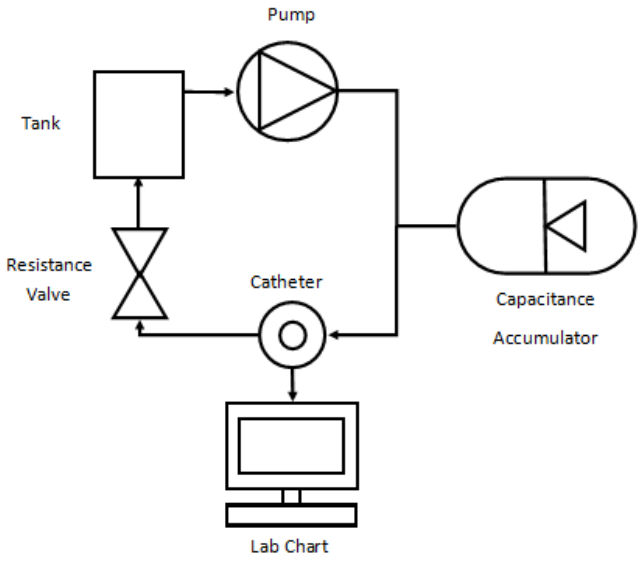

Figure 97:Capacitance experimental setup

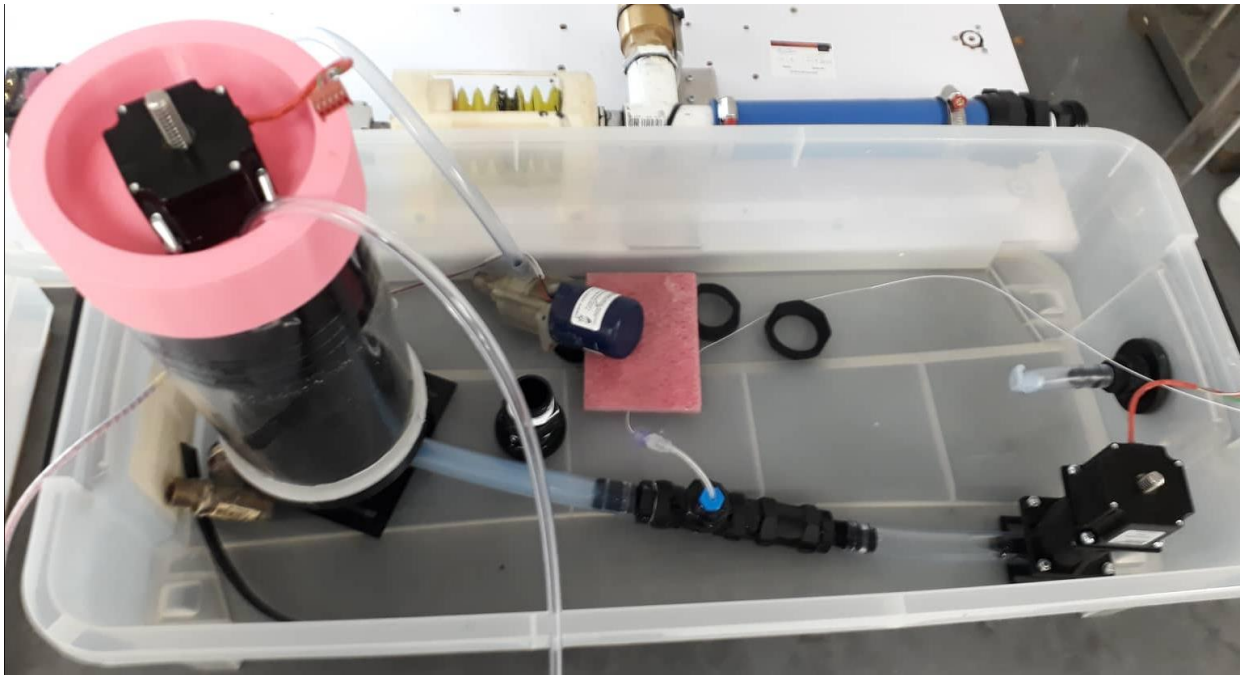

Figure 96: Actual experimental set up

4.2.3.3.2 Experimental Method

1. Calibrating the catheter by measuring two values in a monometer, the first value at 0 mmHg, then at 200 mmHg, inputting the corresponding voltage in the lab chart software.
2. The flow rate was set and measured by timing the flow of water filling a bucket, measured to be 0.88966 m3/s.
3. The capacitance was set at its lowest volume, and the resistor was set to 64×10^6 pa s/m^3 or 8.01 mmHg min/L, water was pumped until the system reached an equilibrium and turned off. This was repeated multiple times to allow measurement of multiple time constants.
4. Measuring the time it takes to reach 36.8% of the maximum value, the time constants can be found for each pulse of the pump.

4.2.3.3.3 Results

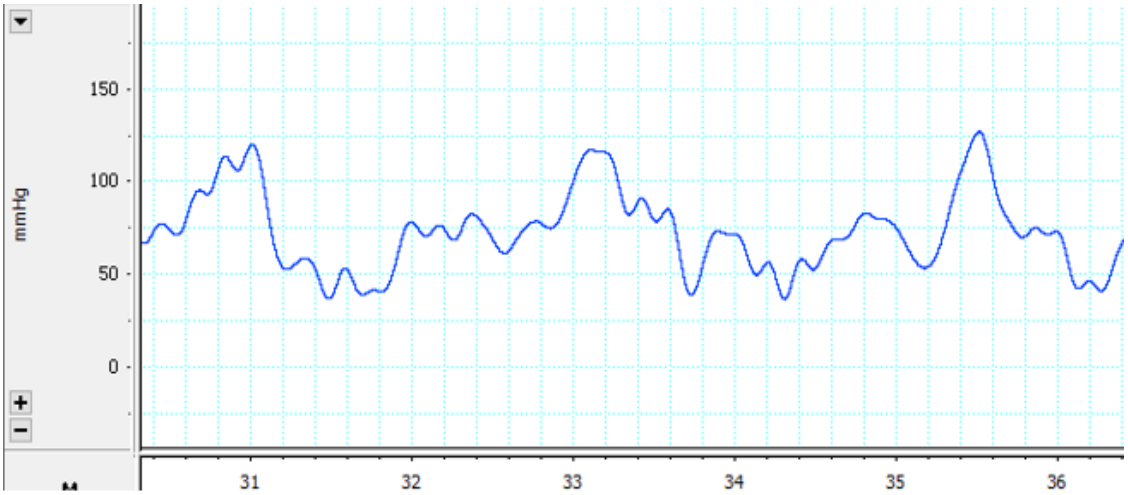

Figure 98: Initial Compliance test plot

	1	2	3	Average
Peak (mmHg)	**121.6**	**125.3**	**122.9**	**123.2**
38.8% of Peak (mmHg)	**30.3**	**31.7**	**34.6**	**32.2**
Time constant (τ)	**0.51s**	**0.42s**	**0.41s**	**0.94s**
C (ml/mmHg)	**1.06**	**0.87**	**0.85**	**0.92**

Table 20: Initial compliance test results

4.2.3.3.4 Discussion

Table 20 illustrates the results of the initial capacitance testing; it was apparent that the compliance chamber was not working as expected. It is known from the literature that the time constant is proportional to RC ($\tau = R.C$) . From these the above capacitance values were determined for the initial test of the MCL. The expected capacitance in this instance was 2 mL/mmHg as the tank was set to the maximum potential value; however, and an average of 0.92 ml/mmHg was observed, this value is less than the minimum value we desire. Under initial pressurisation of the system, bubbles were observed at the base if the capacitance device; it was assumed that air was escaping through the print. Although watertight, it was determined it might not be airtight as some layers may contain small gaps. As the test was set up so that the capacitance to be emulated and the minimum value was barely reached, further testing was done to discover faults in the design and make improvements capacitance system.

4.2.3.4 Changes and improvements

As stated above, during testing, bubbles were observed to be expelled from the base of the 3D printed base. A coat of resin and silicon sealant was added to the capacitance print to observe weather the pressure would be held with this change.

Once this was done, the capacitance was retested using the methods stated above in section 4.2.3.3.2. No significant changes to the compliance values were observed. In the absence of visible bubbles being expelled from the system after intentionally creating bubbles within the loop, it was decided to test the air pressure above the fluid to ensure fluid was not leaving from the top of the system. A manometer was connected to the piston above the system to measure the chamber's air pressure. Maximum pressure of 20 mmHg was observed on the monometer, indicating air leakage from the top of the vessel past the pistons seal through the print. Noting this, the system was redesigned in favour of a design that could constantly seal the air above the system.

The system was redesigned to be based on the bladder accumulator design rather than a piston accumulator. The benefit of the bladder accumulator would be that the bladder itself would seal the air inside it, as well as sealing the water in the pressure vessel as the bladder seals the edges of the vessel during inflation. The overall size and shape of the vessel remained the same. Still, the methods employed here allow a much more consistence seal than the previous design also allow the potential for greater damping as the air in the bladder can be pressurised beforehand rather than being charged at atmospheric pressure.

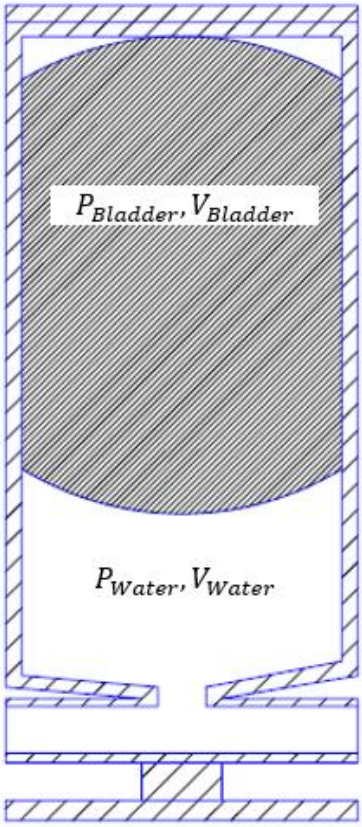

Figure 99: Revised Capacitance design

The methods of determining capacitance for this design are the same as those employed in section 4.2.3.2; we can assume that the bladder's volume can be equated to cylindrical given the tank's shape. The charging procedure can be observed in the following table.

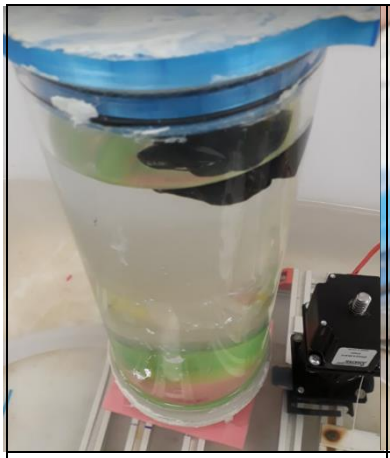		
Step 1: Charge the chamber with water	Step 2: inflate the bladder till the vessel is sealed along the edges	Step 3: continue inflating until required pre-charge pressure is reached, then the system can be run

Table 21: Capacitance charging procedure.

4.2.3.4.1 Testing improvements

The testing methods employed here are the same as those employed in section 4.2.2.2; in this case, the resistance value was set at 75133333 pa*s/m3 or 9.39 mmHg min/l.

Figure 100: Capacitor at min volume

	1	2	3	Average
Peak (mmHg)	**59.1**	**58.5**	**59.4**	**59.0**
38.8% of Peak (mmHg)	**21.5**	**21.6**	**22.0**	**21.7**
Time constant (τ)	**0.62s**	**0.59s**	**0.63s**	**0.614s**
C (ml/mmHg)	**1.11**	**0.99**	**1.12**	**1.073**

Table 22: Min volume capacitance test results

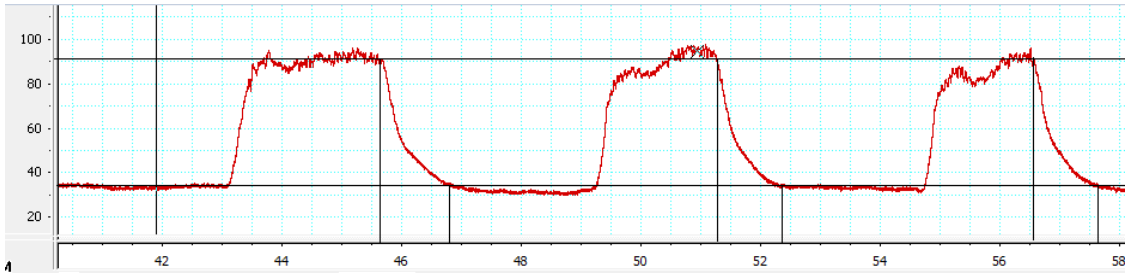

Figure 101: Capacitor at max volume

	1	2	3	Average
Peak (mmHg)	**91.8**	**92.1**	**92.4**	**92.1**
38.8% of Peak (mmHg)	**35.5**	**35.3**	**35.7**	**35.5**
Time constant (τ)	**1.13s**	**1.127s**	**1.125s**	**1.127s**
C (ml/mmHg)	**1.99**	**2.001**	**2.005**	**1.998**

Table 23: Max volume capacitance test results

At the beginning of this project, a range of capacitance was established as 0.9 to 2ml mmHg. From the results above, the minimum value of capacitance determined at the minimum volume was 1.073 ml/mmHg, and the maximum capacitance at the maximum volume was established to be 1.998 ml/mmHg. Observing this test led to the conclusion that the capacitive meets the requirements being within 0.1% of the upper and 19% of the lower range required. The lower limit could be improved by increasing the bladder's volume and or pressure. Also, consistent with the theory of accumulator, the time constant observed decreased as the air volume in the tank decreased.

4.3 Simulation and testing of cardiac conditions

Following the design of the cardiovascular system components, testing was conducted to refine methods and investigate how the separate components interact. This section will describe the tests and refinements conducted on the systems to improve the overall design. Testing was conducted using a catheter to measure pressure and a flow meter to determine fed into a power lab to illustrate the testing results using the lab chart software. A diagram of this setup can be seen in Figure 102. The system was submerged in water and air. This way, we could identify areas where the system leaks.

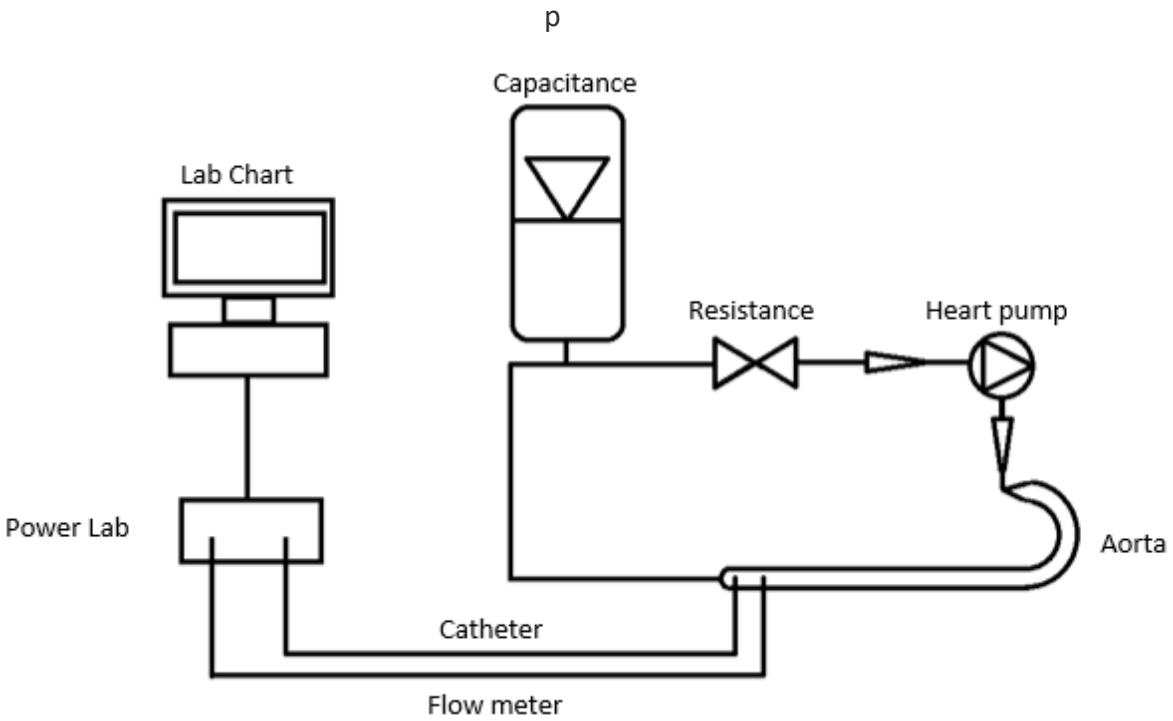

Figure 102: Test Rig Setup

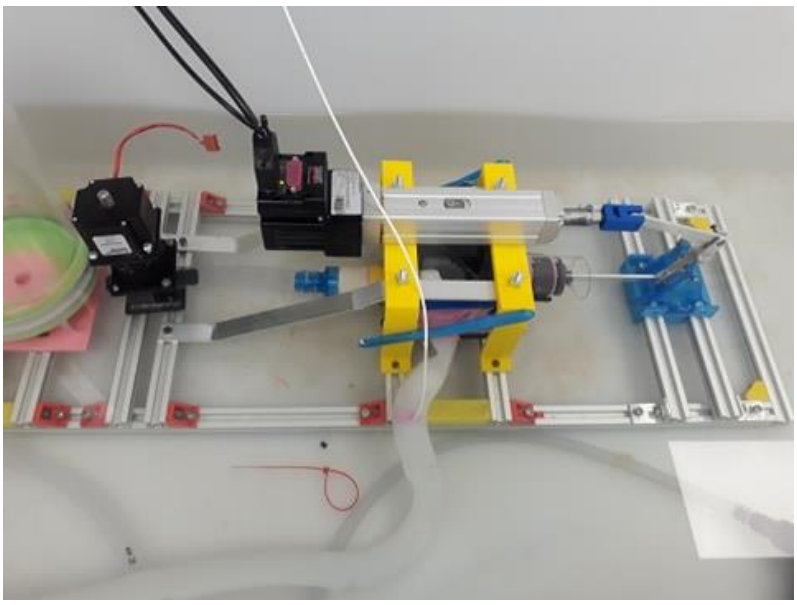

Figure 103: Actual Test setup

The test was conducted, expecting blood pressure and flow within the range of a healthy human being. The system's expected output is an average flow rate of 5 L/min at a pulse rate of 55 bpm, the expected blood pressure being 120/80 mmHg for systolic and diastolic pressure, respectively, at an average of 100 mmHg. Resistance was set to 10.5 mmHg min/L with an expected capacitance of 1 ml/mmHg.

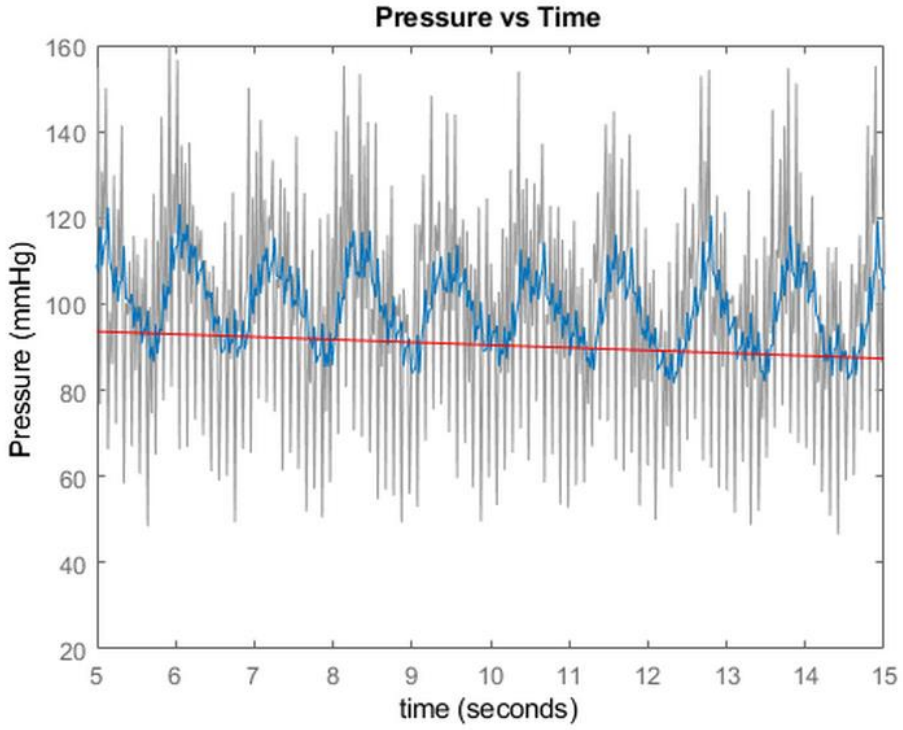

Figure 104: Final test pressure wave

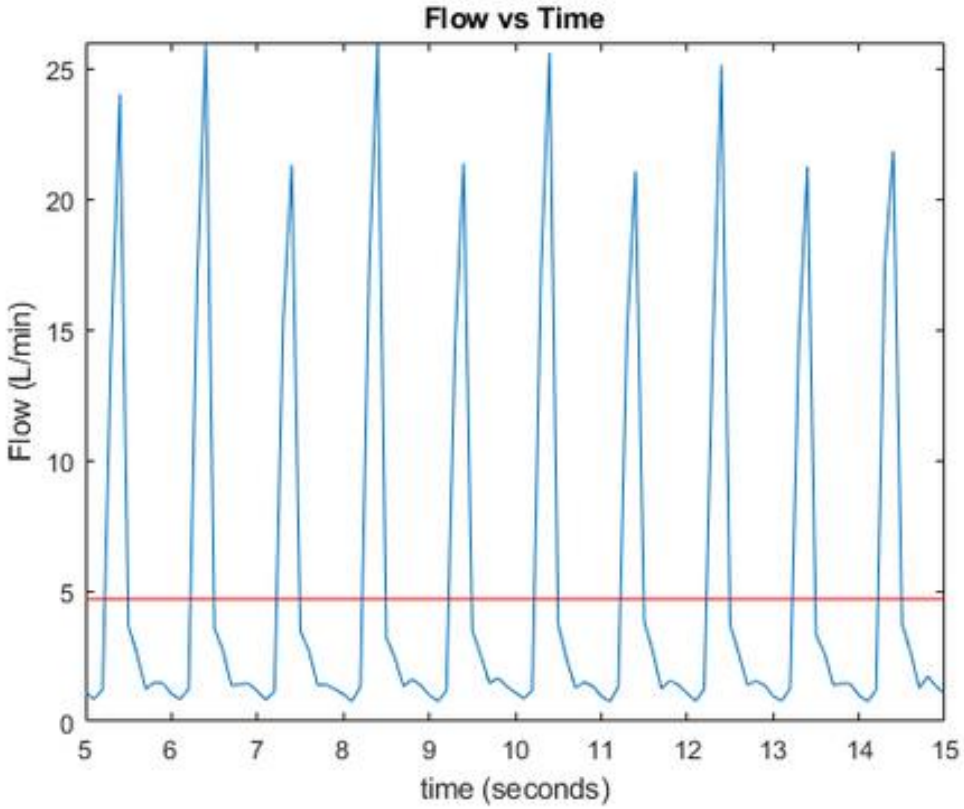

Figure 105:Final flow test wave

Figure 104 and Figure 105 illustrate pressure and flow wave, respectively, from the test conducted on the system. It was observed that the flow rate averaged 4.7 L/min within 6% of the expected value of 5 L/min. The slight variation from the expected and actual flow is likely due to the addition of many different more connections adding to the potential losses in pressure and flow leakages. It was determined that the flow was within a reasonable range as to what the predicted settings were in the motor code. Systolic pressure reached the expected values of an average of 120.1 mmHg with a slightly higher diastolic pressure than expected of 84.3 mmHg, although higher than expected is still with in human resting ranges. The following table is an assessment of the capacitance achieved from this test.

	1	2	3	Average
Peak	**123.8**	**119.8**	**116.8**	**120.1**
38.8% of Peak	**85.84**	**84.14**	**82.93**	**84.3**
Time constant (τ)	**0.62s**	**0.64**	**0.63s**	**0.63s**
C (ml/mmHg)	**0.94**	**1.015**	**1**	**0.998**

Table 24: Final testing capacitance measurements

The capacitance measurements yielded an average of 0.998 ml/mmHg, meaning the actual capacitance is within less than 1% of the desired value. We expect losses in the systems mentioned due to the many fittings required to assemble the different components. These losses can also account for the slope of the average pressure represented in red in Figure 104. The line's slope was measured to be -0.62, indicating that the system is not fully airtight again. Still, reasonably accurate results were yielded none the less, with the pressure averaging 96.6 mmHg throughout the duration of the test.

4.4 Summary

This section aimed to design and develop a method of emulating the circulatory system. The goal was to create a system that can reproduce the pressure and flow waves seen in the literature. This involved developing a pumping method that can adjust pulsatile flow at the required rates and volume, a way to emulate compliance of the arteries and the damping effect it has on blood pressure and systemic vascular resistance to build and throttle pressure in the system. The pumping method designed produced accurate results once the lack of system rigidity and pressure leaks were fixed. The resistance successfully throttled and built pressure within the desired ranges. After a redesign of the initial damping method, the capacitance yielded promising results. When the overall system was assembled, the MCL established healthy human conditions well with the exclusions of minor pressure losses that will require further investigation to rectify.

5 Conclusions and Future Research

5.1 Conclusions

This thesis aimed to present the design and construction of a cardiovascular simulator incorporating a basic phantom simulation of the arterial system to assist in developing and testing a new blood pressure device. A comprehensive literature review aided in identifying the methods, materials and simulation ranges needed in the development of phantom arteries and mock circulatory systems. The methods employed in the literature were employed and modified in a cardiovascular simulation to reproduce values seen in the human body and past experiments. The cardiovascular system and phantom arterial tree were progressed from literature to initial ideas to improvements from testing a retesting method employed. Culminating in a mock circulation system and an arterial tree that emulates findings the properties desired.

5.1.1 Synthetic Artery Design

The design of a phantom arterial tree and methods for creating them successfully reproduced vessels mimicking properties and geometries satisfactorily, using lost core casting methods. The development of the lost core casting process employed in-depth research and testing of the properties of different materials and manufacturing methods, resulting in phantom blood vessels capable of damping pressure as they are observed to do in literature. The materials testing yielded promising results, allowing similar elastic properties to natural arteries as discovered in literature as 150 and 250 kPa. The tests on dragon skin 10 indicated an elastic modulus of 230kPa. The arterial tree was simplified in shape to make moulding easier but still develop the reflection and throttling effects expected. Dimensional accuracy was confirmed through rudimentary tests to validate our process using both vernier measurements and ultrasound imaging of the artery. Tests conducted on the way phantoms preform about what we expect from our testing, and the human body yielded a damping effect of pulse pressure equivalent to that of the upper desired capacitance.

Other moulding method explored proved inconsistent in there results Rotational moulding proved difficult to evenly coat the moulds external surface due to the variety of complex shapes. To make this method effective, a lengthy trial and error process would have to be employed for each specific geometry to determine the precise axial speeds for an even thickness; this led to the abandonment of the moulding process as

the time needed to determine these speeds would outweigh any benefits of using this moulding process. As for the lathe moulding, this method proved very effective for arteries of medium diameter, thickness, and length capable of producing consistent straight arteries at this size. However, the process failed to produce consistent wall thicknesses in smaller vessels due to nozzle size employed, the curing time of the material and the small thicknesses required of the vessel leading to inconsistent wall thicknesses. For the vessels like the aorta, the time needed to create the vessels was too great as the material the dispenser could hold was too small for the large diameter, thickness, and length to be produced without multiple runs of the lathe.

From the development of the phantom arterial tree, the following summary of conclusions can be drawn:

- Lost core casting methods, in conjunction with silicone elastomers particularly Dragon Skin, can yield phantoms with similar mechanical properties to those found in the body.
- Through careful mould design and the procedure outlined in this report, complex shapes could be successfully produced with dimensionally accurate diameters and thicknesses.
- Through the production of the complex shapes found in the artery tree pulse wave reflections can be reproduced.

5.1.2 Mock Circulatory Design

The aim of the mock circulatory system was to create a system that can reproduce the pressure and flow waves seen in the literature. The cardiovascular simulator design was assisted by the in-depth literature review conducted. The features of the loop, including the compliance chamber, resistance, ventricle contraction, flow and pressure examination and recording methods, were all included in the final design. This cardiovascular simulator can reliably emulate the human circulatory system to test new blood pressure measurement devices.

This required developing a device mimicking the pumping of the heart pulsating flow at the desired volume and speed; this was achieved by placing a mock ventricle in a sealed chamber filled with water and actuating a piston to change the outer water volume, thus transferring the change in volume of the ventricle involving the development of a

volume change curve that could be fed to a linear motor. Initially, the transfer of power through the system was not consistent, as the piston would not drive the full length determined by the motor output leading to an undesired rate of flow much lower than expected. The issue was identified as lack of rigidity in the system as the motor stand developed as well as the linkage stage could be seen to flex and move as the system was driven; the issue was fixed by reinforcing the flexing items with aluminium bars. This method successfully replicated the input into the motor to output flow in the system once a lack of system rigidity and pressure leaks were fixed.

The resistance employed a motor actuated gate valve. The valve was successful in throttling flow within the desired ranges, and a flow curve was developed to accurately predict the throttling in relation to the gate height. The compliance chamber was vital in replicating the damping effect seen in the literature. The initial design implemented a position to change the air volume above the system, the trapped air damping the flow. In practice, the design was flawed as the pressure could not be adequately sealed, air escaping through the 3D print releasing the pressure. The redesigned system implements a design using a bladder accumulator design; this design fixed the pressure leaking issues by enveloping the sides leaving no room for any residual air or water to escape; the bladder accumulator also allowed for higher pressures to be employed, broadening the damping capability and successfully dampened the system to what was expected of the design and designs from the literature.

When all the loop elements were implemented, the loop successfully produced the human cardiovascular states desired for both pressure and flow rate or cardiac output. The arterial. The tree was measured for the pulse wave reflection effects that amplify the pressure as it propagates through the system. The result showed a significant increase in wave amplitude at the radial point compared to the aorta, as expected.

The following points can summarise the conclusions drawn:

- Blood flow can be successfully mimicked through the piston and chamber methods described.
- Resistance can be successfully achieved using the gate valve designed.
- The bladder accumulator designed here can damp pulsating flow to within human physiological ranges of capacitance.
- The individual elements when assembled successfully emulate the cardiovascular functions needed for the testing of a new blood pressure device.

5.2 Future Research

5.2.1 Synthetic Artery Design

A basic arterial tree was emulated as per the aims of this research; however, there is room for improvement and further study.

- Imaging of the major arteries in the arterial tree could be undertaken for replication in phantom form.
- This system employed a simplification of arterial shapes more complex anatomically correct phantoms could be produced to simulate the arterial tree more accurately.
- A larger range of material could be employed as different arteries in different area of the body can have a great variance in their properties when compared.

5.2.2 Mock Circulatory Design

Although this design satisfactorily employed methods to replicate human cardiovascular conditions, there is some area for improvement and future research; these are listed below.

- The containment of the ventricle can be improved to provide a method of easily sealing and resealing the pressure vessel to ensure no leaks without the use of sealants as employed in this research.
- The capacitance could be improved to be operated digitally, employing GUI and sensory feedback methods to create a finely controlled pressure vessel and instead of the manually operated method employed.
- More accurate and variant measurement methods can be employed at multiple sites on the MCL, such as the ventricle, for comparison to the downstream readings. This way we can measure the differences between the ventricle and arterial pressure. A replacement for the Arduino flowmeter would be a welcome addition for a device capable of measuring forward and backflow at a higher frequency for more accurate readings.

6 References

AHA. (2019). "The Facts About High Blood Pressure." from https://www.heart.org/en/health-topics/high-blood-pressure/the-facts-about-high-blood-pressure.

Andrade, A., D. Nicolosi, J. Lucchi, J. Biscegli, A. C. Arruda, Y. Ohashi, J. Mueller, E. Tayama, J. Glueck and Y. Nosé (1999). "Auxiliary total artificial heart: A compact electromechanical artificial heart working simultaneously with the natural heart." Artif Organs **23**(9): 876-880.

Aplin, J., P. H. Geoghegan, C. Spence, N. Kabaliuk and M. C. Jermy (2016). "SPIV of natural breathing in Neonatal Airways."

Arabia, M. and T. Akutsu (1984). "A new test circulatory system for research in cardiovascular engineering." Ann Biomed Eng **12**(1): 29-48.

Athanassiou, L., S. M. Hancock and R. P. Mahajan (2005). "Doppler estimation of zero flow pressure during changes in downstream pressure in a bench model of a circulation using pulsatile flow." Anaesthesia **60**(2): 133-138.

Avolio, A. P., L. M. Van Bortel, P. Boutouyrie, J. R. Cockcroft, C. M. McEniery, A. D. Protogerou, M. J. Roman, M. E. Safar, P. Segers and H. Smulyan (2009). "Role of pulse pressure amplification in arterial hypertension: experts' opinion and review of the data." Hypertension **54**(2): 375-383.

Avrahami, I., M. Rosenfeld, S. Raz and S. Einav (2006). "Numerical model of flow in a sac-type ventricular assist device." Artif Organs **30**(7): 529-538.

Ayre, P. J., N. H. Lovell and J. C. Woodard (2003). "Non-invasive flow estimation in an implantable rotary blood pump: a study considering non-pulsatile and pulsatile flows." Physiol Meas **24**(1): 179-189.

Baloa, L. A., J. R. Boston and J. F. Antaki (2001). "Elastance-based control of a mock circulatory system." Ann Biomed Eng **29**(3): 244-251.

Bergel, D. (1961). "The static elastic properties of the arterial wall." The Journal of physiology **156**(3): 445-457.

Biglino, G., P. Verschueren, R. Zegels, A. M. Taylor and S. Schievano (2013). "Rapid prototyping compliant arterial phantoms for in-vitro studies and device testing." Journal of Cardiovascular Magnetic Resonance **15**(1): 2.

Bisaillon, C.-É., M. L. Dufour and G. Lamouche (2011). "Artery phantoms for intravascular optical coherence tomography: healthy arteries." Biomedical Optics Express **2**(9): 2599-2613.

Brunette, J., R. Mongrain, A. Ranga and J.-C. Tardif (2004). "An atherosclerotic coronary artery phantom for particle image velocimetry." Proceedings of the Canadian Engineering Education Association (CEEA).

Cao, P., Y. Duhamel, G. Olympe, B. Ramond and F. Langevin (2013). "A new production method of elastic silicone carotid phantom based on MRI acquisition using rapid prototyping technique." Annu Int Conf IEEE Eng Med Biol Soc **2013**: 5331-5334.

Chee, A. J., B. Y. Yiu, C. K. Ho and C. Alfred (2018). "Arterial phantoms with regional variations in wall stiffness and thickness." Ultrasound in medicine & biology **44**(4): 872-883.

Cornhill, J. F. (1977). "An aortic--left ventricular pulse duplicator used in testing prosthetic aortic heart valves." J Thorac Cardiovasc Surg **73**(4): 550-558.

Dalaq, A. S., D. W. Abueidda and R. K. A. Al-Rub (2016). "Mechanical properties of 3D printed interpenetrating phase composites with novel architectured 3D solid-sheet reinforcements." Composites Part A: Applied Science and Manufacturing **84**: 266-280.

Deplano, V., Y. Knapp, E. Bertrand and E. Gaillard (2007). "Flow behaviour in an asymmetric compliant experimental model for abdominal aortic aneurysm." J Biomech **40**(11): 2406-2413.

Donovan, F. M., Jr. (1975). "Design of a hydraulic analog of the circulatory system for evaluating artificial hearts." Biomater Med Devices Artif Organs **3**(4): 439-449.

Doutel, E., J. Carneiro, M. Oliveira, J. Campos and J. Miranda (2015). "Fabrication of 3d mili-scale channels for hemodynamic studies." Journal of Mechanics in Medicine and Biology **15**(01): 1550004.

Dumont, K., J. Yperman, E. Verbeken, P. Segers, B. Meuris, S. Vandenberghe, W. Flameng and P. R. Verdonck (2002). "Design of a new pulsatile bioreactor for tissue engineered aortic heart valve formation." Artif Organs **26**(8): 710-714.

Dutta, D., K.-W. Lee, R. A. Allen, Y. Wang, J. C. Brigham and K. Kim (2013). "Non-invasive assessment of elastic modulus of arterial constructs during cell culture using ultrasound elasticity imaging." Ultrasound in medicine & biology **39**(11): 2103-2115.

Fiore, G., A. Redaelli, M. Rasponi and R. Fumero (2003). Development of a model left ventricle with physiologic-like diastolic behaviour for studying mitral valve surgical correction.

Fuard, D., T. Tzvetkova-Chevolleau, S. Decossas, P. Tracqui and P. Schiavone (2008). "Optimization of poly-di-methyl-siloxane (PDMS) substrates for studying cellular adhesion and motility." Microelectronic Engineering **85**(5-6): 1289-1293.

Gamble, G., J. Zorn, G. Sanders, S. MacMahon and N. Sharpe (1994). "Estimation of arterial stiffness, compliance, and distensibility from M-mode ultrasound measurements of the common carotid artery." Stroke **25**(1): 11-16.

Garrison, L. A., J. A. Frangos, D. B. Geselowitz, T. C. Lamson and J. M. Tarbell (1994). "A new mock circulatory loop and its application to the study of chemical additive and aortic pressure effects on hemolysis in the Penn State electric ventricular assist device." Artif Organs **18**(5): 397-407.

Geoghegan, P. H., N. A. Buchmann, C. J. T. Spence, S. Moore and M. Jermy (2012). "Fabrication of rigid and flexible refractive-index-matched flow phantoms for flow visualisation and optical flow measurements." Experiments in Fluids **52**(5): 1331-1347.

Ghasemalizadeh, O., M. R. Mirzaee, B. Firoozabadi and K. Hassani (2014). "Exact modeling of cardiovascular system using lumped method." arXiv preprint arXiv:1411.5337.

Gregory, S. D. (2009). Simulation and development of a mock circulation loop with variable compliance, Queensland University of Technology.

Grigioni, M., C. Daniele, G. D'Avenio and V. Barbaro (2000). "Hemodynamic performance of small-size bileaflet valves: pressure drop and laser Doppler anemometry study comparison of three prostheses." Artif Organs **24**(12): 959-965.

Haft, J. W., J. L. Bull, R. Rose, J. Katsra, J. B. Grotberg, R. H. Bartlett and R. B. Hirschl (2003). "Design of an artificial lung compliance chamber for pulmonary replacement." Asaio j **49**(1): 35-40.

Hales, S. (1733). "Haemostaticks." Statistical Essays: Haemostaticks.

Hench, L. and J. Jones (2005). Biomaterials, artificial organs and tissue engineering, Elsevier.

Hoi, Y., S. H. Woodward, M. Kim, D. B. Taulbee and H. Meng (2006). "Validation of CFD simulations of cerebral aneurysms with implication of geometric variations." J Biomech Eng **128**(6): 844-851.

Huetter, L., P. H. Geoghegan, P. D. Docherty, M. S. Lazarjan, D. Clucas and M. Jermy (2015). "Application of a meta-analysis of aortic geometry to the generation of a compliant phantom for use in particle image velocimetry experimentation." IFAC-PapersOnLine **48**(20): 407-412.

Hughes, A. D., J. E. Davies and K. H. Parker (2013). "The importance of wave reflection: A comparison of wave intensity analysis and separation of pressure into forward and backward components." Annu Int Conf IEEE Eng Med Biol Soc **2013**: 229-232.

Ionita, C. N., M. Mokin, N. Varble, D. R. Bednarek, J. Xiang, K. V. Snyder, A. H. Siddiqui, E. I. Levy, H. Meng and S. Rudin (2014). "Challenges and limitations of patient-specific vascular phantom fabrication using 3D Polyjet printing." Proc SPIE Int Soc Opt Eng **9038**: 90380m.

ISO_37 (2017). Rubber, vulcanized or thermoplastic - Determination of tesnislt stress - strain properties.

Koenig, S. C., G. M. Pantalos, K. J. Gillars, D. L. Ewert, K. N. Litwak and S. W. Etoch (2004). "Hemodynamic and pressure-volume responses to continuous and pulsatile ventricular assist in an adult mock circulation." Asaio j **50**(1): 15-24.

Kolff, W. J. (1959). "Mock circulation to test pumps designed for permanent replacement of damaged hearts." Cleve Clin Q **26**: 223-226.

Kozarski, M., G. Ferrari, F. Clemente, K. Górczyńska, C. De Lazzari, M. Darowski, R. Mimmo, G. Tosti and M. Guaragno (2003). "A hybrid mock circulatory system: development and testing of an electro-hydraulic impedance simulator." Int J Artif Organs **26**(1): 53-63.

Lick, S. D., J. B. Zwischenberger, D. Wang, D. J. Deyo, S. K. Alpard and S. D. Chambers (2001). "Improved right heart function with a compliant inflow artificial lung in series with the pulmonary circulation." Ann Thorac Surg **72**(3): 899-904.

Litwak, K. N., S. C. Koenig, R. C. Cheng, G. A. Giridharan, K. J. Gillars and G. M. Pantalos (2005). "Ascending aorta outflow graft location and pulsatile ventricular assist provide

optimal hemodynamic support in an adult mock circulation." Artif Organs **29**(8): 629-635.

Liu, Y., P. Allaire, H. Wood and D. Olsen (2005). "Design and initial testing of a mock human circulatory loop for left ventricular assist device performance testing." Artif Organs **29**(4): 341-345.

Loh, M. and Y. C. Yu (2004). Feedback control design for an elastance-based mock circulatory system.

Mafi, M., S. Rajan, M. Bolic, V. Groza and H. Dajani (2011). "Blood pressure estimation using oscillometric pulse morphology." Conference proceedings : ... Annual International Conference of the IEEE Engineering in Medicine and Biology Society. IEEE Engineering in Medicine and Biology Society. Conference **2011**: 2492-2496.

Marcus, R. H., C. Korcarz, G. McCray, A. Neumann, M. Murphy, K. Borow, L. Weinert, J. Bednarz, D. D. Gretler, K. T. Spencer, P. Sareli and R. M. Lang (1994). "Noninvasive method for determination of arterial compliance using Doppler echocardiography and subclavian pulse tracings: Validation and clinical application of a physiological model of the circulation." Circulation **89**(6): 2688-2699.

Messas, E., M. Pernot and M. Couade (2013). "Arterial wall elasticity: State of the art and future prospects." Diagnostic and Interventional Imaging **94**(5): 561-569.

Meyer, C. A., E. Bertrand, O. Boiron and V. Deplano (2011). "Stereoscopically observed deformations of a compliant abdominal aortic aneurysm model." J Biomech Eng **133**(11): 111004.

Mitchell, J. and J. Wang, Jr. (2014). "Expanding application of the Wiggers diagram to teach cardiovascular physiology." Advances in physiology education **38**: 170-175.

Morsi, Y. S. and A. A. Sakhaeimanesh (2000). "Flow characteristics past jellyfish and St. Vincent valves in the aortic position under physiological pulsatile flow conditions." Artif Organs **24**(7): 564-574.

Munro, B., S. Becker, M. F. Uth, N. Preußer and H. Herwig (2015). "Fabrication and characterization of deformable porous matrices with controlled pore characteristics." Transport in porous media **107**(1): 79-94.

Naemura, K., M. Umezu and T. Dohi (1999). "Preliminary study on the new self-closing mechanical mitral valve." Artif Organs **23**(9): 869-875.

Orime, Y., S. Takatani, K. Tasai, Y. Ohara, K. Naito, K. Mizuguchi, K. Makinouchi, Y. Matsuda, T. Shimono, J. Glueck and et al. (1994). "In vitro and in vivo validation tests for total artificial heart." Artif Organs **18**(1): 54-72.

Pantalos, G. M., S. C. Koenig, K. J. Gillars, G. A. Giridharan and D. L. Ewert (2004). "Characterization of an adult mock circulation for testing cardiac support devices." Asaio j **50**(1): 37-46.

Papaioannou, T. G., D. S. Mathioulakis, J. N. Nanas, S. G. Tsangaris, S. F. Stamatelopoulos and S. D. Moulopoulos (2002). "Arterial compliance is a main variable determining the effectiveness of intra-aortic balloon counterpulsation: quantitative data from an in vitro study." Med Eng Phys **24**(4): 279-284.

Patel, S., P. Allaire, G. Wood and J. M. Adams (2003). DESIGN AND CONSTRUCTION OF A MOCK HUMAN CIRCULATORY SYSTEM.

Qian, M., L. Niu, K. K. L. Wong, D. Abbott, Q. Zhou and H. Zheng (2014). "Pulsatile flow characterization in a vessel phantom with elastic wall using ultrasonic particle image velocimetry technique: the impact of vessel stiffness on flow dynamics." IEEE Transactions on Biomedical Engineering **61**(9): 2444-2450.

Reul, H., B. Tesch, J. Schoenmackers and S. Effert (1974). "Hydromechanical simulation of systemic circulation." Med Biol Eng **12**(4): 431-436.

Richard E. Klabunde, P. (2004). "Cardiovascular Physiology Concepts." Baltimore:Lipincott Williams & Wilkins.

Rosenberg, G. (1981). "Design and evaluation of the Pennsylvania State University mock circulatory system." ASAIO Journal.

Ross, R., M. Toshner, E. Soon, R. Naeije and J. Pepke-Zaba (2013). "Decreased time constant of the pulmonary circulation in chronic thromboembolic pulmonary hypertension." American journal of physiology. Heart and circulatory physiology **305**.

Scotten, L. N., D. K. Walker and R. T. Brownlee (1979). "Construction and evaluation of a hydromechanical simulation facility for the assessment of mitral valve prostheses." J Med Eng Technol **3**(1): 11-18.

Sharp, M. K. and R. K. Dharmalingham (1999). "Development of a hydraulic model of the human systemic circulation." Asaio j **45**(6): 535-540.

Smith, R. F., B. K. Rutt and D. W. Holdsworth (1999). "Anthropomorphic carotid bifurcation phantom for MRI applications." J Magn Reson Imaging **10**(4): 533-544.

Sokolis, D. P., K. M. Lampropoulos, C. A. Dimitriou, E. Balafas, H. Boudoulas and P. E. Karayannacos (2010). "Time-course of mechanical changes of the rat aorta following chronic beta-blocker treatment." Hellenic J Cardiol **51**: 19-26.

Sparks, J. L., N. A. Vavalle, K. E. Kasting, B. Long, M. L. Tanaka, P. A. Sanger, K. Schnell and T. A. Conner-Kerr (2015). "Use of silicone materials to simulate tissue biomechanics as related to deep tissue injury." Adv Skin Wound Care **28**(2): 59-68.

Timms, D., M. Hayne, K. McNeil and A. Galbraith (2005). "A complete mock circulation loop for the evaluation of left, right, and biventricular assist devices." Artif Organs 29(7): 564-572.

Trittenwein, G., A. Zamberger, H. Trittenwein, G. Burda, J. Golej, M. Hermon and A. Pollak (1998). "A simple neonatal mock circulation enabling pulsatility and different hemodynamical states for neonatal ECMO research: application to assess the effect of a centrifugal pump operated neonatal ECMO system on the circulation." Artif Organs 22(5): 414-418.

Vandenberghe, S., J. P. Van Loon, P. Segers, G. Rakhorst and P. Verdonck (2003). "In vitro evaluation of the PUCA II intra-arterial LVAD." Int J Artif Organs 26(8): 743-752.

Verdonck, P. R., K. Dumont, P. Segers, S. Vandenberghe and G. Van Nooten (2002). "Mock loop testing of On-x prosthetic mitral valve with Doppler echocardiography." Artif Organs 26(10): 872-878.

Walther, T., S. Lehmann, V. Falk, J. Köhler, N. Doll, J. Bucerius, J. Gummert and F. W. Mohr (2002). "Experimental evaluation and early clinical results of a new low-profile bileaflet aortic valve." Artif Organs 26(5): 416-419.

Woodruff, S. J., M. K. Sharp and G. M. Pantalos (1997). "Compact compliance chamber design for the study of cardiac performance in microgravity." Asaio j 43(4): 316-320.

Yazdi, S. G., P. H. Geoghegan, P. D. Docherty, M. Jermy and A. Khanafer (2018). "A Review of Arterial Phantom Fabrication Methods for Flow Measurement Using PIV Techniques." Annals of Biomedical Engineering 46(11): 1697-1721.

Yip, R., R. Mongrain, A. Ranga, J. Brunette and R. Cartier (2011). "DEVELOPMENT OF ANATOMICALLY CORRECT MOCK-UPS OF THE AORTA FOR PIV INVESTIGATIONS." Proceedings of the Canadian Engineering Education Association.

7 Appendix

Flow sensor code:

```
int flowPin = 2;    //This is the input pin on the Arduino
double flowRate;    //This is the value we intend to calculate.
volatile int count; //This integer needs to be set as volatile to ensure it updates correctly during the interrupt process.

void setup() {
  // put your setup code here, to run once:
  pinMode(flowPin, INPUT);           //Sets the pin as an input
  attachInterrupt(0, Flow, RISING);  //Configures interrupt 0 (pin 2 on the Arduino Uno) to run the function "Flow"
  Serial.begin(9600);  //Start Serial
}
void loop() {
  // put your main code here, to run repeatedly:
  count = 0;      // Reset the counter so we start counting from 0 again
  interrupts();   //Enables interrupts on the Arduino
  delay (500);   //Wait 1 second
  noInterrupts(); //Disable the interrupts on the Arduino

  //Start the math
  flowRate = (count * 2.25);        //Take counted pulses in the last second and multiply by 2.25mL
  flowRate = flowRate * 60;         //Convert seconds to minutes, giving you mL / Minute
  flowRate = flowRate / 1000;       //Convert mL to Liters, giving you Liters / Minute

  Serial.println(flowRate);         //Print the variable flowRate to Serial
}

void Flow()
{
   count++; //Every time this function is called, increment "count" by 1
}
```

Resistance Motor Code:

```
// Arduino stepper motor control code

#include <Stepper.h> // Include the header file

// change this to the number of steps on your motor
#define STEPS 200

// create an instance of the stepper class using the steps and pins
Stepper stepper(STEPS, 8, 10, 9, 11);

int val = 0;

void setup() {
  Serial.begin(9600);
  stepper.setSpeed(50);
}

void loop() {

  if (Serial.available()>0)
  {
    val = Serial.parseInt();
    stepper.step(val);
    Serial.println(val); //for debugging
  }


}
```